

THERMAL ENHANCEMENT OF PCR USING
TERNARY HYBRID NANOFUIDS

BY

JALAL MOHAMMED ZAYAN

A thesis submitted in fulfilment of the requirement for the
degree of Doctor of Philosophy (Engineering)

Kulliyyah of Engineering
International Islamic University Malaysia

JULY 2021

ABSTRACT

Polymerase chain reaction (PCR) is a vital tool in molecular diagnostics. Still, it is challenged with a host of poor yield, low sensitivity, specificity, contamination, non-specific target amplification, time-consuming, higher cost, energy-intensive, etc. In this study, the performance of PCR as a thermocycler is enhanced from a mechanical engineering perspective by adding additives leading to the enhancement of thermal conductivity of the reaction. In this study, two types of novel ternary hybrid nanoparticles (THNp) or tri-hybrid nanoparticles (GO-TiO₂-Ag and rGO-TiO₂-Ag) were synthesized consisting of three different nanoparticles graphene oxide, titanium dioxide, and silver decorated on each other. The two THNp were synthesized and then characterized using various techniques. The THNp were dispersed in lab-grade DDH₂O and sonicated substantially to form stable ternary hybrid nanofluids (THNf). Zeta potential of the prepared nanofluids was measured to check their stability, and it was in a range of 25 mV to 35 mV. The nanofluids were then serially diluted to 5 levels. Thermal conductivity measurements were performed, and the measurements showed a significant enhancement of about 66% and 83% for both GO-TiO₂-Ag and rGO-TiO₂-Ag, respectively, with THNp in the base fluids. The nanofluids' dynamic viscosity measurements show that the ternary hybrid nanofluids behave as Newtonian and non-Newtonian, where the viscosity decreases with the increase in temperature. Rheological investigations of both the ternary hybrid nanofluids exhibit Newtonian behavior with the stock solution. At the same time, it behaves as non-Newtonian, shear-thinning, or pseudo-plastic fluid when the concentration is diluted. At higher temperatures and low shear rates, the viscosity decreases significantly, which indicates shear thinning behavior. Concentration played a vital role in the change of viscosity due to the variation of temperature. Agglomeration is believed to be the reason for such behavior. Effects of concentration, temperature, and stresses applied in the non-linear viscoelastic fluid revealed linear viscoelastic (LVE) region through amplitude and frequency sweep tests. PCR experiments were performed on the extracted DNA. The initial PCR amplicons from the agarose gel electrophoresis showed that a higher concentration of nanoparticles is not of much significance to PCR, while lower concentration (5×10^{-3} wt.%) of both GO-TiO₂-Ag and rGO-TiO₂-Ag contribute a significant enhancement of PCR reaction while reducing the number of cycles to about 40% when compared to PCR without nanoparticles (control). Subsequent PCR study showed PCR amplicon yield increased by 16.74-folds and 15.30- folds with the addition of GO-TiO₂-Ag and rGO-TiO₂-Ag, respectively. Band intensity study corroborated the same, indicating that the addition of THNp contributes to the thermal enhancement in the reactions. Sanger sequencing results showed the presence of a conserved region, and no DNA damage was observed with the addition of THNp. Separately, DNA denaturation tests were performed with and without the use of THNf for all prepared concentrations. The results showed significantly higher absorbance of UV light in the samples with THNf, indicating earlier denaturation of DNA strands due to the enhancement of thermal conductivity of the reaction. Numerical simulations using ANSYS thermal transient model were performed for a PCR setup with and without THNp. The temperature contours showed a significant enhancement of the heat transfer in the PCR reaction with THNp as an additive. They reduced the overall time by about 40%, corroborating our experimental results.

خلاصة البحث

(أو THNp في هذه الدراسة ، تم تصنيع نوعين من الجسيمات النانوية الهجينة الثلاثية الجديدة) مع ثلاثة من الجسيمات $rGO-TiO_2-Ag$ و $GO-TiO_2-Ag$ الجسيمات النانوية ثلاثية الهجين (النانوية المعروفة ذات السمعة الطيبة وهي أكسيد الجرافين وثاني أكسيد التيتانيوم و فضة. ثم تم تمييز الجسيمتين النانويتين الهجينين باستخدام تقنيات توصيف مختلفة. تم تحضير الموائع النانوية المركب وصوتنة. تم إجراء قياسات جهد زيتا للتحقق من الثبات ثم تم تخفيفها THNp باستخدام بشكل متسلسل إلى 5 مستويات. تم إجراء قياسات الموصلية الحرارية على المخزون ، والسوائل . أظهرت قياسات الموصلية الحرارية أن هناك KD2 pro النانوية المخففة تسلسلياً باستخدام جهاز في السوائل. أظهرت القياسات تحسناً THNp موصلية حرارية معززة للسوائل الأساسية في وجود على التوالي. تُظهر $rGO-TiO_2-Ag$ و $GO-TiO_2-Ag$ كبيراً بنسبة 66% و 83% لكل من قياسات اللزوجة الديناميكية للسوائل النانوية أن السوائل النانوية الهجينة الثلاثية تتصرف كسلوكيات نيوتونية وغير نيوتونية حيث تنخفض اللزوجة مع زيادة درجة الحرارة. أظهرت التحقيقات تظهر سلوكاً نيوتونياً مع محلول GO الريولوجية أن السوائل النانوية الهجينة الثلاثية القائمة على المخزون بينما يتصرف كسلوك ترقق غير نيوتوني أو سائل بلاستيكي زائف عند تخفيف التركيز. في درجات الحرارة المرتفعة ومعدلات القص المنخفضة ، تنخفض اللزوجة بشكل كبير مما يشير إلى سلوك القص الخفيف. لعب التركيز دوراً حيوياً في تغيير اللزوجة في التباين في درجة الحرارة. يعتقد أن التكتل هو سبب هذا السلوك. أظهرت تأثيرات التركيز ودرجة الحرارة والضغوط المطبقة من خلال LVE على اللزوجة المرنة غير الخطية وجود منطقة المرونة اللزجة الخطية (اعتبارات اكتساح السعة والتردد. ثم تم استخدام الموائع النانوية لإجراء تفاعل البوليميراز المتسلسل ، وأظهرت أمبليكونات تفاعل البوليميراز المتسلسل من الرحلان الكهربائي لجيل الاغاروز أن التركيز العالي للجسيمات النانوية يثبط تفاعل البوليميراز المتسلسل بينما التركيز المنخفض يساهم تحسن كبير في $rGO-TiO_2-Ag$ و $GO-TiO_2-Ag$ (بالوزن%) لكل من 5×10^{-3} تفاعل تفاعل البوليميراز المتسلسل مع تقليل عدد الدورات إلى حوالي 40% بالمقارنة مع تفاعل البوليميراز المتسلسل بدون جزيئات نانوية. أكدت دراسة شدة النطاق نفسه. يشير هذا إلى أنه مع في التحسين. بشكل THNp ، يساهم التحسين الحراري في التفاعلات الناتجة عن THNp إضافة منفصل ، تم إجراء اختبارات تمسخ الحمض النووي باستخدام وبدون استخدام السوائل النانوية الهجينة الثلاثية لجميع التراكيز المحضرة. أظهرت النتائج أن هناك امتصاصاً كبيراً لضوء الأشعة ، مما يشير إلى تمسخ سابق لخيوط الحمض THNp فوق البنفسجية في العينات التي تحتوي على النووي والذي يمكن أن يرجع أساساً إلى تعزيز التوصيل الحراري للتفاعل. أظهرت نتائج التسلسل مع الأملاح الموجودة في THNp. قد يكون ذلك بسبب تقارب PCR وجود ضوضاء في منتج PCR الحراري العابر لإعداد ANSYS المنتج. تم إجراء عمليات محاكاة عديدة باستخدام نموذج . أظهرت ملامح درجة الحرارة أن هناك تحسناً كبيراً في انتقال THNp باستخدام وبدون استخدام مع انخفاض كبير بنسبة 40% تقريباً في الوقت الذي THNp مع PCR الحرارة في تفاعل تستغرقه التحسينات الحرارية التي تدعم نتائجنا التجريبية.

APPROVAL PAGE

The thesis of Jalal Mohammed Zayan has been approved by the following:

Ahmed Faris Ismail
Supervisor

Akbar John
Co-Supervisor

Abdul Khaliq Rasheed
Co-Supervisor

Hamzah Mohd Salleh
Co-Supervisor



Sher Afghan Khan
Internal Examiner

Saidur Rahman
External Examiner

Ismail Hassanein Ahmed Mohamed
Chairman

DECLARATION

I hereby declare that this thesis is the result of my own investigations, except where otherwise stated. I also declare that it has not been previously or concurrently submitted as a whole for any other degrees at IIUM or other institutions.

Jalal Mohammed Zayan

Signature.....

Date.....

INTERNATIONAL ISLAMIC UNIVERSITY MALAYSIA

**DECLARATION OF COPYRIGHT AND AFFIRMATION OF
FAIR USE OF UNPUBLISHED RESEARCH**

**THERMAL ENHANCEMENT OF PCR USING TERNARY
HYBRID NANOFLUIDS**

I declare that the copyright holders of this thesis are jointly owned by the student and IIUM.

Copyright © 2021 Jalal Mohammed Zayan and International Islamic University Malaysia. All rights reserved.

No part of this unpublished research may be reproduced, stored in a retrieval system, or transmitted, in any form or by any means, electronic, mechanical, photocopying, recording or otherwise without prior written permission of the copyright holder except as provided below

1. Any material contained in or derived from this unpublished research may be used by others in their writing with due acknowledgement.
2. IIUM or its library will have the right to make and transmit copies (print or electronic) for institutional and academic purposes.
3. The IIUM library will have the right to make, store in a retrieved system and supply copies of this unpublished research if requested by other universities and research libraries.

By signing this form, I acknowledged that I have read and understand the IIUM Intellectual Property Right and Commercialization policy.

Affirmed by Jalal Mohammed Zayan

.....
Signature

.....
Date

To Almighty Allah for means; And to my beloved family and friends for support.....

ACKNOWLEDGMENTS

In the Name of Allah, the Most Compassionate, the Most Merciful

Allah - beginning with the name of - the Most Gracious, the Most Merciful Most Auspicious is he whose control is the entire kingship, and he can do all things [67:1]. All Praise to Allah, the Lord of the creation, and countless blessings and peace upon our Master Mohammed, the leader of the Prophets (peace be upon Him).

My humble thanks to my supervisor, Professor Dr. Ahmed Faris Ismail, for being a pillar of support during the entire journey of my study. My special heartfelt gratitude to both of my brotherly co-supervisors, Dr. Akbar John and Dr. Abdul Khaliq Rasheed, for always being there for me to not only help in my academics but also for their patience and for knowing me very personally, for being my guiding light during my entire study and before. Words are not enough to thank them for their immense help in my studies and their guidance. My sincere acknowledgment to Prof. Dr. Mohammed Khalid and his team Priyanka and Mahesh Vaka from the Graphene advance research lab at Sunway University for their help with my rheological and denaturation experiments.

My sincere thanks to Anton-Paar, Malaysia, for helping us with the equipment for many of our experiments. Also, my sincere thanks to all my colleagues and friends in the “ECTRMG post-graduate lab” for their cooperation and support. And not to forget Br. Oualid from the preparation lab. My sincere acknowledgment and gratitude to Sis Batoul Allam from Kuliyyah of Pharmacy, Kuantan, for her help with my PCR experiments and also to Dr. Mohammed Abdulmalek Aldheeb for his help in my ANSYS simulations and finally, my heartfelt gratitude and thanks to my good friend Dr. Abdul Aabid from S&M Research Lab., Prince Sultan University, Riyadh, KSA for his immense help in guiding me how to write my thesis and all his immense help to complete this thesis as what it is today.

Special thanks to my Parents for their faith and tremendous patience to complete this study and to my siblings for their constant encouragement and prayers throughout my life.

TABLE OF CONTENTS

Abstract	ii
Abstract in Arabic	iii
 Approval Page	iv
Declaration	v
Aknowledgements	viii
Table of Contents	ix
List of Tables	xii
List of Figures	xiii
List of Symbols	xvi
List of Abbreviations	xvii
CHAPTER ONE: INTRODUCTION	1
1.1 Overview	1
1.2 Background of the Study	1
1.2.1 NanoPCR	5
1.2.2 Hybrid NanoPCR	6
1.3 Statement of the Problem	7
1.4 Research Philosophy	8
1.5 Research Objective	9
1.6 Research Scope	9
1.7 Thesis Outline	10
CHAPTER TWO: LITERATURE REVIEW	12
2.1 Overview	12
2.2 NanoPCR	12
2.3 Types of Nanoparticles and their Properties	19
2.3.1 Nanoparticles Made of Carbon and Their Allotropes	19
2.3.1.1 Diamond	21
2.3.1.2 Graphite	22
2.3.1.3 Lonsdaleite	22
2.3.1.4 C60 (Buckminsterfullerene or Buckyball)	22
2.3.1.5 C540	23
2.3.1.6 C70	23
2.3.1.7 Amorphous Carbon	24
2.3.1.8 Single and Multi-Walled Carbon Nanotube	24
2.3.1.9 Graphene	25
2.3.2 Metallic Nanoparticles	25
2.3.2.1 Gold	26
2.3.2.2 Silver	27
2.3.2.3 Platinum	27
2.3.2.4 Rhenium	28
2.3.2.5 Ruthenium	28
2.3.2.6 Palladium	28
2.3.3 Metallic Oxide Nanoparticles	29
2.3.3.1 Aluminium Oxides	29

2.3.3.2 Titanium Dioxide.....	29
2.3.3.3 Silicon Dioxides	30
2.4 Thermal Conductivity of Nanofluids.....	30
2.5 Rheological Investigations of Nanofluids	34
2.6 Critical Analysis of Literature	38
CHAPTER THREE: RESEARCH METHODOLOGY	41
3.1 Overview.....	41
3.1.1 Preparation of GO-TiO ₂ -Ag and rGO-TiO ₂ -Ag nanocomposites	41
3.2 Material Characterization	43
3.2.1 Scanning Electron Microscopy (SEM)	43
3.2.2 Raman Spectroscopy	43
3.2.3 Fourier-Transform Infrared Spectroscopy (FTIR)	44
3.2.4 X-Ray Powder Diffraction (XRD)	44
3.2.5 Particle Size Distribution	44
3.3 Synthesis of Ternary Hybrid nanofluids.....	45
3.3.1 Zeta Potential	45
3.4 Thermal conductivity measurements.....	46
3.5 Dynamic Viscosity and rheological Measurements	47
3.6 Molecular Technique	48
3.6.1 Gene Selection	48
3.6.2 DNA Isolation	48
3.6.3 PCR Protocol and Amplicons Quantification	49
3.6.4 Sequencing Analysis	51
3.7 Evaluation of DNA denaturation by UV spectroscopy	51
3.8 Numerical Simulation.....	52
CHAPTER FOUR: RESULTS AND DISCUSSION.....	54
4.1 Synthesis of Ternary Hybrid Nanoparticles, Characterization, and Preparation of Nanofluids.....	54
4.1.1 Materials Characterization	54
4.1.1.1 Scanning Electron Microscopy (SEM).....	54
4.1.1.2 Raman Spectroscopy	56
4.1.1.3 Fourier-Transform Infrared Spectroscopy (FTIR)	57
4.1.1.4 X-Ray Powder Diffraction (XRD)	58
4.1.1.5 Particle Size Distribution.....	59
4.1.2 Synthesis of Hybrid nanofluids.....	60
4.1.2.1 Zeta Potential	60
4.2 Thermal conductivity measurement	62
4.2.1 Effect of Concentration.....	62
4.2.2 Effect of Temperature	63
4.3 Rheological Investigations of Graphene Based Ternary Hybrid Nanofluids	67
4.3.1 Viscosity Vs Temperature.....	68
4.3.1.1 Effect of Ternary Hybrid Nanoparticle Type on Temperature	72
4.3.2 Viscosity Vs Shear Rate.....	74
4.3.2.1 Effect of Ternary Hybrid Nanoparticle Type on Viscosity	74

4.3.2.2 Effect of Ternary Hybrid Nanoparticle Type on Concentration.....	76
4.3.3 Shear stress Vs Shear rate	78
4.3.3.1 Effect of Ternary Hybrid Nanoparticle Type on Shear Rate	78
4.3.3.2 Effect of Ternary Hybrid Nanoparticle Type on Concentration.....	81
4.3.3.3 Effect of Ternary Hybrid Nanoparticle Type on Temperature	83
4.3.4 Amplitude sweep.....	83
4.3.5 Frequency sweep.....	87
4.4 Effect of Ternary Hybrid Nanoparticles on DNA Denaturation, PCR Enhancement and Sequencing	90
4.4.1 Effects of THNp in Reduction of PCR Reaction Times / PCR Efficiency.....	90
4.4.2 Effects of THNp on PCR yield	92
4.4.3 Effects of THNp on DNA/PCR Amplification	96
4.4.4 Effects of THNp on DNA Sequencing	97
4.4.5 Effects of THNp on DNA Denaturation	101
4.4.6 Absorbance at 260nm.....	107
4.5 Numerical Simulation of PCR Using ANSYS	109
4.5.1 Finite Element Method.....	109
4.5.1.1 Finite Element Modelling	111
4.5.1.2 Meshing and Boundary Conditions	113
4.5.2 Results	115
4.6 Chapter Summary	117
CHAPTER FIVE: CONCLUSION AND RECOMMENDATIONS	121
5.1 Conclusion	121
5.2 Recommendations for future	126
REFERENCES.....	127
PUBLICATIONS	149
APPENDIX A: SEQUENCING FASTA FORMAT	151

LIST OF TABLES

Table 2.1 A brief Summary of Nanoparticles used in the enhancement of PCR	17
Table 2.2 NanoPCR findings with the best concentration for PCR enhancement	18
Table 3.1 PCR mix and thermal cycling conditions for four sets of GO-TiO ₂ -Ag and rGO-TiO ₂ -Ag nanomaterial-assisted PCR (nanoPCR) for 35 cycles	50
Table 3.2 PCR mix and thermal cycling conditions for four sets of GO-TiO ₂ -Ag and rGO-TiO ₂ -Ag nanomaterial-assisted PCR (nanoPCR) for 25 cycles	51
Table 4.1 Material properties	113

LIST OF FIGURES

Figure 1.1 Overview of Research Methodology Flowchart	
Figure 2.1 Various carbon allotropes.	20
Figure 3.1 Flow chart represents an overview of Research Methodology	41
Figure 3.2 Schematic of ternary hybrid nanofluids preparation	46
Figure 3.3 PCR process	50
Figure 4.1 Scanning electron microscope (SEM) images of GO-TiO ₂ -Ag Hybrid Nanoparticles in magnification 60000x, 30000x and 16000x	55
Figure 4.2 Scanning electron microscope (SEM) images of rGO-TiO ₂ -Ag Hybrid Nanoparticles in magnification 1000x, 30000x and 60000x	56
Figure 4.3 Raman spectroscopy of THNp	57
Figure 4.4 FTIR of THNp	58
Figure 4.5 XRD of THNp	59
Figure 4.6 Particle Size Distribution of THNp	59
Figure 4.7 Zeta potential of THNp	60
Figure 4.8 Zeta potential of THNp with respect to time	61
Figure 4.9 (a) and (b): Thermal conductivity of THNp GO-TiO ₂ -Ag, rGO-TiO ₂ -Ag at various temperature (where A, B, C, D and E are serial dilutions)	64
Figure 4.10 Schematic of thermal conductivity mechanism of THNp in the nanofluids	65
Figure 4.11 (a) Viscosity of THNp GO-TiO ₂ -Ag, (b) Viscosity of THNp rGO-TiO ₂ -Ag, (c) Viscosity Vs Shear rate of THNp GO-TiO ₂ -Ag (d) Viscosity Vs Shear rate of THNp rGO-TiO ₂ -Ag, (e) Shear stress Vs Shear rate of THNp GO-TiO ₂ -Ag (f) Shear stress Vs Shear rate of THNp rGO-TiO ₂ -Ag	70
Figure 4.12 (a) and (b): Viscosity Vs Temperature at different temperature and concentrations of ternary hybrid nanoparticles. A, B, C, D and E are serial dilutions	73
Figure 4.13 (a) and (b): Shear rate Vs viscosity at different temperatures and at a concentration of 5×10^{-5} ternary hybrid nanoparticles	76

Figure 4.14 (a) and (b): Viscosity Vs Concentration at different temperature of ternary hybrid nanofluids. A, B, C, D, and E are serial dilutions 78

Figure 4.15 Shear Stress Vs Shear rate. Plots a, b, c, d and e are GO- TiO₂-Ag samples of concentrations A(5x10⁻¹)wt%, B(5x10⁻²)wt%, C(5x10⁻³)wt%, D(5x10⁻⁴)wt% ,and E(5x10⁻⁵)wt%, and f, g, h, I and j are rGO-TiO₂-Ag samples of concentrations A(5x10⁻¹)wt%, B(5x10⁻²)wt%, C(5x10⁻³)wt%, D(5x10⁻⁴)wt%, and E(5x10⁻⁵)wt% 80

Figure 4.16 Amplitude sweep – Storage modulus and Loss Modulus Vs Shear stress and their damping factor (Inset) at different temperatures Plots a, b, c, d and e are GO-TiO₂-Ag samples of concentrations A(5x10⁻¹)wt%, B(5x10⁻²)wt%, C(5x10⁻³)wt%, D(5x10⁻⁴)wt%, and E(5x10⁻⁵)wt%, and f, g, h, I and j are rGO-TiO₂-Ag samples of concentrations A(5x10⁻¹)wt%, B(5x10⁻²)wt%, C(5x10⁻³)wt%, D(5x10⁻⁴)wt%, and E(5x10⁻⁵)wt% 87

Figure 4.17 Frequency sweep – Storage modulus and Loss Modulus Vs Angular frequency and their damping factor (Inset) at different temperature at different temperatures Plots a, b, c, d and e are GO-TiO₂-Ag samples of concentrations A(5x10⁻¹)wt%, B(5x10⁻²)wt%, C(5x10⁻³)wt%, D(5x10⁻⁴)wt%, and E(5x10⁻⁵)wt%) and f, g, h, I and j are rGO-TiO₂-Ag samples of concentrations A(5x10⁻¹)wt% B(5x10⁻²)wt%, C(5x10⁻³)wt%, D(5x10⁻⁴)wt%, and E(5x10⁻⁵)wt% 89

Figure 4.18 (a) and (b): The Lane control is for the marker, and the S is for positive control. The tag 2A to 2D represent the GO-TiO₂-Ag ternary hybrids mixture while the 3A to 3D represents the rGO-TiO₂-Ag ternary hybrid mixture. The term A to D represents the concentration of the nanoparticles in the mixture. 93

Figure 4.19 : The Lane control is for the marker, and the S is for positive control. The tag 2A to 2D represent the GO-TiO₂-Ag ternary hybrids mixture while the 3A to 3D represents the rGO-TiO₂-Ag ternary hybrid mixture. The term A to D represents the concentration of the nanoparticles in the mixture. 93

Figure 4.20 (a) lanes (1 and 3) 1kb ladder; (2,5,7,9,and 11) PCR amplicon amplified using 25 cycle for negative control, sample treated with GO-TiO₂-Ag nanofluid at different concentration. (4,6,8,10,and 12) PCR amplicon amplified using 35 cycle for negative control, sample treated with GO-TiO₂-Ag nanofluid at different. 93

Figure 4.21 (b) lanes (1) 1kb ladder; (2,4,6,8, and 10) PCR amplicon amplified using 25 cycle for negative control, sample treated with rGO-TiO₂-Ag nanofluid at different. (3,5,7,9, and 11) PCR amplicon amplified using 35 cycle for negative control, sample treated with rGO-TiO₂-Ag nanofluid at different concentrations. 94

Figure 4.22 : Quantification of band intensity of the gel electrophoresis of GO-TiO₂-Ag and rGO-TiO₂-Ag with 25 and 35 cycles. 94

Figure 4.23 chromatogram noise observed in sequences 98

Figure 4.24 Bio-edit sequence alignment tool shows base pair mismatch after multiple pairwise sequence analysis using Clustal W v2. 98

Figure 4.25 Conserved region of cytochrome oxidase 1 gene showed in stars 100

Figure 4.26 A graphical representation of nanoparticle interaction in the DNA sequencing is depicted.	101
Figure 4.27 DNA – 12, plots a, b, c, d, e are GO-TiO ₂ -Ag samples of concentrations A(5x10 ⁻¹)wt%, B(5x10 ⁻²)wt%, C(5x10 ⁻³)wt%, D(5x10 ⁻⁴)wt%, and E(5x10 ⁻⁵)wt%, and f, g, h, I, j are rGO-TiO ₂ -Ag samples of concentrations A(5x10 ⁻¹)wt%, B(5x10 ⁻²)wt%, C(5x10 ⁻³)wt%, D(5x10 ⁻⁴)wt%, and E(5x10 ⁻⁵)wt%	105
Figure 4.28 DNA – 27, plots k, l, m, n and o are GO-TiO ₂ -Ag samples of concentrations A(5x10 ⁻¹)wt%, B(5x10 ⁻²)wt%, C(5x10 ⁻³)wt%, D(5x10 ⁻⁴)wt%, and E(5x10 ⁻⁵)wt% and p, q, r, s and t are rGO-TiO ₂ -Ag samples of concentrations A(5x10 ⁻¹)wt%, B(5x10 ⁻²)wt%, C(5x10 ⁻³)wt%, D(5x10 ⁻⁴)wt%, and E(5x10 ⁻⁵)wt%	107
Figure 4.29 Absorbance at a wavelength of 260 nm for 2 samples of DNA (a) 12 (Wavelength 260) (b) 27 (Wavelength 260)	108
Figure 4.30 3D model of a 0.2mL PCR tube	112
Figure 4.31 3D model of the thermo-cycler Aluminum plate	112
Figure 4.32 Section view of the PCR tube inside the Aluminum well setup with the PCR reaction mixture.	113
Figure 4.33 Sectioned view of meshing in the assembly	115
Figure 4.34 Temperature contours of the simulation, with three different PCR steps (a) 28°C–92°C (denaturation), (b) 92°C–55°C, (annealing), and (C) 55°C–72°C (extension) using the ANSYS.	117

LIST OF SYMBOLS

ρ	Density
φ	Volume Fraction
k	Thermal Conductivity
C	Specific Heat Capacity
μ	Viscosity of Hybrid nanofluids
f	Fluid
p	nanoparticles
eff	Hybrid nanofluids
T	Temperature

LIST OF ABBREVIATIONS

3D	Three-dimensional
PCR	Polymerase chain Reaction
RT-PCR	Reverse transcriptase Polymerase chain Reaction
THNp	Ternary Hybrid Nanoparticles
THNf	Ternary Hybrid Nanofluids
GO	Graphene oxide
rGO	Reduced Graphene oxide
TiO ₂	Titanium Oxide
Ag	Silver
SEM	Scanning electron microscopy
FTIR	Fourier-transform infrared spectroscopy
XRD	X-ray powder diffraction
DNA	Deoxyribonucleic acid
UV	Ultraviolet
FEA	Finite Element Method
GC	Guanine-Cytosine
ATGC	Adenine (A), Cytosine (C), Guanine (G), And Thymine (T).

CHAPTER ONE

INTRODUCTION

1.1 OVERVIEW

This introductory chapter covers the research background, problem statement, research philosophy, scope, methodology, and objectives. This presentation includes a brief overview of the topic followed by the research problem and reasoning to the solution based on the philosophy of the study. The scope of the research is briefly clarified along with a specific end goal to answer the problem statement and followed by the research objectives laid down in steps. Then, the critical flow of the current study is explained in the research methodology. Finally, the outline of the thesis is presented.

1.2 BACKGROUND OF THE STUDY

The polymerase chain reaction (PCR) is an *In vitro* reaction technique that enables us to multiply an available DNA of any organism from a few strands to multiple billion copies of the targeted DNA. The PCR was an invention of Kary Mullis in 1984 based on the concept devised by Kjell Kleppe and H. Gobind Khorana by using assays of enzymes to replicate DNA templates with primers (Kleppe et al., 1971). The PCR is a fundamental building block of all genetic testing by multiplying copies of targeted DNA (Dwyer et al., 2002; M. Li, 2005; Siqueira and Rôças, 2003). This fundamental technique is widely used in contemporary molecular biology research and clinical medicine. PCR is an inexpensive, rapid, and simple means of producing large numbers of copies of DNA molecules from a small number of source DNA material (Goodman et al., 1993; Mullis et al., 1986; Ponce and Micol, 1992).

PCR mainly relies on thermal cycling, where the temperature of the DNA and its additive reactants are rapidly changed in many heating and cooling stages to allow different temperature-dependent reactions in each stage (Marie et al., 2003). The reactions are rapidly done in many cycles, where the DNA is multiplied exponentially with each cycle. A small amount of DNA strands from materials like tissues, skin, hair, saliva, or blood peripherals are multiplied exponentially until a desired copy of the DNA is obtained. PCR is a crucial technique used in almost all medical and biotechnological laboratories and research centers for numerous applications like criminal forensics, genotyping, biomedical researches, cloning of DNA, cloning or duplication of genes, monitoring of infectious diseases, pathogen detection (Giovannini and Concilio, 2002), amplification of ancient DNA in archaeology, diagnosis of hereditary diseases, genetic fingerprint and identity analysis as in parentage testing and many more research-based applications. PCR is highly significant to be used when a specific set of DNAs is amplified within minutes in an automated machine called a thermocycler. That is called specificity, wherein only the target set of DNA or genomic material is amplified. The PCR has several challenges which researchers are working hard to address to make it a better technique.

Some of its challenges include the inadequate availability of DNA in the sample, template's high GC content, low specificity in amplification, lower efficiency, the requirement of higher melting temperature in some samples, difficulty in amplifications of some DNA samples due to its secondary structure, the higher formation of impurities or primer- dimer, etc. (Pan. et al., 2012). The typical PCR reaction consists of a three-step recycling process: denaturation, annealing, and extension. The main components of a PCR reaction include PCR buffer solution of about ten times, deoxynucleotide triphosphate (dNTP) mixture, Mg^{2+} , DNA templates, and Taq enzyme.

The PCR relies on thermal cycling in which the content mixture goes through repeated temperature changes called cycles consisting of three temperature steps, as mentioned above. The initialization is done by heating the reaction mixture to a temperature of 94-96 °C for about 1 -10 minutes. The first step of the cycle is denaturation, which consists of heating the reaction mixture to 94–98 °C for about 20–30 seconds. This stage causes the DNA to melt and de-naturate or open strands by breaking the hydrogen bonds between complementary bases, which yields two single-stranded DNA molecules. The next step is annealing, in which the reaction temperature is lowered to about 50–65 °C for about 20–40 seconds. This reduction in temperature allows the primers of each single-stranded DNA template to bind itself to the target region. This is also known as a hybridization stage in which the primers (short DNA fragments) of different strands attach themselves to the denatured strands of DNA. The next stage in the reaction is the elongation or extension in which the temperature is raised to 75–80 °C. This helps synthesize a new DNA strand complementary to the DNA template strand by adding free dNTPs from the reaction mixture. This cycle is repeated as required to amplify the DNA target to millions of copies as required. The general formula used for a given number of cycles is 2^n where n is the number of cycles in the reaction.

PCR is a very widely used method for many applications to simulate *In vivo* DNA replication in many fields of scientific research like DNA cloning for sequencing, gene manipulation, and cloning, construction of DNA-based phylogenies, gene mutagenesis monitoring and diagnosing of hereditary diseases; ancient DNA amplification (Markwell, 2009) analyzing of DNA for profiling to be used in forensic sciences and diagnosis of infectious diseases by detection of pathogens in nucleic acids. However, PCR is still compromised with its low specificity, sensitivity, and false-

negative results, especially in GC-rich fragments (Cao et al., 2009). PCR is prone to have errors due to contamination and primer-dimer formation, where other unwanted DNA is also multiplied by the targeted ones due to the *in vitro* nature of the reaction. Efforts have been made to increase PCR efficiency by various means to improve specificity, sensitivity, reduction of time per cycle, and increase the yield, especially in the GC-rich regions.

PCR is a vital tool with many applications, and it is highly desirable to enhance efficiency using various methods. Some of the conventional methods used are by selecting high-fidelity enzyme such as pfx DNA polymerase, optimizing the PCR reaction conditions, and adding special chemical reagents such as glycerol, etc. (Chisholm et al., 2002; D Cui and al., 2004; Sellner, Coelen, and Mackenzie, 1992; Tomblin et al., 1996). Other biochemical analysis methods require a significant number of biological materials, whereas PCR requires very little, and it has the ability of higher sensitivity, detection, and amplification. It is known from the literature that metal ions such as Mg^{2+} significantly increase the PCR efficiency by maintaining the highest activity of Taq enzyme.

It is imperative to develop newer ways and techniques to enhance the amplification efficiency and specificity (He et al., 2016). Many researchers have found that a few materials such as dimethyl sulfoxide (DMSO), glycerol, formamide, betaine, etc. (Henke, 2008; Varadaraj and Skinner, 1994) enhance the amplification of PCR. Even though these methods can slightly improve the specificity and efficiency of PCR, there is still a considerable void that should be addressed to improve the efficiency of PCR. Few other ways to increase the efficiency of the PCR are to develop better thermocycler machines or by adding additives such as nanoparticles into the PCR reaction known as NanoPCR. The latter is an inexpensive method that has led to

intense investigation due to their fascinating physical and chemical properties (J. Wang et al., 2015). It has attracted considerable attention from researchers in the last decade. Various types of nanoparticles have been tried and used in the PCR to enhance its efficiency and obtained better results.

1.2.1 NanoPCR

In the last decade, nanoparticles have attracted more considerable attention and gradually penetrated various engineering and life sciences fields because of their unique chemical and physical properties, such as large surface area and small size effect, which significantly promoted the development of life science and technology. Their high thermal conductivity and surface-to-volume ratio have led many researchers to adopt them in PCR and named them NanoPCR (Shen et al., 2009). NanoPCR using Gold nanoparticles has proved to increase- the sensitivity of PCR detection 5- to 10-fold in a slower PCR system (i.e., conventional PCR) (S. H. Hwang et al., 2013). Khaliq et al. observed that TiO₂ nanoparticles effectively enhanced the PCR efficiency of low as well as high GC- rich DNA templates, with maximal augmentation up to 6.9- fold at 0.4 nM concentration (Khaliq et al., 2010). Platinum nanoparticles capped with β -cyclodextrins helped improve the overall efficiency of the PCR and increased the sensitivity while reducing the use of reagents (Petralia et al., 2012).

Carbon-coated silica nanocomposites or hybrid nanoparticles were found to be effective PCR enhancers which also induced strong interaction between polymerase and primers (J. Y. Park et al., 2015a). ZnO-TiO₂ hybrid nanoparticles were found to enhance the overall efficiency and specificity of PCR reaction while reducing overall time to about 50% (Fadhil, 2014). Better PCR enhancements can be obtained from other novel nanoparticles, which are yet to be studied. This technology has become a current

research hotspot. The mechanism and application of PCR amplification technology based on various nanoparticles are being explored. Nonspecific amplification and primer mismatch significantly affect PCR amplification. The addition of nanoparticles highly improves the sensitivity, specificity, and yield of PCR due to their excellent surface properties, heat conduction, and specific binding to single-stranded DNA or protein.

1.2.2 Hybrid NanoPCR

Hybrid NanoPCR is a term given to PCR in which a combination of more than one nanoparticle is used. Since the nanoparticles to be added in the PCR reaction are initially mixed with either water or the PCR buffer solution, they are called nanofluids. When one or more nanoparticles are used to prepare the nanofluids to be used as additives to PCR, they are called hybrid NanoPCR. Hybrid NanoPCR is a very new concept. A significant number of studies reported to date has mainly focused on single material nanoparticle as PCR enhancers. At the same time, very few studies have been done on the bi-hybrid or two-material nanoparticles, which can also be referred to as nanocomposites. The aim of synthesizing a multiple-material nanoparticle is to enhance the overall efficiency of PCR and increase the specificity, yield, and efficiency in profiling less abundant, low expressive genes. It also aimed to reduce the time taken per cycle, the overall reaction time of the PCR. At the same time, it should also try to eliminate or at least reduce the formation of primer-dimer or the formation of another unwanted potential by-product of PCR. NanoPCR has the advantage of exhibiting more than one characteristic to improve more aspects in enhancing PCR. The rationale behind the use of hybrid nanoparticles could be because:

- Possibility of modification in the DNA molecular structure and its biochemical and bio-thermal activities due to interactions between the nanoparticles and DNA molecules (M. Li, 2005)
- They exhibit higher heat conduction since nanoparticles have a large surface area (Abdul Khaliq et al., 2010)
- Approximately 20% of atoms of particles measuring less than 20 nm are carried on their surface, facilitating them instantly open for heat transfer (Zhizhou Zhang et al., 2008)
- Enhanced heat transfer due to micro-convection of fluid as a result of the movement of the nanoparticles attributable to the infinitesimal size (Mi et al., 2007)
- Small size and less weight of the particles evade the problem of particles sedimentation (Zhizhou Zhang et al., 2008)
- Percolation structures also help faster transfer heat within the nanoparticles and surrounding fluid (X. Cao et al., 2011).

1.3 STATEMENT OF THE PROBLEM

PCR is one of the fundamental tools in molecular biology. Various nanomaterials have opened up newer opportunities for improving PCR. Several reports have confirmed that an optimal concentration of various nanoparticles acts as enhancers that enhance the yield, specificity, and overall reduction of the PCR reaction time. However, scores of debates prevail concerning the underlying mechanisms. NanoPCR efficiency is affected by parameters such as size, shape, concentration, and type of nanoparticles used, either metallic or non-metallic/carbon-based. All these parameters were also found to have a substantial effect on the thermal conductivity of nanoparticle-

based suspensions. Therefore, it is imperative to investigate the role of enhanced thermal conductivity effect of nanoparticles and their rheological properties on PCR along with interactions between DNA, primers, and enzymes.

It is strongly believed that the potency of nanomaterials to enhance the PCR through uniform heat transfer exclusively relies on the complete dispersal of nanoparticles in nuclease-free water/PCR buffer, besides maintaining their structural integrity due to the sonication process. Understandably, some nanoparticles, such as silver nanoparticles, cause structural damage to the gene under study. Hence, it is essential to study the effect of adding nanoparticles (in this case, graphene nanoflakes based ternary hybrid nanoparticles, GO-TiO₂-Ag and rGO-TiO₂-Ag) that causes any gene mutation or damage to the test gene under study. In this study, ternary hybrid or the trihybrid nanoparticles was synthesized and used as PCR enhancing material. Graphene oxide (GO) is a mono-atomic layer of thick particles formed with the hybridization of carbon atoms. The silver and titanium oxide nanoparticles are decorated on top of graphene nanoparticles to form a ternary hybrid nanoparticle.

Two ternary hybrid nanoparticles consist of graphene oxide, and reduced graphene oxides are coated with two other silver and titanium dioxide nanoparticles. The selection of the three nanoparticles to synthesize a ternary hybrid nanoparticle was based on the consideration of their high thermal conductivity, their hydrophilic nature, solubility in water samples, chemically inert, cost-effective, high mechanical strength, thermal diffusivity, and its easy availability, and the ability to synthesize.

1.4 RESEARCH PHILOSOPHY

Integration of nanotechnology into real-life sciences by the addition of hybrid nanoparticles into PCR is studied. The nanoparticles are known thermal conductivity

enhancers. Hence, the addition of nanoparticles into PCR will enhance the PCR amplification at a considerably low cost and reduce its cycle time while significantly improving specificity, amplification efficiency, and sensitivity of PCR.

1.5 RESEARCH OBJECTIVE

The main objective of this research is

- To develop a novel ternary-hybrid nanoparticle.
- To determine its thermo-physical characteristics
- To enhance the PCR efficiency using THNp.
- Perform systematic investigation on
 - The effects of nanoparticles on DNA amplification,
 - Damage of DNA, and
 - Optimize the concentration of ternary hybrid nanoparticles.

1.6 RESEARCH SCOPE

To study the effect of dispersing ternary hybrid nanoparticles in nuclease-free DD-H₂O and then to perform the PCR to check the enhancement. The enhancement due to the addition of ternary hybrid nanoparticles into PCR is the solution to our problem statement. It is aligned with the research objectives laid out in the previous section. The scope of this current study are as follows:

- Synthesis of ternary hybrid nanoparticles and then characterize them using various instruments.
- Study the thermal conductivity characteristics and rheological behavior for various levels of concentrations and serial dilutions.

- Perform PCR using isolated DNA samples by adding ternary hybrid nanoparticles of various concentrations to the reaction and checking the PCR enhancement using gel electrophoresis.
- Study the concentration of the ternary hybrid nanoparticles in the PCR, which gives the maximum enhancement and optimize the same.
- Perform sequencing analysis to the amplified product and check whether there is damage to the DNA.
- Perform a DNA denaturation experiment using the THNp and check the effect of nanoparticles to the denaturation.
- Numerical investigations of PCR reactions with and without the THNp will allow us to optimize the PCR.

1.7 THESIS OUTLINE

This thesis is organized as follows:

- Chapter 1: As explained above
- Chapter 2: A detailed literature study on PCR enhancements using ternary hybrid nanoparticles is presented. A brief study of different types of nanoparticles, their characteristics are listed. Thermal conductivity and rheological characteristics of the selected nanoparticles to be synthesized are studied and summarized.
- Chapter 3: Detailed methodology of preparation, characterization and experimental measurements are presented.
- Chapter 4: This chapter illustrates the synthesis of ternary hybrid nanoparticles, characterization, and preparation of nanofluids. Thermal conductivity measurement is recorded. The effects of various characteristics like particle size,

concentration, temperature, and various mechanisms responsible for enhancing thermal conductivity are illustrated. Detailed rheological measurements, including various characteristics like particle size, concentration, the temperature of the ternary hybrid nanofluids, are explained. Measurements of various stresses on nanofluids like amplitude sweep and frequency sweep to measure the loss and storage moduli in the nanofluids are presented. PCR experiments using DNA samples with and without ternary hybrid nanoparticles were conducted. The analysis of samples for PCR enhancements, amplification, the effect of nanoparticles on PCR inhibitions, and DNA damage is explained. The effects of ternary hybrid nanoparticles of DNA denaturation are illustrated. Three-dimensional modeling of the PCR tube and the thermocycler wells were designed using solid works, and then numerical simulations using ANSYS software are detailed in this chapter.

- Chapter 5: It deals with the study's overall conclusion and recommends the scope of future works based on this research.

CHAPTER TWO

LITERATURE REVIEW

2.1 OVERVIEW

This chapter overviews all the previous research and articles that have been published related to the PCR enhancements using nanoparticles. It also details the vast number of nanoparticles based on their types, characteristics, and applications. A brief literature survey on thermal conductivity and the rheological properties of the nanoparticles-based nanofluids are presented.

2.2 NANOPCR

The detection of selective DNAs, which are highly sensitive and selective, has extensively been studied as it has many vital applications in the field of biological sciences such as clinical research, diagnosis, genetically modified food monitoring, and detection of environmental contamination (Dhanekar and Jain, 2013; Gupta et al., 2010; Rodríguez-Lázaro et al., 2007). However, when DNA amplification is lower due to some reasons like contamination, lower quality, it becomes a significant bottleneck to quantitatively and qualitatively analyze genetic information. Many types of DNA amplification methods have been developed. Polymerase chain reaction (PCR) is one method which is the best way to amplify DNA since its discovery in the 1980s (Pérez-Pérez and Hanson, 2002; Schmid-Burgk et al., 2013) (Garibyan and Avashia, 2013).

The PCR is performed under in vitro conditions, and it is composed of three main steps, denaturation, annealing, and extension. Despite its extensive utilization, PCR is a delicate and temperature-sensitive technique for amplifying DNA. Therefore, the efficiency and specificity of PCR become a significant challenge. Recent advances

in nanotechnology have made it possible to address such issues by adding nanomaterial to assist PCR using nanoparticles from materials such as metals, carbon-based nanomaterials, semiconductor quantum dots (QDs), and silicon nanowires. That has proven to enhance the efficiency and specificity of PCR (Li, 2005; Liang et al., 2009). This nanomaterial-assisted PCR is referred to as NanoPCR, coined from nanoparticles assisted PCR technology by the early researchers who used nanoparticles to enhance PCR efficiency. The addition of nanoparticles to a PCR reaction significantly improved specificity, amplification, the efficiency of PCR, and sensitivity and accelerated the reaction by reducing the number of cycles (Sang et al., 2017).

After a thorough search, it was found that the earliest study to use nanoparticles in a PCR reaction was in 2004. They used a single-walled carbon nanotube to increase the amount of PCR product (Daxiang et al., 2004). Then metallic nanoparticles like gold were used to assist the PCR process in demonstrating higher PCR amplification concerning yield and specificity (Haikuo et al., 2005). This technological trend to use nanoparticles to assist PCR reaction picked up as a research hotspot, and many researchers used various type of nanoparticles for a variety of applications like biosensors in the detection of specific bacterium (Xu and Yao, 2013) and viruses (Huang et al., 2008), general PCR enhancements (Khaliq et al., 2012) in profiling less abundant low expressive genes (Sailapu et al., 2018), etc. using a variety of types of nanoparticles like gold (Lou and Zhang, 2013), silver (Thamilselvi and Radha, 2017), TiO₂ (Khaliq et al., 2010), graphene (Sharma et al., 2016), ZnO (Upadhyay et al., 2020), Iron Oxide (Kambli and Kelkar-Mane, 2016), CNT (Zhang et al., 2008), carbon nano powder (Zhang et al., 2007a), CuO (Gao et al., 2019), quantum dots (Sang et al., 2015), platinum (Nejdl et al., 2017), magnesium (Narang et al., 2016) and hybrid

nanocomposites like graphene-ZnO (Sharma et al., 2016), ZnO-TiO₂ (Fadhil, 2014), Gold-graphene (Jeong et al., 2015), etc.

The nanoparticles are a hotspot of research and application in almost all recent technological advancements. They have many unique properties, which makes them desirable in a variety of applications. The most important property is their high thermal conductivity due to minimal size and larger surface area. Moreover, the nanoparticles share many common properties such as biocompatible, solubility in water, and are highly stable. Various nanoparticles, both metallic and non-metallic nanoparticles, have their unique characteristics. The nanoparticles are used as a PCR enhancer for more than a decade. Single material nanoparticles like gold nanoparticles are active enhancers of PCR because of its mediated surface interaction rather than higher thermal conductivity, and also gold nanoparticles in PCR are target dependant (Shen and Zhang, 2013); likewise, graphene nanoparticles enhance the yield and specificity of the PCR (Khaliq et al., 2012). TiO₂ nanoparticles in PCR tend to enhance the denaturation of genomic DNA through efficient thermal conductivity of the reaction buffer (Khaliq et al., 2010).

The nanomaterials provide exceptional physical and chemical properties like a large surface area to volume ratio, a reasonable heat transfer rate, and potential binding sites for biological materials. Among the various types of nanomaterials, GO has been considered one of the most exciting materials because of its intrinsic properties and potential applications. GO, a two-dimensional material composed of sp²-bonded carbon atoms is enriched with oxygen functional groups such as carboxyl, hydroxyl, and epoxy groups (Jung et al., 2010), rendering it water dispersible and functional building blocks for constructing hybrid nanomaterials. In particular, GO exhibits a capability for anchoring biomolecules without any surface modification or coupling reagents due to

weak van der Waals and p-p interactions. Despite the merits and capabilities of GO, a severe level of agglomeration leads to a limited surface area, which may impede PCR performance (Chen and Xie, 2010; Uddin et al., 2013).

Gold nanoparticle (Au-NP) based hybrid nanomaterials have been considered an alternative to meet these requirements to overcome such challenges. Hybrid nanomaterials maintain the beneficial features of both precursor materials and provide advantages unique to the hybrid material through the combination of functional components (Sanchez et al., 2003). GO plays a role as a template and building block for developing graphene-based hybrid materials (Li et al., 2014). GO also prevents the self-aggregation of Au-NPs by serving as a substrate (Hotze et al., 2010). The Au NPs on individual GO sheets can also be exploited to maintain the GO sheets at a certain distance from each other. Furthermore, Au NPs commonly exhibit biocompatibility, chemical stability, and simplicity in preparation and surface modification for immobilization of biomolecules (Jia et al., 2008; Jung et al., 2010; Li and Rothberg, 2004).

These advantages provide more adhesion layers that can be immobilized together in the exact location as the PCR components, thereby significantly increasing the possibility of the amplification reaction (Mi et al., 2007; Yuce et al., 2014; Zhang et al., 2008). Therefore, Au and GO are suitable to increase the efficiency and the fidelity of PCR. However, the mechanism of Au and GO hybrids during PCR remains a mystery. The rationale behind the use of nanoparticles could be because of; Possibility of modification in DNA molecular structure and its biochemical and bio-thermal activities due to interactions between the nanoparticles and DNA molecules (Li et al., 2005). They exhibit higher heat conduction since nanoparticles have a large surface area. Approximately 20% of atoms of particles measuring less than 20 nm are carried

on their surface, facilitating them instantly open for heat transfer (Eastman et al., 1996). Enhanced heat transfer due to the micro-convection of fluid due to the nanoparticles' movement attributable to the infinitesimal size (Eastman et al., 2001).

Small size and less weight of the particles evade the problem of particle sedimentation (Cui and al., 2004). Percolation structures also help in the faster transfer of heat within the nanoparticles and surrounding fluid. Several reports have confirmed that several nanoparticles are potential enhancers of PCR. The addition of nanoparticles to PCR has shown enhancements in increased yield and enhanced specificity with inhibitory effects in some cases. It is difficult to explain the exact mechanism behind enhancements due to the complexity involved in a PCR reaction, which contains several reagents such as a polymerase, primers, template DNA, dNTP, Mg²⁺, buffer solution, etc. additives.

Nevertheless, some mechanisms including binding of DNA with nanoparticles (Koo et al., 2005), the interaction of polymerase and nanoparticles (Khaliq et al., 2010), electrostatic interaction between the nanoparticles and PCR components, enhanced heat transfer effect of nanoparticles, nanoparticle bound primers (Jung et al., 2010), etc., have been proposed for such PCR enhancements. Many attempts were made to utilize different nanoparticles to enhance the product yield in conventional PCR techniques. Table 2.1 below summarises the nanoparticles used in the enhancement of PCR, and table 2.2 summarises the nanoparticles used in the literature for PCR enhancement along with their best concentrations.

Table 2.1 A Summary of Nanoparticles used in the enhancement of PCR

Reference	Materials Used	Findings
Cui and al., 2004	Single-walled CNT	The DNA templates and Taq enzymes are attached to bundles of SWCNTs in PCR products. Increased PCR efficiency
Li, 2005	Gold Nanoparticles	Reaction time is decreased, the yield is improved
Zhang et al., 2007b	Carbon Nano Powder	DNA could be obtained with a certain amount of CNP in the sixth-round amplification. Specificity was improved and significantly improved the amplification efficiency for prolonged PCR reactions.
Haber et al., 2008	Gold Nanoparticles	Au-NPs altered the PCR amplification profile, and they conclude that effects on the assay detection system must be carefully evaluated before Au-NPs are included in any qPCR assay
Wan et al., 2009	silver and titanium dioxide nanoparticles	complex interaction mechanism exists between AgNPs and TiO ₂ NPs with PCR reagents
Khaliq et al., 2010	Titanium oxide Nanoparticles	TiO ₂ augmented the denaturation of genomic DNA, indicating more efficient thermal conductivity through the reaction buffer
Cao et al., 2011	polyethyleneimine (PEI)-modified multi-walled carbon	specificity and efficiency of an error-prone two-round PCR are significantly impacted by the surface charge polarity of the PEI-modified MWCNTs
Suresh et al., 2011	Al ₂ O ₃ -Cu	Thermal Conductivity enhancement
Khaliq et al., 2012	Graphene Nano flakes	Superior thermal conductivity affected the enhancement of PCR
Tong et al., 2012	PEI-stabilized gold nanoparticles	Enhancement of efficiency and specificity
Cao et al., 2012	Dendrimerentrapped gold nanoparticles	A novel class of PCR enhancers improved interaction with the PCR components and the thermal conductivity, which allow them to be used for enhancing different error-prone PCR systems
Fadhil, 2014	Zinc oxide and titanium dioxide	there is about a 50 % reduction in overall PCR reaction time
Jeong et al., 2015	Gold-Graphene hybrid	PCR performance is improved, chemical interaction of the hybrid composite and the PCR components and the potential mechanism behind the hybrid composite-assisted are studied

Park et al., 2015b	PDA-coated silica and carbonized PDA Silica Nanoparticles	strong interaction between the nanocomposites and PCR reagents, including polymerase and primers, regulate the PCR performance
Zhong et al., 2016	Graphene Oxides	demonstrate that the size, reduction degree, and surface charge affect the specificity of PCR
Dantas et al., 2017	Gold and Titanium dioxide Nanoparticles	Formation of well-defined bands, being able to inhibit the occurrence of false negatives. Increased detection of Lxx by PCR
Dhabaan et al., 2018	silver, zinc, and gold	The DNA yield was enhanced, and the sensitivity of random amplified polymorphic DNA (RAPD) PCR products was increased
Maleki et al., 2019	Green graphene oxide/gold (GO/Au)	nanocomposite can improve both endpoint and real-time PCR methods at the optimum concentrations
Wang et al., 2019	Gold nanoparticles	The sensitivity of DPO-NanoPCR was at least 100-fold higher than that of conventional PCR. The specificity detection showed that the DPO-NanoPCR was able to detect BRV, BPV, and BVDV accurately.
Upadhyay et al., 2020	ZnO nanoflowers	Significant enhancement of the PCR assay concerning its sensitivity and specificity for the diagnosis of two important CVBDs

Table 2.2 NanoPCR findings with the best concentration for PCR enhancement

References	Nanoparticles used	Size of the nanoparticle	Best concentration	PCR property enhanced
Wang et al., 2017	Graphene oxide sheets	1nm	< 1 µg/mL	Eliminate the nonspecific products
Li et al., 2005	Au	12nm	-	PCR efficiency (time reduction)
Dantas et al., 2017	Au – TiO ₂	13nm	1.6 g/L	improvement in the DNA yield and purity
Xu & Yoa, 2013	Ag -TiO ₂	0.6&0.9	40 pg/µL	Enhancing PCR efficiency
Khaliq et al., 2010	TiO ₂	~25 nm	0.4 nM	Enhancing PCR efficiency
Khaliq et al., 2012	Graphene NF	8nm	1 mg/ml	65% reduction in Number of Cycles
Gabriel et al., 2018	GO, Al ₂ O ₃ and CuO	-	0.04 µg / mL	Enhance the detection of pathogenic free-living amoebae.
Lou et al., 2013	Au	1nm	172 µg/mL	AuNPs inhibit and enhance PCR by

					polymerase adsorption under varied situations.
Upadhyay et al., 2020	ZnO flower	Nano	-	5 μ L	Reduction in PCR reaction time and Enhancement of PCR efficiency

2.3 TYPES OF NANOPARTICLES AND THEIR PROPERTIES

2.3.1 Nanoparticles Made of Carbon and Their Allotropes

Nanoparticles have attracted considerable attention in recent years. They are used in the medical field as medicines and as a target medicine delivery agent in recent times. They are also widely used to improve the diagnosis and treatment of human diseases (Bhaskar et al., 2010). The exceptional properties of nanoparticles, including high resistance to oxidation and high thermal conductivity, make them desirable to be used in a wide array of applications in the medical and biotechnological arena. Carbon-based nanoparticles come in many shapes and sizes. It was discovered about three decades ago, in 1991. These particles are arranged in a hexagonal network of carbon atoms having a diameter of one nanometre and lengths varying from 1 to 100 nm in a cylindrical manner. There are many configurations of carbon-based nanoparticles; some of them are listed in Figure 2.1.

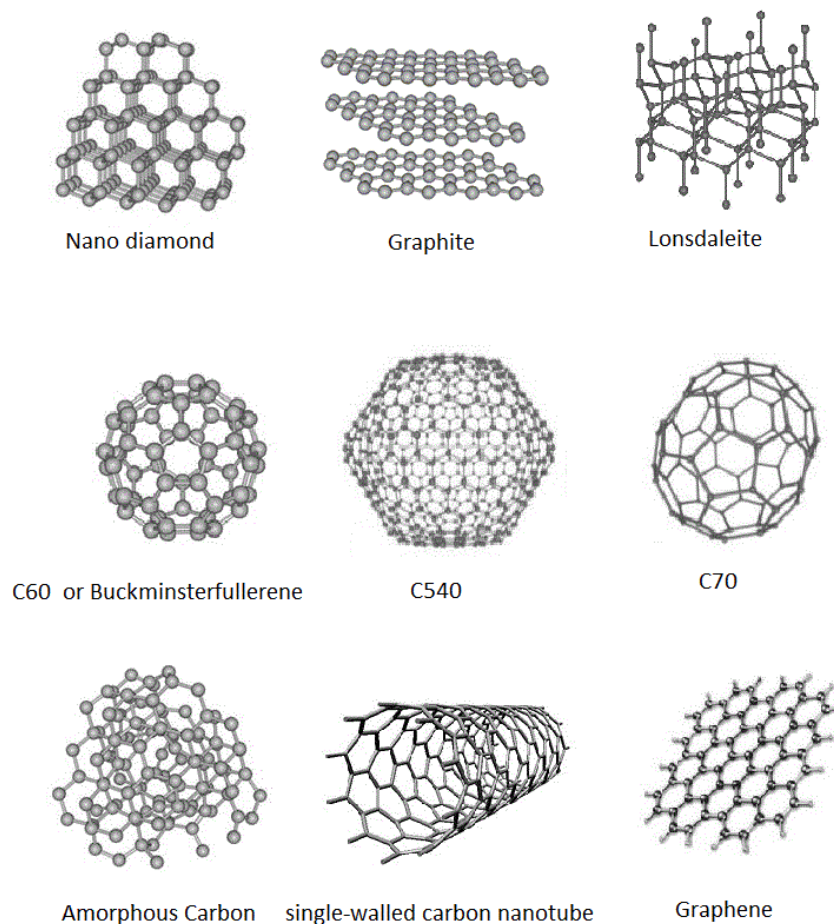


Figure 2.1 Various carbon allotropes. (Image adapted from multiple websites)

The size, geometry, and surface characteristics of these nanoparticles make them remarkably highly useful in various applications, starting from DNA sequencing to additives of lubrication in automotive engines. PCR, as mentioned previously, is a standard tool in biological research. It is an indispensable tool in biotechnology, genetic testing, forensic applications, and many other research fields. In recent times carbon and other material-based nanoparticles are added as an additive to enhance the PCR; hence they are called NanoPCR. These nanoparticles help speed up the process of PCR to a considerable amount of time, enhancing specificity, sensitivity, and mechanisms. That is mainly due to its excellent thermal conductivity, Physico-chemical, and microbial properties. There are various types of carbon-based nanoparticles used in a variety of applications. Some of them are listed below.

2.3.1.1 Diamond

Diamond Nanoparticles or Nano-Diamond were first discovered about 50 years ago in an explosive shock process (DeCarli and Jamieson, 1961). This discovery of Nano-Diamond led to their enormous studies and is used in various applications, including in biotechnologies. Diamond particles at the nanoscale length ~1 to 100 nanometres are carbon nanoparticles with a truncated octahedral architecture available in many types such as diamond particles, pure-phase diamond films, 1-D diamond nanorods, and 2-D diamond nanoplatelets (Schrand et al., 2009). These Nano-diamonds measuring about a few nanometres have a nucleus like an onion-shaped shell and are packed in complex chemical composition with a typical diamond density and optical nuclear potential (Aleksenskii et al., 1999; Mochalin et al., 2012).

The Diamond nanoparticle's atomic structure has very distinctive properties like extreme mechanical rigidity, high hardness, and a combination of high thermal conductivity (Field, 2012). They also possess superior physical and chemical properties over conventional materials. Nano-Diamond is used in various applications like bio-labeling (Chao et al., 2007), high-performance Micro and Nano Electro-Mechanical Systems (Williams et al., 2007; Williams et al., 2010). Since diamond nanoparticles are carbon-based nanoparticles, they are non-toxic (Schrand et al., 2007), stable (Yang et al., 2002), and also facile functionalization (Krüger et al., 2006). They are widely used in many bio-applications, such as targeted drug delivery and biomarkers (Huang et al., 2007). However, no studies have been reported on the use of diamond nanoparticles for PCR applications.

2.3.1.2 Graphite

Graphite nanomaterials also referred to as carbon nanotubes (CNTs), are an allotrope of carbon. They are multi-layered and have a planar structure. The carbon atoms of graphite are arranged in a honeycomb lattice. Graphene is the name given to graphitic nanomaterials when they occur in a single layer. Graphite nanoparticle has a high thermal conductivity property. They also possess good mechanical and electrical properties with excellent dimensional stability and excellent optical properties (Depez and McLachlan, 1988). Due to their superior characteristics and promising potential, they are immensely used in many applications ranging from a simple pencil to transistors, batteries, super-capacitor, composites, fuel cells, coolants, and an additive to many biotechnological applications like PCR.

2.3.1.3 Lonsdaleite

Experimental Lonsdaleite is another allotrope of carbon nanoparticle. It usually forms under the heat and stress impact from graphene to diamond (Nakamuta and Toh, 2013) but retains the crystal lattice of the graphitic form. It is known as the most complex material on earth. A tiny amount of lonsdaleite is available in nature. It is a hexagonal 2H polytope of the diamond. Hence, it is also referred to as a hexagonal diamond (Greshnyakov and Belenkov, 2017). They are about 58% harder than the diamond due to their hexagonal lattice structure (Németh et al., 2014). Recent analysis has shown that it has a higher indentation strength than diamond (Pan et al., 2009).

2.3.1.4 C60 (Buckminsterfullerene or Buckyball)

C60 or Buckminsterfullerene or buckyball is an allotrope of carbon nanoparticle which contains about 60 vertices and 32 faces with carbon atoms at vertices of each polygon

connected by bonds along each of the edges. The nuclei distance diameter of the molecule is about 0.71nm. Their atomic structure is similar to graphene but rolled up in a spherical shape with a closed structure (Aschberger et al., 2010). It resembles a similar shape and structure to a soccer ball. They exhibit the spheroidal carbon molecules when analyzed by a mass spectrometer (Katz, 2006). Buckyball molecules are incredibly stable withstanding high temperatures and pressures. C60 molecules form bonds and are locked with each other against rotation at low temperatures (Liu et al., 2014). Since the electron-attracting capability of C60 is very strong, other functional compounds can be easily added to it. Since they have high thermal conductivity and are readily soluble in water-based primers, C60 and its derivatives are used as additives in an extensive range of biomedical applications and biotech experiments (Kadish and Ruoff, 2000).

2.3.1.5 C540

Fullerenes are closed carbon clusters containing sheets of stacked graphitic hexagons closed by 12 pentagons. C540s present all their atoms on the surface of the clusters. They are similar to graphite in terms of their atomic structure. The C540 is very stable, but it is nonreactive. C540 is extensively used in many biotechnological and biomedical applications, including designing high-performance MRI and X-ray contrast agents, drug and gene delivery (Lalwani and Sitharaman, 2013).

2.3.1.6 C70

The C70 carbon nanoparticles, as the name suggests, it has 70 carbon atoms. These atoms bond along each polygon edge at the vertices. The molecular structure resembles that of a rugby ball shape. C70 is closely similar to C60 in its atomic structure, except its equator is connected by a belt of 5 hexagons. The C60 bond length ranges between

0.137 and 0.146 nm in about eight bonds. Each carbon atom in the structure is bonded covalently with three others (Rao et al., 1995). The C70 nanoparticles are insoluble in water (Talyzin and Engström, 1998).

2.3.1.7 Amorphous Carbon

Coal, soot, carbide-derived carbon are few types of amorphous carbon. They are the impure forms of carbon, which is neither graphite nor diamonds. They are polycrystalline and do not have any particular shape (McNaught and Wilkinson, 1997). They are thermodynamically in a metastable state. Their properties vary depending on the methods of formation. Hydrogenated amorphous carbon is the one whose bonds are terminated with hydrogen. The ratio of sp² and sp³ determines the property of amorphous carbon (Robertson, 2002). Amorphous carbon has a high mechanical hardness, high thermal conductivity, and low friction coefficient (Zhu et al., 2009). They also have high electrical conductivity and are used as electrode materials for super-capacitors (Barranco et al., 2010).

2.3.1.8 Single and Multi-Walled Carbon Nanotube

The single-walled carbon nanotube (SWNTs) or Buckytube are cylindrical in their nanostructure. They are a member of the fullerene structural family. The diameter of these SWNTs is usually about 1nm. The length to width ratio can be many million times more massive. They have very high mechanical stiffness in tensile strength and elastic modulus (Yu et al., 2000). Their solid density is very low (Collins and Avouris, 2000). SWNTs are excellent electricity conductors (Mintmire et al., 1992). They are widely used as additives in biotechnological and biomedical applications. The biological applications of the SWNTs depend on the methods they have produced, mainly the

dispersed property and its diameter (Zhang et al., 2008). A multi-walled Carbon nanotube consists of more than one layer of carbon atoms rolled up in layers. The morphology of the multi-walled carbon nanotubes is similar to that of SWNT. Carbon nanotubes are good thermal conductors compared to most other metallic nanoparticles. Carbon nanotubes are widely used in biomedical applications like drug delivery (Liu et al., 2009), gene therapy, immunotherapy, tissue regeneration, and different ailments (Rosen and Elman, 2009).

2.3.1.9 Graphene

Graphene is an allotrope of carbon belonging to the fullerene family. It has a two-dimensional atomic structure. The carbon atoms are densely packed in a hexagonal pattern (Cooper et al., 2012). Graphene is unique due to its mechanical, functional, physical, and functional properties. It is the strongest in mechanical strength and has very high thermal conductivity (Balandin et al., 2008). They are very widely used in many technological fields of application like electronic devices (Wei and Liu, 2010), energy storage, sensors (Avouris and Dimitrakopoulos, 2012), biomedical devices, and bulk scale composites for structural applications. They are also used as PCR enhancers (Khaliq et al., 2012).

2.3.2 Metallic Nanoparticles

Metallic nanoparticles are widely popular over the past few decades. The discovery of nanoparticles has brought about a great revolution in science and technology. Extensive research has been done on these nanoparticles. Nanoparticles have fascinated researchers and engineers alike over the past decade due to their vast potential, fabulous properties, and the ease of making/manufacture them in vast quantities. The electrical, optical, and other functional properties can be easily manipulated precisely by

manipulating their chemical properties at the nanoscale. These nanoparticles have a huge potential in various application areas, starting from biological applications to industries such as the aerospace and automotive industry.

Metallic nanoparticles are those nanoparticles that are synthesized from metals and their oxides. Few examples of metallic nanoparticles include iron, gold, silver, platinum, etc. metallic nanoparticles are applied in a wide range of applications like electronic storage (Kang et al., 1996), targeted drug delivery (Rudge et al., 2001), cancer therapy (Sokolov et al., 2009) and many more. These nanoparticles are classified into metallic and metallic oxides. A few of them are discussed in brief in the following texts.

2.3.2.1 Gold

Gold nanoparticles or Nanogold or colloids of gold is a suspension of nano-sized particles of gold of about 1 to 100 nm in size. The color of the colloids varies from intense red color to dirty yellowish (Tong et al., 2009). Gold nanoparticles are of particular interest to researchers due to their high thermal conductivity enhancements (Das et al., 2006). They are very consistent and are biocompatible with biological applications. Hence the gold nanoparticles are used in various medical applications like targeted drug delivery system (Han et al., 2007), tumor detection (Qian et al., 2008), gene-therapy (Giljohann et al., 2009), Photothermal agents for ablation components for cancer, and other targets (Niidome et al., 2006), Radiotherapy dose enhancer (McMahon et al., 2011), detection of toxic gas, as a biosensor to enhance sensitivity, stability, and selectivity (Zhang et al., 2014), and other applications like signal amplification (Wang et al., 2002) and as a highly sensitive electrochemical biosensor (Gole et al., 2001).

2.3.2.2 Silver

Silver is one of the noble metals used in various applications apart from being used in jewelry. It plays a vital role in nanoscience and nanotechnology. The nanoparticles of silver with sizes ranging between 1 and 100 nm are primarily available in diamond, octagonal, and thin sheet-shaped with an extensive surface area (Graf et al., 2003). Silver nanoparticles have some unique and peculiar properties like high thermal and electrical conductivity. Their unique chemical properties make them highly desired components in many fields like household appliances, industrial and healthcare applications. They are also used as coatings in some medical devices. Silver nanoparticles are used in cancer research and targeted drug delivery (Chernousova and Epple, 2013).

2.3.2.3 Platinum

Platinum is another noble metal that is highly scarce in terms of earth deposits. The platinum nanoparticles come in sizes varying from 2 to 100 nm. They are usually brownish-red or black in colloids or liquid suspensions, just like other noble metal nanoparticles. Platinum nanoparticles come in spherical, cubical, and rod-shaped (Harris, 1986). Platinum nanoparticles have unique chemical and physical properties; hence they are widely used for many research applications like optics, enzyme immobilization, and electronics. They are also used as hybrids and other nanoparticles in the application of newer technologies like hydrogen fuel cells and methanol fuel cells (Chen and Holt-Hindle, 2010). They are used in many biological applications like drug delivery (Pelka et al., 2009) and Genotoxicity (Elder et al., 2007).

2.3.2.4 Rhenium

Rhenium is a scarce metal obtained mainly as a by-product during the extraction and refining of molybdenum and copper ores. Rhenium nanoparticles usually are sized between 20 to 100nm. They are spherical shaped and are brown. They are from the group 7 metal transition ores. They have the second-highest melting point (Haynes et al., 2011). So, they are very high-temperature resistant material. It has a meager standard reduction potential. All these unique properties make rhenium very desirable to many applications, like manufacturing jet engine components and improving engine efficiency. Rhenium nanoparticles are also used in medical applications like targeted magnetic radiotherapy and silica coating (Cao et al., 2004). When used as a catalyst, Re nanoparticles are resistant to carbon monoxide and Sulphur poisoning. Hence, they are widely used as catalytic converters in automotive exhaust systems.

2.3.2.5 Ruthenium

Ruthenium is another rare transitional metal from the platinum group. The nanoparticles of ruthenium are usually spherical-shaped brown-colored particles. The nanoparticles are usually sized from 2 to 100nm. Ruthenium is a chemically inert metal that hardly reacts with any chemicals. Ruthenium has excellent electrical conductivity and high specific capacitance; hence they are used to make super-capacitors. Ruthenium is widely used in medical fields by manipulating or hybridizing with graphene or other noble metallic nanoparticles to manufacture anti-cancer agents (Bergamo and Sava, 2011), anti-malarial, and immuno-suppressive drugs (Allardyce and Dyson, 2001).

2.3.2.6 Palladium

Palladium is a rare earth metal belonging to the platinum group of metals with the lowest melting point, less dense, and has similar chemical properties as other platinum group

metals. Palladium nanoparticles are available in sizes from 2 to 100 nm. They have unique structure versatility (Kim and Hyeon, 2013), and hence they are used in several applications like biocatalysts, anti-microbial, anti-viral, anti-cancer (Mittal et al., 2013). When hybridized with reduced glutathione, palladium nanoparticles showed prolonged blood circulation, accumulation in tumors, and no apparent toxicity during clinical trials on mice (Tang et al., 2014). Hence, they have the potential for the treatment of cancer cells.

2.3.3 Metallic Oxide Nanoparticles

2.3.3.1 Aluminum Oxides

Aluminum oxide nanoparticles are almost spherical and are about 2 to 10 nm. They have a very high specific surface area. They have high hardness and excellent dimensional stability. When they are water dispersed, they improve the density of ceramics. The aluminum oxide nanoparticles have excellent thermal conductivity and are also resistant to corrosion. The water-dispersed aluminum oxide nanoparticles also improve the thermal fatigue resistance, wear resistance in polymers while improving fracture toughness. Hence these aluminum oxide nanoparticles are used in rubber, ceramic, and plastic industries. The aluminum oxide nanoparticles are also used in medical industries and bio applications as antimicrobial agents, drug delivery, and diagnosing agents for diseases (Mukherjee et al., 2011). They are also used as catalysts in some chemical reactions.

2.3.3.2 Titanium Dioxide

Titanium dioxide is a naturally occurring oxide of titanium, which is also called titania. The titanium oxide nanoparticles are usually about 2 to 100nm, which is available in many shapes, including spherical and tube-shaped structures. Titanium dioxide is one

of the widely used materials in many applications. They have some unique properties, including biocompatibility, resisting the effects of the body fluids in bio-applications. They have corrosion resistance, tensile strength, and flexibility (Roy et al., 2011). They have high durability, and hence they are also used as implant materials (Mihov and Katerska, 2010). They are inert and are biologically stable. Titanium dioxide nanoparticles are nowadays widely used to enhance the specificity of PCR (Khaliq et al., 2010). They are used as a UV-resistant material and also in the manufacture of cosmetic products.

2.3.3.3 Silicon Dioxides

Silicon dioxide or silica are oxides of silicon, and it is a principal constituent of sand. Since it is very readily available, it is used in a wide range of applications. The nanoparticles of silicon dioxide are widely used as an additive for rubber and plastics, as a strengthening agent for concrete. These nanoparticles are the lower conductor of heat and electricity; hence they are widely used as an insulating material (Talib et al., 2015). Since the nanoparticles of silicon dioxides are nontoxic, they are also used in many biomedical applications such as drug delivery and theranostics (Park et al., 2015a). Silicon nanoparticles are also used in the reconstruction of bone defects (Xu et al., 2014).

2.4 THERMAL CONDUCTIVITY OF NANOFLUIDS

Removal of excess heat from engines, power-plant equipment, manufacturing processes, electronics, and transmission systems has been challenging. Water, ethylene glycol, and mineral oils are commonly used heat transfer fluids. These fluids have lower thermal conductivity, thus, limiting their performance and applications.

Thermal conductivity in such fluids can be enhanced by adding or dispersing solid metallic particles, a concept first demonstrated by Maxwell in 1881 (Chrystal, 1882). He dispersed micro-sized particles in liquid to study the thermal conductivity enhancement, which gave him limited success. It was noticed that the dispersed micro-size particles settled down after some time due to their higher density. Recent scientific advancements opened up the opportunity to produce nano-sized particles, which can be suspended for a longer time in the fluids due to the low density (Choi, 1995). The lesser the particle size, the higher the surface area it will have, thus, making the solid-liquid interaction more effective (Rasheed et al., 2016). Fluids suspended with nanoparticles are also popularly known as nanofluids, with higher thermal conductivity, which is desired for efficient thermal energy transfer in most systems.

Studies have shown that the coefficient of thermal conductivity increases considerably in the nanofluids, even with a meager amount of nanoparticle concentration compared to the standard base fluids (Wen and Ding, 2004). Nanofluids could replace the existing coolants in several sectors like energy, electronics, transportation, and manufacturing. The enhancement of the heat transfer in the nanofluids is greatly influenced by many factors like the concentration of the nanoparticles, particle sizes, particle materials, particle shapes, and types of base fluids. It is always desirable to have higher stability of nanoparticles in the standard base fluid to achieve a lasting thermal conductivity enhancement.

A few nanofluids show a more significant enhancement in the thermal conductivity performance despite containing a minimal concentration of nanoparticles ($\phi < 1\%$). The thermal conductivity enhancements differ based on the type of nanofluids. Generally, the thermal conductivity is higher in nanoparticles, which are metallic-based compared to non-metallic and metallic oxide-based nanoparticles. Several studies were

done on single-material nanoparticle-based nanofluids in the past few decades, and the results are well-established. Modern-day applications require a combination of many characteristics such as high thermal conductivity, together with stable rheological properties, longer stability time, and homogeneity. These characteristics can be achieved by hybridizing the single-material nanoparticles with other nanoparticles. Although different hybrids have emerged in the past decade, new nanoparticle combinations continue to evolve due to advancements in synthesis routes. These hybrid nanoparticles offer many intriguing properties along with considerably higher thermal conductivity compared to single material nanoparticles. This includes the extended stability of the suspended particles in the fluid (Choi et al., 2001).

The hybrid nanoparticle combination could comprise two or more nanoparticle types. The compositions of the binary-hybrid and ternary-hybrid nanoparticles (THNp) are selected according to the desired outcome of the application requirements. The goal of synthesizing a hybrid nanoparticle is to accomplish improved and better thermo-physical, hydrodynamic, and heat transfer properties by trading off the advantages and disadvantages compared to the single-material nanoparticle. It can be attributed to a better thermal network of the nanoparticles and other general factors such as good aspect ratio and synergistic effect. An appropriate hybridization can achieve a better heat transfer characteristic, even at a lower concentration of nanoparticles (Esfe et al., 2017).

The hybrid nanoparticles or a nanocomposite has many advantages such as high thermal conductivity, better stability in base fluids, large surface area, crystallinity, and higher zeta potential. Preliminary studies to investigate carbon-based hybrid nanoparticles have been done till now. Graphene is an atom-thick sheet of sp² carbon atoms arranged in a hexagonal pattern attached to the carbon atoms present in a

honeycomb crystal mesh structure. The graphene oxide and the reduced-graphene oxide are functional groups of graphene.

Graphene is hydrophobic, which does not dissolve easily in water and other water-based solvents. It can be made hydrophilic by attaching suitable functional groups to form Graphene oxide (Du and Cheng, 2012). Graphene-oxide is then heavily oxygenated along with other functional groups that contain oxygen, such as epoxide hydroxyl, carbonyl, and carboxyl groups. The interfacial interaction of the polar polymer matrices is higher due to the functional groups. Reduced graphene oxide (rGO) nevertheless has a lesser amount of other functional groups that contain oxygen. Reduced graphene-oxide are produced by chemical and thermal reduction method. Hydrazine hydrate and ascorbic acid are usually preferred reducing agents used in the preparation of the rGO. Different reduction agents will give different carbon to oxygen ratios and chemical composition (Velasco-Soto et al., 2015).

Various research findings were reported that hybrid nanoparticles' heat transfer characteristics are more significant compared to single nanoparticles. Silver nanoparticles are another type of metallic nanoparticle that has been widely used. The linear and nonlinear optical properties of silver nanoparticles are affected by many factors such as size, shape, inter-particle spacing, environment, spectral, and geometrical properties (Bruzzone et al., 2005). Silver nanoparticles are used in many fields, including the detection of heavy metals in water and as coatings for glass slides. In developing analytical sensors, silver nanoparticles are used as excellent conductors of heat. They are used as thermal conductivity enhancers in various fluid mediums such as ethylene glycol, water, and oils.

Titanium dioxide (TiO₂) is another nanoparticle used in the preparation of various nano-fluidic applications. They are mainly used because of their stability

without forming sedimentation for more extended periods (Thamilselvi and Radha, 2017). TiO_2 is a transitional metal oxide that is one of the most widely used nanoparticles in numerous applications. Many methods can be used to synthesize TiO_2 . It is widely used as a thermal conductivity enhancer in various applications like refrigerant (Peng et al., 2011), pool boiling, conduction enhancers, convective heat transfer, PCR enhancements (Khaliq et al., 2010), as well as antifogging coatings due to its light-reflective property. Another advantage is its adaptability to high-pressure applications with varying concentrations, which is the desired property (Naphon and Thongjing, 2014).

2.5 RHEOLOGICAL INVESTIGATIONS OF NANOFLUIDS

Nanofluids are colloidal suspensions of nanoparticles in a base fluid. The nanoparticles are generally dispersed in base fluids such as water, EG, oils, and synthetic fluids such as liquid paraffin oil and polyesters. Metallic nanoparticles include gold, silver, titanium, aluminum, iron oxide, etc. The non-metallic nanoparticles in use are predominantly carbon-based nanoparticles such as diamonds, graphene, CNT, fullerenes, etc. some other non-carbon, non-metallic nanoparticles include sodium, ceramic, carbides, etc. (Chakraborty and Panigrahi, 2020)

Generally, the rheological behavior of nanofluids is of prodigious significance in a wide variety of applications (Sidik et al., 2016). There is a proportional relationship between various factors such as viscosity, shear rates, pumping power, pressure drop, and convective heat transfer in the fluids. The change in viscosity is mainly due to two common factors: a change in temperature and an increase/decrease of nanoparticle concentration in the fluid. Other factors increase the viscosity, such as the relationship

between k and viscosity of nanofluids. Many studies have also shown that the viscosity is also influenced by the k factor (Tsai et al., 2008).

Nanofluids are emerging and essential fluids in many applications today in all major industrial and biomedical applications, where rapid heating and cooling are vital. Since the nanofluids enhance the heat transfer or the thermal conductivity of the base fluids, they are used in a wide range of applications of heat transfer such as engines, power plants, pharmaceutical processes, PCR, and vehicle thermal management, to name a few (Yang et al., 2020). Many industries require fluids that have higher thermal conductivity and excellent rheological properties in a working fluid.

These enhanced heat transfer fluids will reduce time and energy consumption. Rheology is the study of viscosity, which is the fluid's resistance to deformation or a frictional force against the flow. It is a fundamental tool to characterize the material and fluid properties. Rheology is the correlation of stress and strains, which can be used to study and understand the fundamental behavior of fluids. They are also crucial in designing models of viscosity. The rheological study will help us to interpret and measure the mechanical and flow behavior of the fluids. It is also important to note that the rheological analysis of fluids will help to investigate the structural evolution in a solid-liquid dispersion. Dispersing nanoparticles in the base fluids enhances the thermal conductivity and affects the fluids' rheological behavior.

The fluids may tend to become either Newtonian or non-Newtonian. The addition of nanoparticles to fluid will change the property of the fluids drastically. Hence it is essential to study the rheological properties of the nanofluids to determine their characteristics, behavior, and optimal performance for the desired application. The rheological study is also essential for many other factors, like calculating the pumping power required to pump the nanofluids. The addition of solid nano-sized particles to

standard base fluids can also cause a pressure drop in the system. An example is the shear thinning of nanofluids due to various shapes of the particles, which can lead to agglomeration of particles in the fluids, thereby affecting the performance. Considering all these factors, it is highly essential to study the effects of dispersing the nanoparticles in the fluids to the fluids structure and its rheological behavior under various stress and temperature conditions (Babar et al., 2019).

Various other factors affect the rheological properties like the pH of the nanofluid, nanoparticle volume fraction, the shearing rate of the particle with the liquid layer, the selection of the base fluid, the nanoparticle size, and shape. The stability of the nanoparticle in the fluid and its duration without sedimentation also affects the viscosity of the nanofluids. While considering these factors, it is essential to study the rheological properties of nanofluids. Viscosity plays a significant role in determining the characteristics of the fluid, either Newtonian or non-Newtonian. Nanofluids, which contain more than one type of single material nanoparticles, are called hybrid nanofluids.

Hybrid nanofluids are the hot area of research widely investigated by many researchers in the current decade. The hybrid nanoparticles are a combination of two or more nanoparticles synthesized or decorated on top of another. Their dispersion into the base fluids is known as hybrid nanofluids. They have the unique characteristic of enhanced thermal conductivity and tailor-made rheological properties, making them favorable to numerous applications. These characteristics of nanofluids attract numerous researchers to investigate the applications of hybrid nanofluids in various fields of application (Sidik et al., 2017).

Few other aspects of studying a hybrid nanoparticle are the ability of the particles in the nano-scale level to adapt and respond uniquely to the changing

environmental conditions. Hence, most researchers are interested in analyzing the hybrid nanoparticle at their structural level and their reactions with varying temperature, chemical, and biological conditions. The hybrid nanoparticles can be metallic types like a silver-gold hybrid (Bhatia and Banerjee, 2020) or maybe a combination of carbon-metallic nanoparticles like silver and graphene (Xu et al., 2011) name a few. Each of these hybrid nanoparticles exhibits different characteristics and behavior.

Many studies and reviews have reported the nanofluid's preparation methods (Devendiran and Amirtham, 2016), characterization (Arshad et al., 2019), thermal conductivity enhancements (Azmi et al., 2016), thermal conductivity models (Aybar et al., 2015), mechanisms of thermal conductivity (Pinto and Fiorelli, 2016), the effect of particle size and shape on the thermal conductivity (Esfahani et al., 2016), rheological effects on the addition of nanoparticles (Babar et al., 2019), rheological behavior (Sharma et al., 2016), viscosity (Murshed and Estellé, 2017), viscosity models (Meyer et al., 2016), the effect of particle size and shape on the viscosity (Koca et al., 2018) and stability (Chakraborty and Panigrahi, 2020).

Researchers have further studied the effects of the nanoparticles and also on the type of nanoparticles used like graphene (Rasheed et al., 2016), gold (Das et al., 2011), aluminum (Sridhara and Satapathy, 2011), hybrid nanofluids (Babar et al., 2019) and other nanoparticles based nanofluids and its applications (Babar and Ali, 2019). Few studies have reported an increase in thermal conductivity, which has enhanced the outcomes of their applications. One study has proven to accelerate the thermal conduction in PCR reaction and lead to a substantial reduction in the number of cycles employed using graphene nanoflakes (Khaliq R et al., 2012) and titanium nanoparticles (Khaliq et al., 2010).

Few other studies have reported the applications yielding better results in areas like medical (Mekheimer et al., 2018), nuclear reactors (Sharma et al., 2017), oil recovery (Zakaria et al., 2015), etc. Studies based on hybrid nanofluids have gain momentum only very recently (Babar and Ali, 2019). Bi-hybrid nanoparticles have been used in various studies like CuO-MWCNT (Esfe et al., 2018), Al₂O₃- TiO₂ (Kumar and Sarkar, 2019), SiO₂-MWCNT (Amini et al., 2019), MWCNT-GNPs (Hussien et al., 2017), to name a few. But a minimal study has been done to date on the rheological behavior of trihybrid/ternary hybrid nanoparticles with various levels of concentrations along with their sweep characteristics such as amplitude sweep and frequency sweep-based storage and loss moduli.

Few reports have also mentioned that the viscosity is also dependant on the particle size of the nanomaterials, with a difference of over 5% (Hamzah et al., 2017). The viscosity of the nanofluids varies with the type of material behavior and is influenced by either metallic or non-metallic nanoparticles. Another important aspect is the shape of the nanoparticle (Park and Kim, 2014). Further, very few studies have reported the rheological effects of dispersing minute quantities or low concentration of nanoparticles on the base fluids (<1% wt), which can be classified as dilute (Chen et al., 2007). The other aspect absent in the literature is the deficiency of proper rheological data through experiments for a tri hybrid or ternary hybrid nanoparticles dispersed into DI water.

2.6 CRITICAL ANALYSIS OF LITERATURE

The literature on nanoparticle-based PCR was extensively studied and found that the nanomaterials possess unique physical and chemical properties. During the extensive search, it was found that more than 90% of the existing studies addresses the problem

from a biological perspective, and very few studies have addressed the issue in a mechanical/thermal enhancement perspective, which is through improving the thermal conductivity of the PCR reagent and the reaction mixture inside the PCR tube. Nanomaterials enhance the efficiency of PCR both in terms of sensitivity and specificity. The effects of nanomaterials on PCR are due to the interaction between the surface of nanoparticles and PCR components. Hence it was agreed upon to choose the nanoparticles which have all the characteristics necessary to not only improve/enhance the PCR but also to cater for reduction of the time taken, reduction of the number of cycles of the PCR, improving the efficiency of the PCR product, improve the sensitivity and specificity of PCR to amplify low expressing genes.

Very few hybrid nanomaterials have been used, and new materials are being explored with surface modification effects known to play a vital role in achieving enhanced PCR efficiency. Three incredibly superior nanoparticles like graphene oxide, titanium oxide, and silver were selected considering all these factors. The selection of the three nanoparticles to synthesize a ternary hybrid nanoparticle was based on the consideration of their high thermal conductivity, their hydrophilic nature, solubility in water samples, chemically inert, cost-effective, high mechanical strength, thermal diffusivity, and its easy availability, and the ability to synthesize.

In this study, graphene oxide and reduced graphene oxide were decorated with two other metallic nanoparticles: titanium dioxide and silver. Both silver and titanium dioxide nanoparticles are well established in the literature (Sharma et al., 2016). Graphene is a unique material famous for its exceptional properties (Aravind and Ramaprabhu, 2013), particularly when it comes to its high thermal conductivity, as well as its specific surface area. (Bumataria et al., 2019). And also, it was noted that the effect of nanoparticles on DNA denaturation had been largely ignored in the literature.

The Impact of nanoparticles on DNA sequencing is never explored, and also, the numerical simulation of nanoparticle augmented heat transfer in PCR has not been reported ever for hybrid nanoparticles.

CHAPTER THREE

RESEARCH METHODOLOGY

3.1 OVERVIEW

The overall aim of this study is to synthesize novel graphene-based ternary hybrid nanoparticles (GO-TiO₂-Ag and rGO-TiO₂-Ag) and disperse them in double distilled water at different concentrations (5x10⁻¹, 5x10⁻², 5x10⁻³, 5x10⁻⁴, and 5x10⁻⁵wt %). The ternary hybrid nanofluids will be used in the PCR to enhance the PCR yield, reducing the reaction time and the number of cycles without compromising the PCR output. The detailed methodology of the current work has been shown in Figure 3.1.

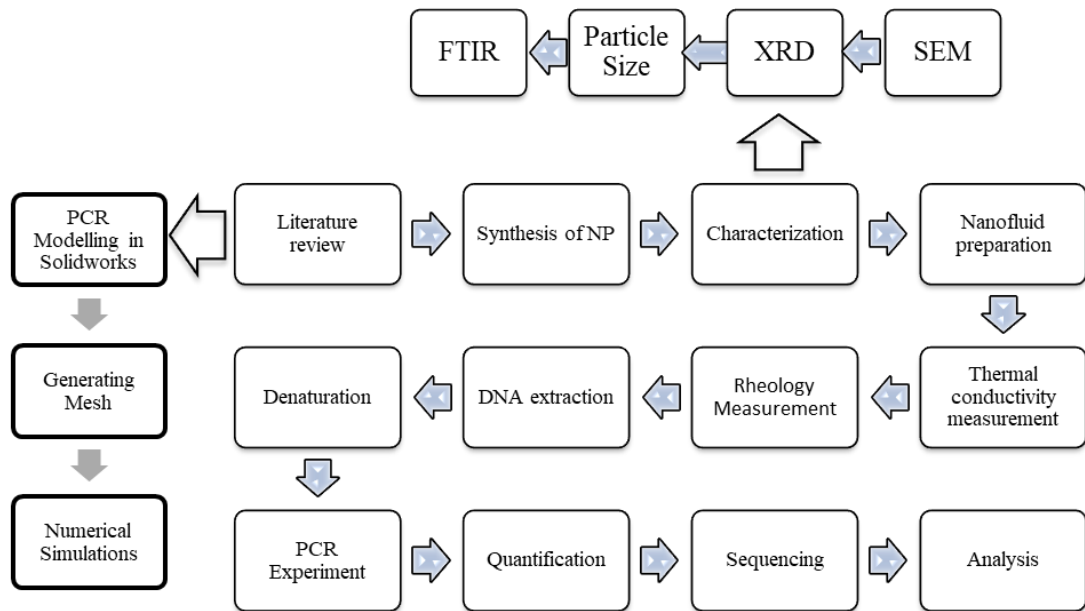


Figure 3.1 Flow chart represents an overview of Research Methodology

3.1.1 Preparation of GO-TiO₂-Ag and rGO-TiO₂-Ag nanocomposites

The selected nanoparticles are then synthesized/decorated onto another to form a hybrid nanoparticle. In this study, graphene oxide and reduced graphene oxide are decorated with titanium oxide and silver to form a novel ternary hybrid nanoparticle (GO-TiO₂-

Ag and rGO-TiO₂-Ag). Both GO-TiO₂-Ag and the rGO-TiO₂-Ag nanocomposite were synthesized using a hydrothermal method (Perera et al., 2012). Graphene oxide (GO) of about 0.25g was suspended in 250 mL deionized water using an ultrasonic stirring treatment for about two hours. After that, 10 mL of titanium isopropoxide (TTIP) was dissolved in 10 mL isopropyl alcohol, and the combination was added dropwise into the 50 mL of GO suspension. Then, 10ml of 0.2M AgNO₃ was added dropwise into the GO-TTIP combination and then stirred for 1 hour approximately. After stirring for about an hour, the pH was adjusted to 1.1, and the stirring continued for another two hours to get a uniform solution. The solution was then transferred and heated at 160 °C for 24 hours in a Teflon-lined stainless-steel autoclave. After the hydrothermal treatment, the resulting product was first strained and washed using ethanol.

Further washing was done using DI water to remove unreacted ions and possible remnants in the nanoparticle. The obtained GO-TiO₂-Ag nanocomposite was dried overnight at 80°C. The same procedure was repeated to synthesize rGO-TiO₂-Ag. The difference is that 2 mL of hydrazine and ammonia were added to aid and adjust the pH to neutral. Hydrazine was used to remove the oxygen molecules from graphene oxide sheets and their functional groups. Different hybrid nanofluid samples were prepared by blending different ratios of nanomaterials in DI water. The homogeneous formulation was obtained after sonication and stirring using a bath-type sonicator (JAC Sonicator 1505, 4 kHz) for about 4 hours. Physical monitoring of samples was done to examine the settling of nanoparticles.

3.2 MATERIAL CHARACTERIZATION

3.2.1 Scanning Electron Microscopy (SEM)

A field emission scanning electron microscopy (FE-SEM) at 30 kV was used to measure the surface topography. For the GO-TiO₂-Ag ternary hybrid nanoparticle, crumpled and rippled GO sheets were decorated by two types of nanoparticles, the TiO₂ and the Ag. The quality of SEM depends on the nanoparticle sample preparation. The tools used to prepare the nanoparticles SEM samples were clean and made sure to be stored in a dry place where the air quality is preferred to be of high-efficiency particulate air (HEPA) filtered air. The substrate is be filled with a smaller number of nanoparticles so that uniform analytical samples are prepared. The sample substrate is then placed on a chamber where the high beam of electrons will be focussed. The SEM is adjusted depending on the position of the stage. The middle of the substrate is placed directly under the beam by adjusting the stage in the x-and y-direction. This will define the zero-point coordinate for the sample. The resolution was adjusted based on the clarity of the images of the nanoparticles to be obtained.

3.2.2 Raman Spectroscopy

He-Ne laser (model RENISHAW in via Raman Microscope) was used to measure the Laser Raman spectroscopy (LRS) at room temperature in the 200-3000 cm⁻¹ region through a UV excitation at 325 nm. The light beam was focussed on a cylindrical glass vial containing the nanoparticles' samples. The Raman-scattered radiations were collected by oblique geometry on a large aperture convex lens focussed on an optical fiber. A holographic notch filter was used at the front end of the optical fiber, with the desired Raman signals passing through. The measurements were performed in a dark room to avoid desensitization of the sensitive detection system by ambient light.

3.2.3 Fourier-Transform Infrared Spectroscopy (FTIR)

Bruker IFS66/S infrared spectrometer was used in recording Fourier transform infrared spectroscopy (FT-IR) spectra. FTIR spectrometer comprises a source, sample cell, detector, amplifier, A/D converter, and computer. The radiation from the infrared light source reaches the detector after it passes through the interferometer. This light signal is amplified and converted to a digital signal by the A/D converter and amplifier. The amplifier amplifies the signal and feeds them to the computer, where the signal is quantified, and the Fourier transform is calculated. The scanning was completed with a scan number of 16 and a resolution of $\pm 4 \text{ cm}^{-1}$ in the range of $4000\text{-}400 \text{ cm}^{-1}$. This will give the required recorded spectra.

3.2.4 X-Ray Powder Diffraction (XRD)

The crystallographic structure of the synthesized GO-TiO₂-Ag and rGO-TiO₂-Ag nanocomposites were gauged with XRD. The diffraction occurs when a periodic array of long-range scatters x-ray focuses on a nanomaterial, producing constructive interference at specific angles. This scattering of x-ray from the atoms produces a diffraction pattern containing information about the atomic pattern of the nanoparticles. The samples are deposited on a flat plate with a smooth surface, and it was ensured that the nanoparticles are densely packed in them. The X-ray is then beamed onto the samples, and electrons in the atoms make the light scattered. The diffraction is measured.

3.2.5 Particle Size Distribution

The particle-size distribution of the THNp in the nanofluids was carried out using a dynamic light scattering method. The measurements were performed by using Anton Paar Particle Size Analysers PSA 990. The scattering ranged from $0.2 \mu\text{m}$ to $500 \mu\text{m}$,

and it has an accuracy of <3% with less than a minute measuring time. The ternary-hybrid nanofluids were filled in the vial and placed in the analyzer.

3.3 SYNTHESIS OF TERNARY HYBRID NANOFLUIDS

The challenge in the application of the nanofluid is its preparation and long-term stability. To achieve an even dispersion and obtain the desired characteristics require the nanofluid to be stable without sedimentation. The ternary-hybrid nanofluids were prepared by dispersing the two types of graphene-based hybrid nanoparticles (GO-TiO₂-Ag and rGO-TiO₂-Ag) in the base fluid (molecular biology-grade sterile/DI water). An electronic balance [Sartorius Entris® Analytical balance] was used to measure the nanoparticles before the dispersion into the base fluid. A stock solution was prepared with 50ml of deionized water and 2.5mg of THNp, which constitutes a concentration of 0.05 wt%. Ultrasonic probe sonication was done on this nanofluid for about 10 minutes. The nanofluids were sonicated using a bath-sonicator for 4 hours until the nanoparticles were dissolved entirely in the deionized water to form a homogenous mixture without any sedimentation. The stock solution is then serially diluted to about five levels of dilution (5×10^{-1} , 5×10^{-2} , 5×10^{-3} , 5×10^{-4} , and 5×10^{-5} wt %). These are known as ternary hybrid nanofluids. The schematic of the preparation of the ternary hybrid nanofluids is as presented in Figure 3.2.

3.3.1 Zeta Potential

Dispersion stability of the nanofluids and Surface charge at the solid-liquid interface were measured in terms of Zeta potential. The surface charge of the nanoparticles influences their physical state in the liquids. The zeta potential of the THNp based nanofluids was measured using the Anton Paar Electrokinetic Analyzer SurPASS 3.

The Electrostatic repulsion forces of the suspended nanoparticles and the Zeta potential are directly related. The prepared nanofluids were transferred to a measuring cuvette. Then they are placed into the measuring chamber. UV-VIS light beamed to the sample chamber, where the absorption rate is measured. The measured data is then analyzed.

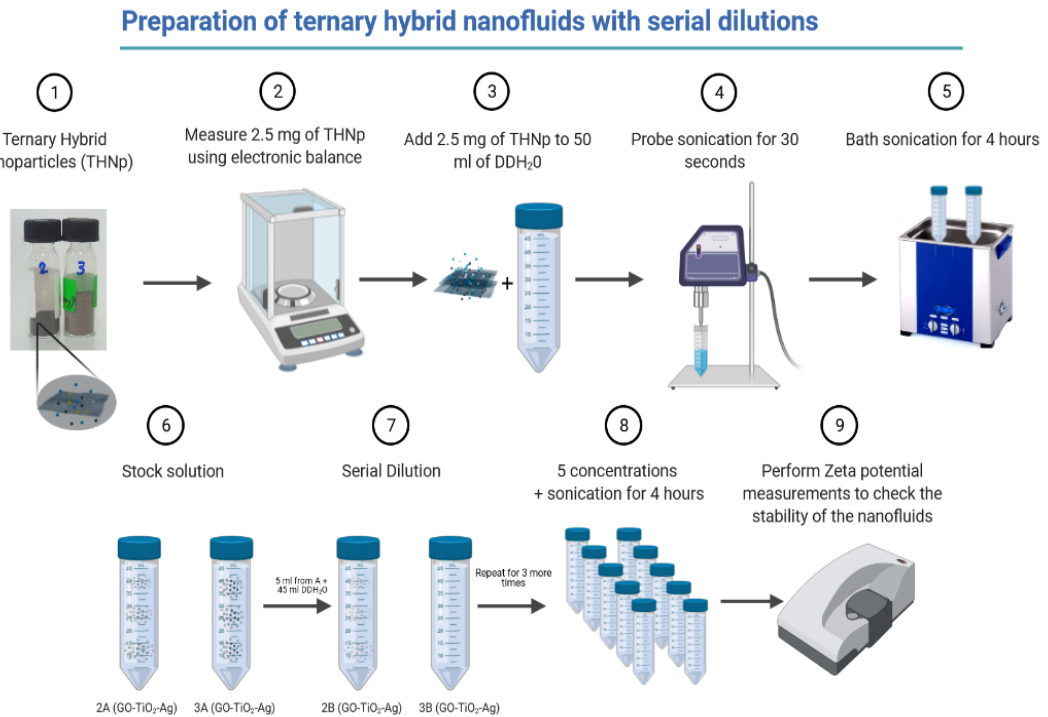


Figure 3.2 Schematic of ternary hybrid nanofluids preparation

3.4 THERMAL CONDUCTIVITY MEASUREMENTS

Thermal conductivity measurements on the ternary hybrid nanofluids were carried out on all the samples using a handheld thermal analyzer named KD2 pro (Decagon Devices). This thermal analyzer has a transient line heat source method. The heat-flow equation with an exponential integral solution is attached to the device for both single and dual-needle-type sensors. The device calculates the thermal conductivity and specific heat using a mathematical non-linear least-squares-inverse procedure for differential equations solutions.

The samples were immersed in a thermostat bath in equilibrium to minimize free convection. The thermal analyzer was kept in an isolated place to avoid any disturbances and vibrations from other adjacent equipment, inducing vibrations during the measurements. The transient line source was a single needle (1.3mm diameter and 60mm length) used for the thermal conductivity measurements. The sensor needle was calibrated inside the standard liquid (DI water and glycerine, Thermal conductivity = 0.633 and 0.285 W/m-K respectively. at ambient temperature) provided by the equipment manufacturer for accuracy of the measuring instrument. Measurements were taken at various temperatures starting at 25°C with 5°C increments till 50°C. Non-linear least squares were done for exponential integral functions for curve fitting of the measured values. The measurements were iterated about four times for each temperature value to give us a well-averaged value and eliminate uncertainty within $\pm 5\%$.

3.5 DYNAMIC VISCOSITY AND RHEOLOGICAL MEASUREMENTS

Dynamic viscosity measurements were done using Anton Paar's (GmbH, Austria) MCR302 modular compact rheometer. This rheometer uses a C-PTD200 gauging cell, and the temperature of the measurement sample is maintained with the Peltier system 1-100 1/s. CC45 DIN spindle was used in measuring viscosity, shear rate, and shear stress at temperatures ranging from 25°C to 50°C with an increment of 5°C. The ternary hybrid nanofluids were placed in the rheometer's sample chamber. The double-gap system spindle was immersed and rotated against the ternary hybrid nanofluid against the viscous drag. The drag force was measured by the deflection of the calibrated spring. The viscosity shear strain and shear stress were measured at room temperature, and the equipment's data logger recorded the data. The accuracy of the rheometer is guaranteed

to be within $\pm 1\%$ of the full-scale range. The reproducibility is within ± 2 for the spindle speed combination. The viscous effect was developed in the ternary hybrid nanofluids against the spindle rotation. Viscosities of the ternary hybrid nanofluids were measured at various temperatures ranging from 25°C to 50°C with 5°C increments.

3.6 MOLECULAR TECHNIQUE

3.6.1 Gene Selection

pCDNA3-GFP was procured from Martine Roussel (Addgene # 74165) (Vo et al., 2016).

3.6.2 DNA Isolation

This procedure was carried out at Kulliyyah of Pharmacy, IIUM, and the cultured plasmid sample was prepared. The extraction was done using a PV92 PCR Informatics (1662100EDU–Bio-Rad Laboratories, Hercules, CA) extraction kit. Briefly, pCDNA3-GFP was first propagated from their agar stab upon receiving in *Escherichia coli* (*E. coli*) DH5 α by first streaking them in LB (Luria-Bertani) Agar (35 mg/mL of distilled water) containing 100 $\mu\text{g/mL}$ of ampicillin and incubated overnight at 37°C , inverted. LB Broth was prepared by dissolving LB Broth powder 20 g in 1 L of distilled water. A single colony was added into 20mL of the LB Broth medium. This was incubated in a shaker at 37°C , 180 rpm for 8 hours. Following culture in LB broth, the plasmids were extracted and purified using a Pure Yelidminiprep plasmid kit (Promega, Madison, USA) according to the manufacturer's instructions. The plasmid DNA concentration was determined using Quantus™ Fluorometer (Promega, Madison, USA), and they were adjusted to 100 ng/ μl in nuclease-free water and stored at 4°C until used in PCR.

3.6.3 PCR Protocol and Amplicons Quantification

The term amplicon refers to a single strand of DNA. The PCR was carried out to amplify a target DNA segment in EGFP plasmid using gene-specific primers, forward primer (5'-CCCACTGCTTACTGGCTTATC-3'), EGFP reverse primer (5'-CCATGTGATCGCGCTTCT-3'). Amplification was performed using the PCR master mix (Bio-Rad, California, USA). The typical PCR reaction mixture contained the following final concentrations: 100 ng of template DNA was mixed with 20 μ L of PCR master mix, one μ L each forward/reverse primer, and nuclease-free water to a final volume of 50 μ L. For nanoparticle samples, nuclease-free water was replaced by different concentrations (10^{-1} , 10^{-2} , 10^{-3} , and 10^{-4}) of nanoparticles GO-TiO₂-Ag and rGO-TiO₂-Ag. The PCR was run on Bio-Rad PCR thermocycler (California, USA) using the following thermal condition: denaturation step for 10 min at 95°C; followed by 35 cycles of (95°C denaturing step for 30 S; 55°C annealing step for 30 S and 72°C extension step for 30 S) then a final step of 72 °C for 7 min and finally held at 4 °C. Then an equal volume of the amplification product was subjected to 1% w/v agarose gel and run for 60 min at 120 V.

The amplified PCR products were quantified by measuring band intensities using ImageJ software (NIH, Bethesda, MD, USA). The band intensities were calculated to determine the effect of nanoparticles on PCR products, and they were expressed as relative fold intensity compared to a positive control (sample without nanoparticles). PCR products were sequenced using the Sanger sequencing technique in an ABI sequencer at Apical Scientific SDN BHD, Malaysia. The comprehensive PCR process is as presented in figure 3.3

- Supplementary material u might need:
- Target gene: T2 sequence in EGFP

- Forward primer: sequence, Tm: 5'-CCCACTGCTTACTGGCTTATC-3', 55.5 °C
- Reverse primer: sequence, Tm: 5'- CCATGTGATCGCGCTTCT -3', 54.7 °C
- Amplicon size: 801 PB

Table 3.1 PCR mix and thermal cycling conditions for four sets of GO-TiO₂-Ag and rGO-TiO₂-Ag nanomaterial-assisted PCR (nanoPCR) for 35 cycles

PCR Mix Components	PCR Mix 1	PCR Mix 2	PCR Mix 3	PCR Mix 4	Thermal Cycling conditions for PCR		
	(with GO-TiO ₂ -Ag nanomaterial solution)	(without GO-TiO ₂ -Ag nanomaterial solution)	(with rGO-TiO ₂ -Ag nanomaterial solution)	(without rGO-TiO ₂ -Ag nanomaterial solution)			
PCR master mix (1st base)	20 µL	20 µL	20 µL	20 µL	95 °C	10 min	1 cycle
Primer (forward/reverse)	2 µL	2 µL	2 µL	2 µL	95 °C	30 S	35 cycle
					60 °C	45 S	
					72 °C	30 S	
ddH ₂ O	NA	27 µL	NA	27 µL	72 °C	7 min	1 cycle
GO-TiO ₂ -Ag Nanomaterial solution	27 µL	NA	NA	NA			
rGO-TiO ₂ -Ag Nanomaterial solution	NA	NA	27 µL	NA	4 °C	∞	
DNA (salmon fish)	1 µL ~ 68 ng	1 µL ~ 68 ng	1 µL ~ 68 ng	1 µL ~ 68 ng			

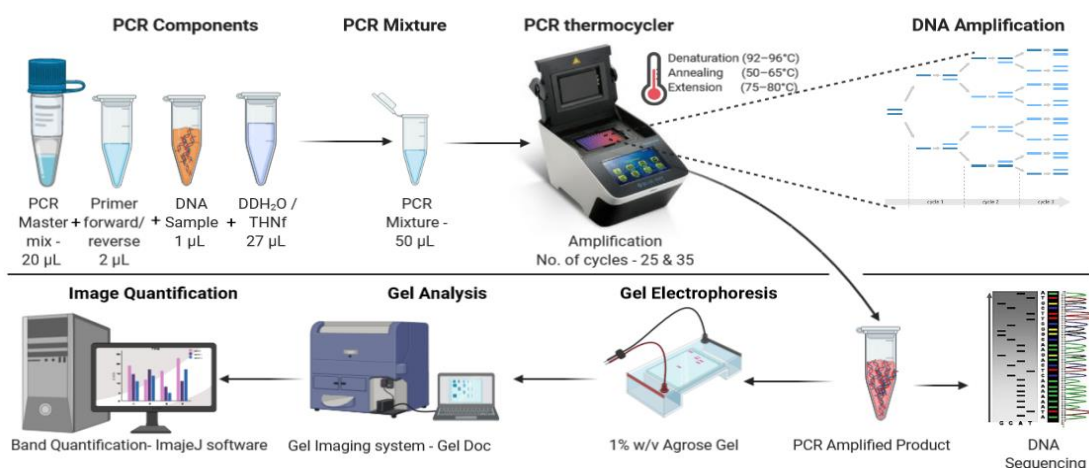


Figure 3.3 PCR process

Table 3.2 PCR mix and thermal cycling conditions for four sets of GO-TiO₂-Ag and rGO-TiO₂-Ag nanomaterial-assisted PCR (nanoPCR) for 25 cycles

PCR Mix Components	PCR Mix 1 (with GO-TiO ₂ -Ag nanomaterial solution)	PCR Mix 2 (without GO-TiO ₂ -Ag nanomaterial solution)	PCR Mix 3 (with rGO-TiO ₂ -Ag nanomaterial solution)	PCR Mix 4 (without rGO-TiO ₂ -Ag nanomaterial solution)	Thermal Cycling conditions for PCR		
PCR mater mix (1st base)	20 μL	20 μL	20 μL	20 μL	95 °C	10 min	1 cycle
Primer (forward/reverse)	2 μL	2 μL	2 μL	2 μL	95 °C	30 S	25 cycle
					60 °C	45 S	
					72 °C	30 S	
ddH ₂ O	NA	22 μL	NA	22 μL	72 °C	7 min	1 cycle
GO-TiO ₂ -Ag Nanomaterial solution	22 μL	NA	NA	NA			
rGO-TiO ₂ -Ag Nanomaterial solution	NA	NA	22 μL	NA	4 °C	∞	
DNA (salmon)	1 μL ~ 60ng	1 μL ~ 60 ng	1 μL ~ 60 ng	1 μL ~ 60 ng			

3.6.4 Sequencing Analysis

The sequence chromatogram was visualized in Bioedit 2V (Hall, 1999), the 5' and 3' ends were trimmed for chromatogram noise, and sequences were BLAST analyzed. Clustal W (Larkin et al., 2007) for multiple pairwise analyses to identify sequence gaps and sequence similarity. Nanoparticle interference, in terms of base-pair changes, was visually observed in Clustal W align file (.Aln).

3.7 EVALUATION OF DNA DENATURATION BY UV SPECTROSCOPY

DNA denaturation occurs at a temperature of about 92°C to 96°C. DNA has a characteristic UV/Visible spectrum exhibiting an absorption peak at 260 nm. Two DNA

samples (Named 12 and 27) were prepared, and then their concentration was measured using Thermo Qubit 3.0 Fluorometer. The concentration was found to be 11.47ng/ μ l and 6.493 ng/ μ l (12 and 27 resp.). The measured sample A260/A280 was found to be 1.793 and 1.895. The A260/280 ratio of \sim 1.8 is considered pure for DNA samples. Lower than the above said values may be considered impure and may indicate the presence of protein, phenols, or other contaminants in the measured DNA samples, which will have higher absorbance of UV/visible light. Temperature controlled Perkin Elmer UV spectrophotometer was used to measure the thermal denaturation of the 2 DNA samples along with the synthesized graphene-based ternary hybrid nanofluids (GO-TiO₂-Ag and rGO- TiO₂-Ag) with five levels of concentrations (named as A(5×10^{-1})wt% B(5×10^{-2})wt% C(5×10^{-3})wt% D(5×10^{-4})wt% and E(5×10^{-5})wt%). The measurements were performed by mixing 5 μ l DNA samples, 2 μ l of the nanofluid, and then it was filled to the marked level in a clean 5mm spectrometer Cuvette cell made of quartz. The absorbance was measured at various temperature ranges starting at 80°C with 2°C increments till 96°C.

3.8 NUMERICAL SIMULATION

Three-dimensional geometrical models of the PCR tube and thermocycler plate will be created using Solid Works. The transient-thermal equation will be solved for the 3D simulation of the PCR tube using transient temperature distribution. Unstructured meshing generated and simulations will be performed with the geometry such that it replicates the test section of the PCR tube, which is filled with its reagents. The boundary conditions will be chosen according to the actual conditions in a PCR thermocycler. Simulations were performed using an adaptive time-stepping method. The transient regions of various temperature levels will be analyzed to distinguish the

PCR tube with and without ternary hybrid nanoparticles. The main reason to choose a FEM instead of a CFD simulation in this study is that the PCR problem involves only heat transfer, and there is no fluid flow. Hence the author feels that it is sufficient to study the thermal transient equation for PCR optimization.

CHAPTER FOUR

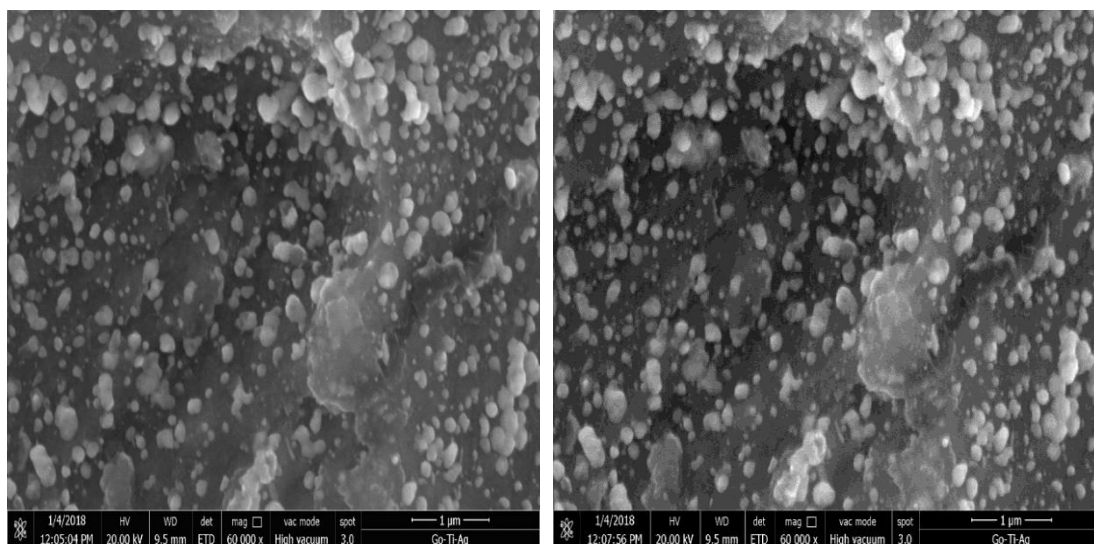
RESULTS AND DISCUSSION

4.1 SYNTHESIS OF TERNARY HYBRID NANOPARTICLES, CHARACTERIZATION, AND PREPARATION OF NANOFLUIDS

4.1.1 Materials Characterization

4.1.1.1 Scanning Electron Microscopy (SEM)

A field emission scanning electron microscopy (FE-SEM) at 30 kV was used to measure the surface topography. The GO-TiO₂-Ag ternary hybrid nanoparticle, crumpled and rippled GO sheets were decorated by two types of nanoparticles, the TiO₂ and the Ag, as shown in Figure 4.1. In the rGO-TiO₂-Ag ternary hybrid nanoparticle, the rGO appeared more as layered and wrinkled nano-sheets decorated with the TiO₂ and the Ag (Leong et al., 2015). This indicates the successfulness of the deposition of the Ag and the TiO₂ nanoparticles on the rGO nano-sheet (Figure 4.2).



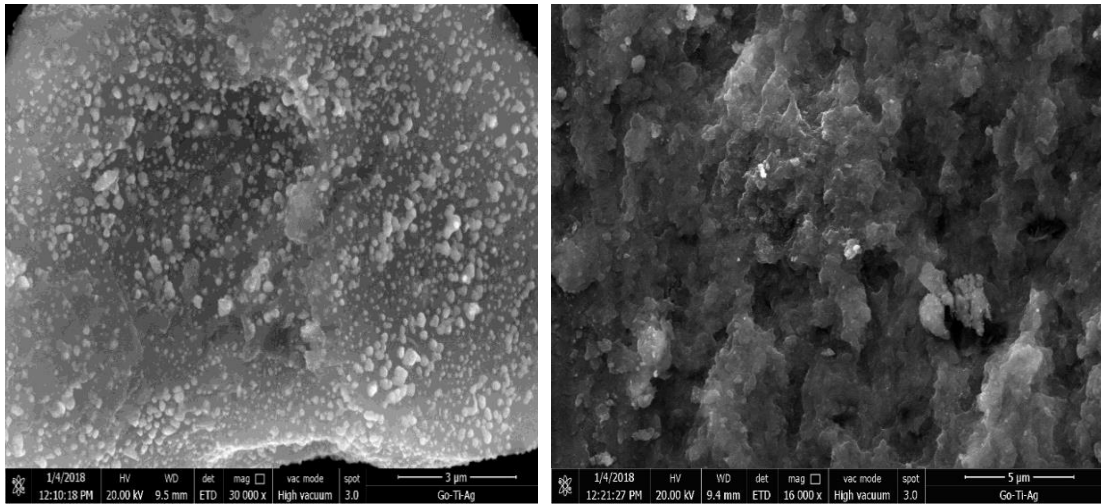
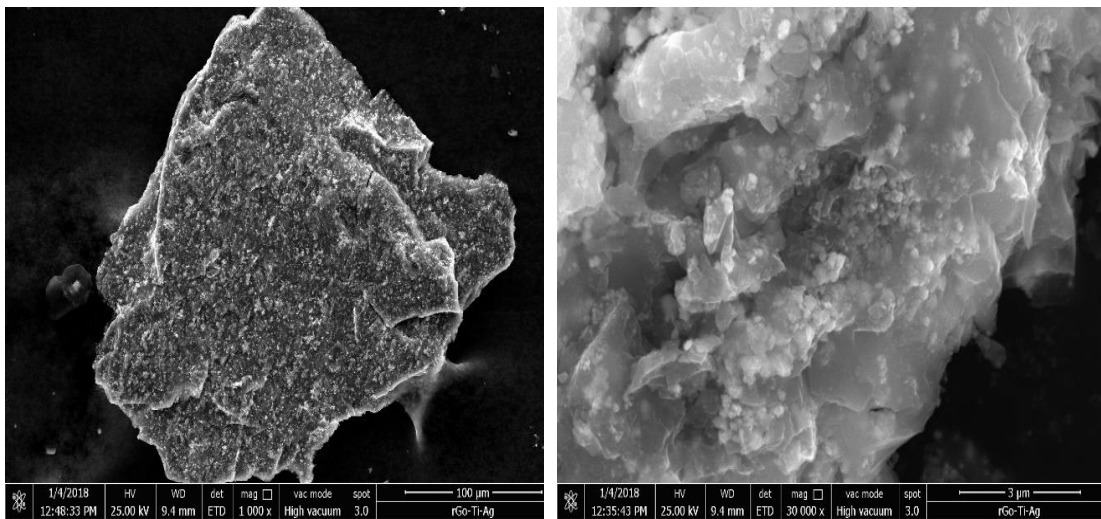


Figure 4.1 Scanning electron microscope (SEM) images of GO-TiO₂-Ag Hybrid Nanoparticles in magnification 60000x, 30000x and 16000x

The above figures show the SEM images of GO-TiO₂-Ag Hybrid Nanoparticles in magnification 60000x, 30000x, and 16000x respectively. In the figures, we can observe that the flakes are scattered. A uniform distribution pattern of the flakes can be observed.



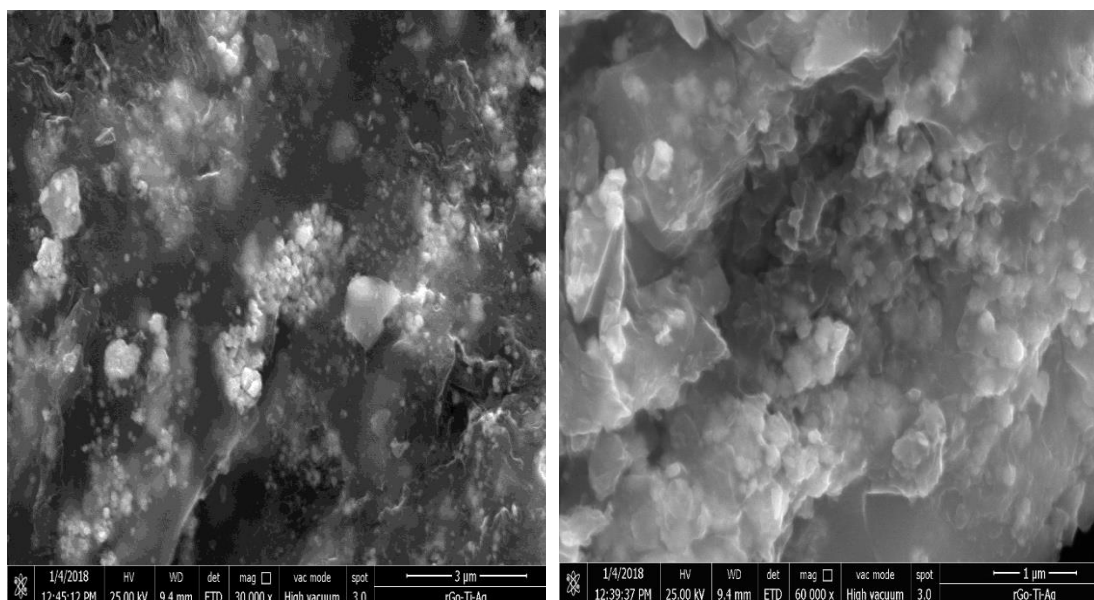


Figure 4.2 Scanning electron microscope (SEM) images of rGO-TiO₂-Ag Hybrid Nanoparticles in magnification 1000x, 30000x and 60000x

The above figures show the SEM images of rGO-TiO₂-Ag Hybrid Nanoparticles in magnification 1000x, 30000x, and 60000x respectively. In the figures, we can observe that the flakes are not as scattered as the GO-TiO₂-Ag. A non-uniform distribution pattern of the flakes can be observed.

4.1.1.2 Raman Spectroscopy

Figure 4.3 shows the Raman scattering spectra of the GO-TiO₂-Ag and rGO-TiO₂-Ag. The structural defects in the sp²-hybridized carbon system are determined mainly by analyzing the D- and G- bands in Raman spectra. These bands represent the presence of first-order scattering of the E_{2g} phonons of sp² carbon atoms. The peaks of D- and G- the band are presented alongside 637 cm⁻¹, the E_g peaks. This is due to the symmetric stretching vibration of the O-Ti-O bonds in both nanocomposites (B.-K. Choi et al., 2018). Nonetheless, the peak intensity ratio I_D/I_G of rGO-TiO₂-Ag increased to 1.41 compared to the GO-TiO₂-Ag (0.96). This may be mainly due to higher defects in its graphitic domains during the chemical reduction of the GO (Tan et al., 2013).

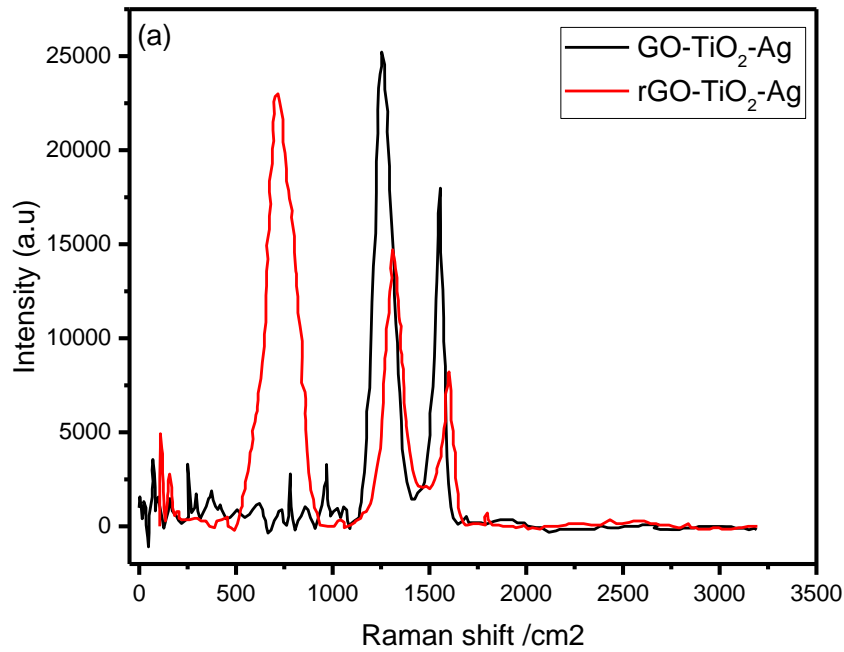


Figure 4.3 Raman spectroscopy of THNp

4.1.1.3 Fourier-Transform Infrared Spectroscopy (FTIR)

The FTIR spectrum of the nanocomposites (GO-TiO₂-Ag and rGO-TiO₂-Ag) are as shown in figure 4.4. The FTIR spectrum of the GO-TiO₂-Ag possesses strong absorption bands at 1,723, 1,620, 1,223 cm⁻¹, corresponding to stretching vibration of C=O, C-C, and C-O, respectively (Gurunathan et al., 2015). There are essential oxygen molecules present in the GO alongside a broad hydroxyl peak at 3300 cm⁻¹. The peaks at 1,620 and 1,223 cm⁻¹, together with a small peak at 596 cm⁻¹ may also attribute to the stretching vibration of (NH) C=O group of silver nanoparticles (Gurunathan et al., 2015). Moreover, the peak at 1,000 cm⁻¹ in composites is attributed to the Ti-O=Ti and Ti-O-C groups (Wen et al., 2001). However, some peaks are still present in the rGO-TiO₂-Ag spectra, but the oxygen peak appears at lower intensity due to the exclusion of oxygen molecules during the reduction process (Zhang et al., 2018). The essential peak of Ag and TiO₂ is still present in the FTIR of rGO-TiO₂-Ag, which indicates the successful manifestation of the silver and titanium nanoparticles on the rGO.

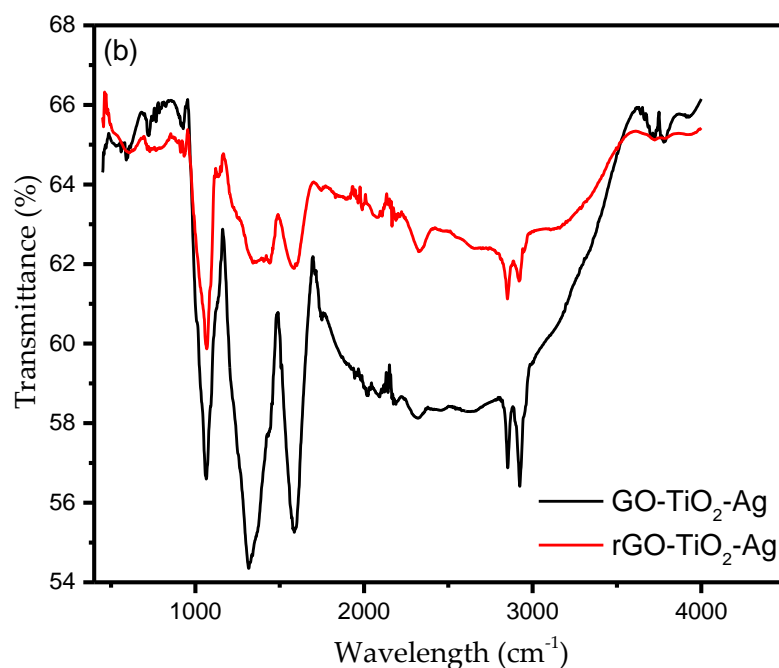


Figure 4.4 FTIR of THNp

4.1.1.4 X-Ray Powder Diffraction (XRD)

The XRD spectra are as shown in Figure 4.5. It is a series of reflections which peaks at 24.5° (101), 38.9° (004), 49.5° (200), 55.4° (105), and 64.2° (204) corresponding to the anatase phase of titanium (Thomas et al., 2014). Moreover, the peaks at 70.5° (220) and 79.5° (311) belong to silver nanoparticles (Fan et al., 2016). The diffraction peaks of the GO-TiO₂-Ag are not distinguishable with the rGO-TiO₂-Ag due to the lower crystallinity degree of the GO and the rGO as compared to the TiO₂, which resulted in the shielding of the peaks (Liu et al., 2014).

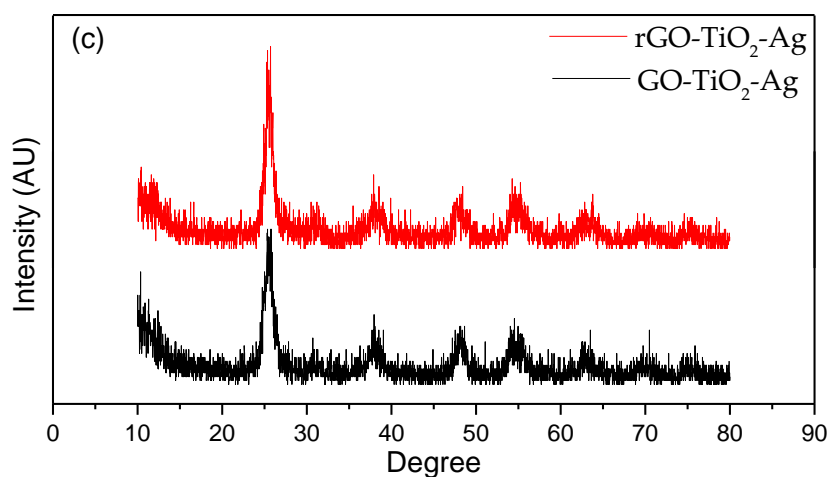


Figure 4.5 XRD of THNp

4.1.1.5 Particle Size Distribution

Graphene-based-hybrid nanofluids are usually well-dispersed colloids since they are polar and hydrophilic. Figure 4.6 shows the aggregate size of the ternary hybrids. The GO-based-ternary hybrid has particle size peaks at 750nm, while the rGO based-ternary hybrid is at the peak of 1750 nm.

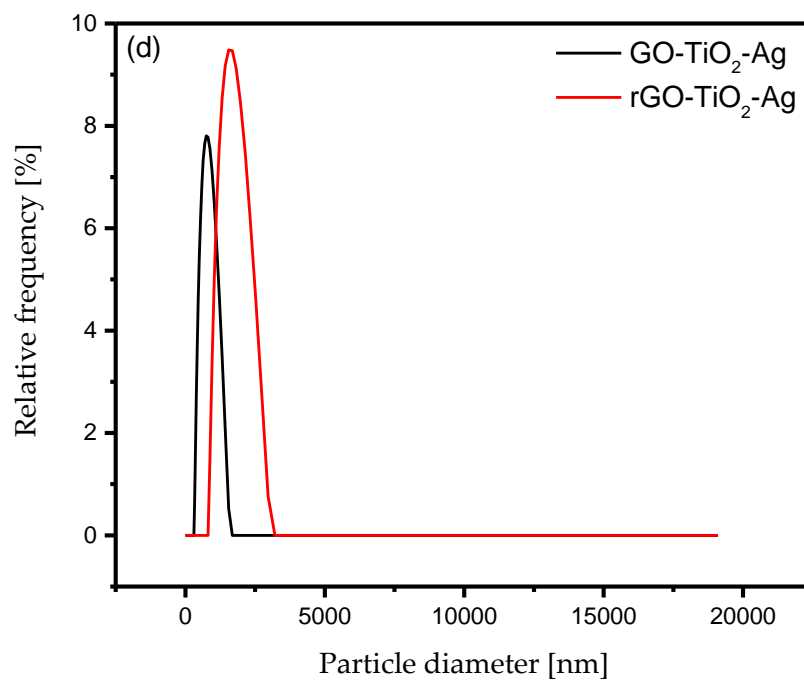


Figure 4.6 Particle Size Distribution of THNp

4.1.2 Synthesis of Hybrid nanofluids

The detailed preparation of the nanofluids is as mentioned in section 3.2.

4.1.2.1 Zeta Potential

The attraction forces for the precipitation should be lesser than the Electrostatic repulsion force (Ghadimi and Metselaar, 2013). The absolute zeta potential of 30 mV is considered suitable for the stability of solid in liquid colloids, which have low ionic strength. Figure 4.7 shows that the peak of the hybrid nanoparticles ranges from 25 mV to 35 mV, which is within a stable range. On the other hand, a lower zeta potential of about 20 mV is considered unstable dispersion. Figure 4.8 shows the zeta potential of the ternary hybrid nanofluids with respect to time.

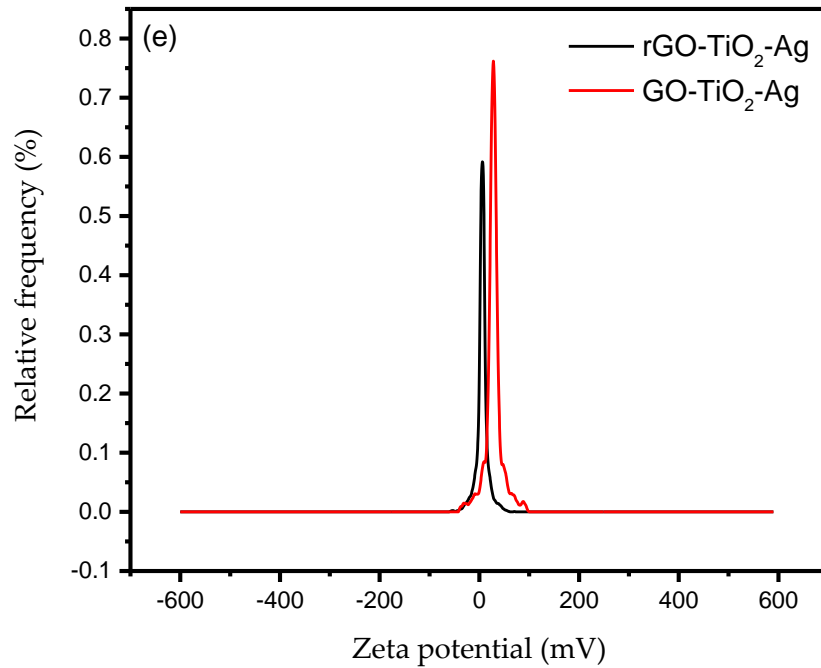


Figure 4.7 Zeta potential of THNp

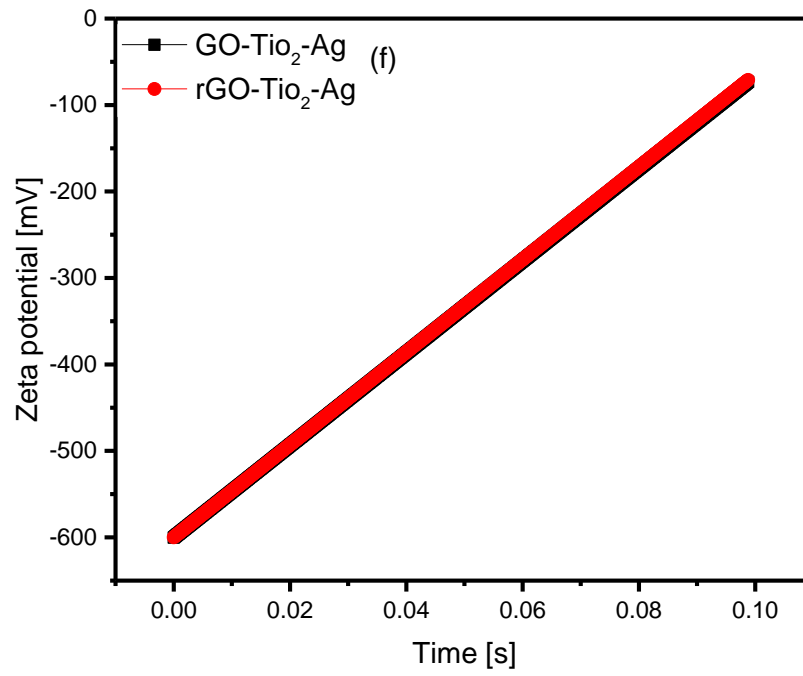


Figure 4.8 Zeta potential of THNp with respect to time

4.2 THERMAL CONDUCTIVITY MEASUREMENT

The thermal conductivity of any nanomaterial is an essential aspect. The importance of studying thermal conductivity and dynamic viscosity is discussed in sections 1.2.1, 1.2.2, and 2.4. The methodology of thermal conductivity measurements is as mentioned in section 3.3.

4.2.1 Effect of Concentration

The thermal conductivity of ternary-hybrid nanofluids with different volumetric concentrations that ranged from 0.05 wt % to 0.0005 wt% was measured. The results are presented in figure 4.9(a) and (b). The measurements were carried out for the ternary-hybrid nanofluids with temperatures ranging from 25°C to 50°C, and with increments of 5°C. It can be observed that the heat transfer characteristics of the nanofluids increase linearly with the increase in volume fraction/concentration. The thermal conductivity of the carbon-based nanofluids is generally said to be higher, as reported by many research observations (Jabbari et al., 2017). The thermal conductivity of the nanofluids is usually higher than the standard-base fluids. This increase is attributed to the thermal conductivity of the nanoparticles in the nanofluids.

The thermal conductivity also increases significantly with the increase of the temperature of the fluid. Significant enhancements in thermal conductivity can be observed from the plots in all samples, as shown in Figures 4.9 (a) and (b). The duration of sonication plays a vital role in the increase of the thermal conductivity of the nanofluid. It was reported that the particle size could be controlled by applying ultrasonication. The surface area in the nanofluid can be increased by making the particle shape and size more uniform. The uniformity of the particle will increase the thermal conductivity of the fluid. A lower concentration of nanoparticles is chosen to prevent

the undesirable increase in the viscosity of the nanofluids. The measurements show that the thermal conductivity increases even with a low concentration of THNp. The enhancement of the thermal conductivity at 25°C is about 10%, whereas the enhancement at 50°C is about 60%. This enhancement is excellent, considering such a small volume fraction. The substantial increment in the thermal conductivity can be attributed to the greater surface area of the THNp. The concentration of nanoparticles has a direct impact on the thermal conductivity of the nanofluids. For instance, Heat transfer takes place through the surface of the particles; therefore, nanofluids with higher concentration shows higher thermal conductivity. This is due to the effect of Brownian motion on the surface of the particles (Kwek et al., 2010). It can be observed from figures 4.9 (a) and (b) that the nanofluids with lower concentrations have lower thermal conductivity. In contrast, nanofluids with higher concentrations have slightly higher thermal conductivity. It may be due to the surface-to-volume ratio, 1000 times smaller for particles of 10 nm diameter in every serially diluted nanofluid.

4.2.2 Effect of Temperature

The nanofluids are used in several applications where a general change of temperature is expected. Many studies establish that thermal conductivity and fluid temperature are directly related (Colangelo et al., 2016). Thus, thermal conductivity enhances with the increase in temperature of the fluid. The enhancement of thermal conductivity in nanofluids is the function of the nanoparticles and temperature. In this study, the temperature of the nanofluid is increased from 25°C to 50°C, and the thermal conductivity of the standard-base fluid added with ternary hybrid nanoparticles increased steadily as well. The enhancement of thermal conductivity is because of the increase in temperature due to the natural phenomena of the thermal conductivity

materials. The thermal conductivity of most nanomaterials increases with the increase in temperature that transfers higher energy between the particles in the standard-base fluid. The increase in the fluid's temperature increases the molecular movements, which enhance energy transfer (Wong and Castillo, 2010).

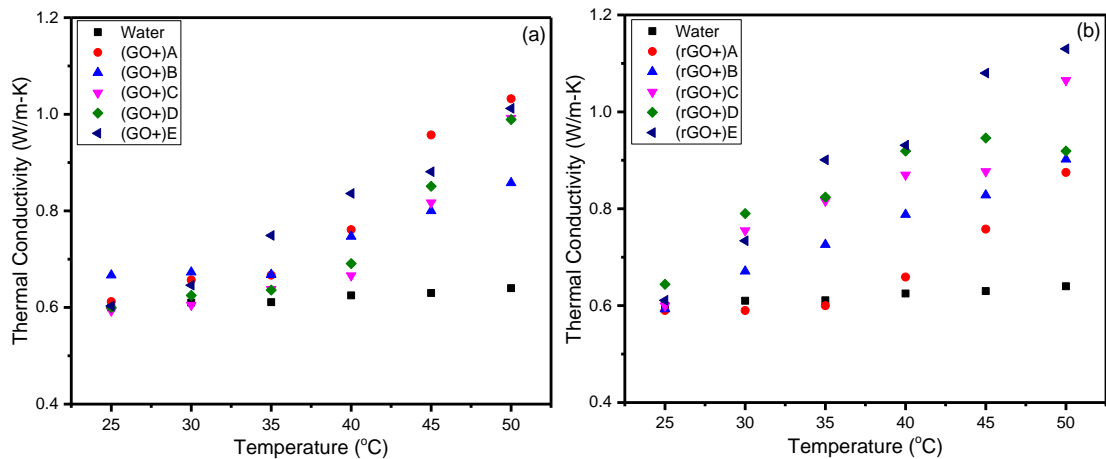


Figure 4.9 (a) and (b): Thermal conductivity of THNp GO-TiO₂-Ag, rGO-TiO₂-Ag at various temperature (where A, B, C, D, and E are serial dilutions)

The enhancement of thermal conductivity is a function of concentration. The THNp in the nanofluids enhances the thermal conductivity in a linear increment. The random motion of particles in a liquid is called Brownian motion. The continuous interaction between the molecules and the particles results in the transfer of heat. The Brownian motion of particles and the clustering of nanoparticles are directly proportional to the change in the nanofluid's temperature, which increases the thermal conductivity. At the nano-scale level, the Brownian motion of nanoparticles governs the thermal behavior of the nanofluids. If there is any change in the dispersion characteristics of the nanofluids, it can be detrimental to the heat transfer process of the nanofluids. The non-linear thermal conductivity enhancement process was observed by Wen and Ding (D. Wen and Ding, 2004) for CNT/water nanofluid. They observed an increase in the

thermal conductivity due to higher temperatures and smaller particle size, which was higher than that of the lower temperature and larger particle size.

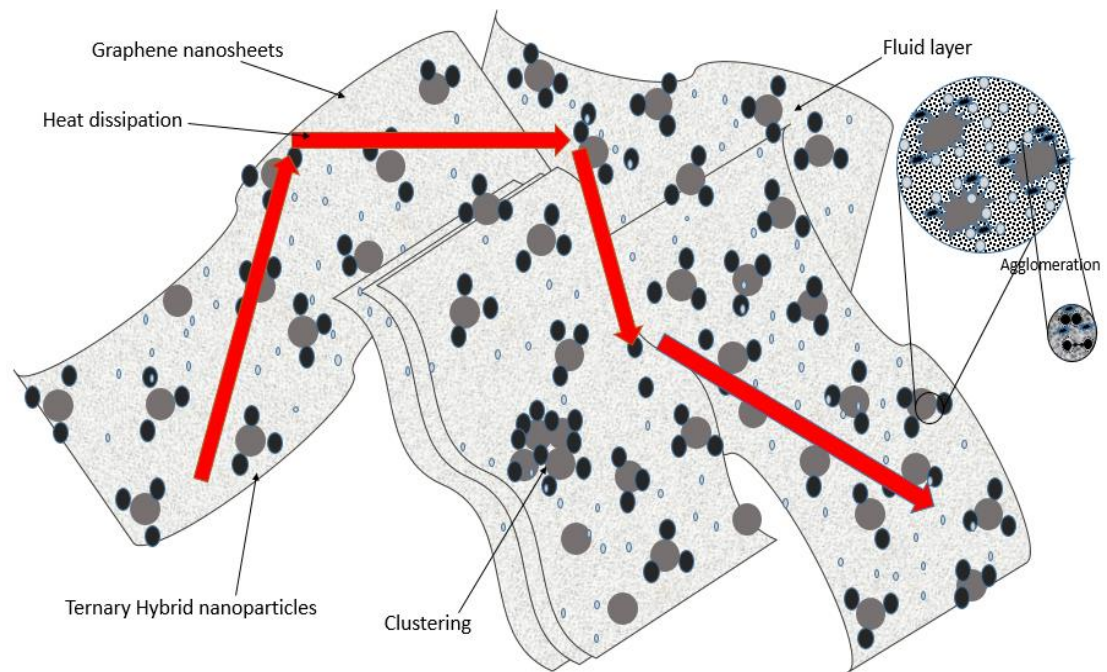


Figure 4.10 Schematic of thermal conductivity mechanism of THNp in the nanofluids

Many researchers studied thermal conductivity and rheological measurements of nanofluids with metal oxides for the concentration of $> 1\%$. However, minimal experimental data are available for effective thermal conductivities and viscosities of the nanofluids made of hybrid nanoparticles at low volume concentration ($< 1\%$) and higher temperatures. The present study is very significant in fulfilling this gap (Godson et al., 2010). Clustering is another important mechanism in the enhancement of thermal conductivity in nanofluids, and it is the aggregation of particles as a result of interacting forces. They are also referred to as agglomerations, responsible for fluctuations in effective thermal conductivity in the nanofluids. These agglomerations are against the dispersal of particles. These agglomerations cause the particles to be packed together to form a solid zone in colloids (Kole and Dey, 2013).

The thermal energy in a solid crystalline lattice tends to move faster than in any other liquid. Hence, the THNp increases the effective thermal conductivity in a colloidal solution. Typically, clustering reduces inter-particle distance, which increases the energy transfer by lowering the thermal energy pathway. The increase in thermal conductivity may also be due to interfacial resistance between the particles. The inherent thermal conductivity of the ternary-hybrid nanoparticles resulted from the advantage of forming clusters of the THNp by concomitant degradation of convection. A suggestive schematic of the thermal conductivity mechanism is shown in figure 4.10. The graphene layers or flakes are stacked above each other with titanium and silver nanoparticles agglomerating on the flakes. Transitional motion and structural limitation of the rotational motion in the nanofluids lead to the clustering of the nanoparticles in higher viscous nanofluids.

A percolation network occurs when the agglomerated nanoparticles hit each other, transferring heat energy from one particle to another called phonon transport. The percolation networks with anisotropic thermal conductivity of the nanoparticles result in higher thermal conductivity. The thickness of the fluid layer depends on the intensity of the particle-fluid interactions. When the magnitude of the stable fluid versus the solid-liquid interface's total area increases, the nanofluids' viscosity increases. Meanwhile, phonon transports in nanofluids have a wide range of free-mean paths. Other mechanisms contributing to higher thermal conductivity in a nanofluid could be phase change, liquid layering, and surface chemical effects.

The thermal conductivity of the THNp may also be influenced by the phonon-phonon transport, which may increase its energy transfer with the increase in temperature. It can be observed from figures 4.9 (a) and (b), the thermal conductivity enhances with the increase of temperature from 25°C to 50°C. Heat conduction in solid

materials is more complicated than liquids (Kikugawa et al., 2009). In the absence of a proper definitive model that proves the transmission of energy modes across the solid-liquid interface, it can only be assumed that the thermal phonon transfer occurs in the solid-liquid interfaces to transport heat energy effectively solid-liquid interface of the nanofluid effectively. The thermal percolation index is the permeation of nanoparticle clusters in the nanofluid. The higher thermal percolation leads to higher thermal conductivity in nanofluids. Few studies reported that nanoparticles act as the carriers of heat energy due to translational movements (Ghosh et al., 2011).

There are few other debates on this theory that claim that the diffusion of thermal energy in a fluid medium is faster than the translational movements (Xue et al., 2004). The other possible phenomenon is the micro-convection effect, which is the conventional heat transfer resulting from the micro-mixing effect and translational displacement because of the fast rotation of the THNp in the nanofluids. There is no doubt that the nanoscale rotation of particles will increase the movement of the fluid molecules when the temperature is increased, which leads to an increase in the thermal conductivity of the nanofluids.

4.3 RHEOLOGICAL INVESTIGATIONS OF GRAPHENE-BASED TERNARY HYBRID NANOFUIDS

Rheological measurements were carried out at various temperature intervals of viscosity versus shear rate and temperature. Other rheological parameters like amplitude sweep and frequency sweep with the loss and storage moduli were also measured at various temperatures ranging from 25°C to 50°C at 5°C intervals. The importance of studying dynamic viscosity is discussed in the literature. The complete methodology is presented in section 3.4.

4.3.1 Viscosity Vs. Temperature

The methodology for the dynamic viscosity measurements is as discussed in section 3.5. The dynamic viscosity measurements were carried out only for the stock solution to check the viscosity characteristics of the nanofluids. It is noted from figure 4.11 (a) and (b) that the viscosity of the hybrid nanofluids is almost linear, which indicates that it is a Newtonian fluid. The ternary nanofluids' measurement shows substantially higher viscosities than the base fluids (Godson et al., 2010).

Rheological measurements of both the THNp (GO-TiO₂-Ag and the rGO-TiO₂-Ag) based nanofluids were done at a concentration of 0.05 wt%. It can be observed that viscosity is lower at higher temperatures. The hybrid nanoparticle shows signs of Newtonian individuality in all the temperature ranges that were measured. The rheological behavior of hybrid nanofluids is imperative to its application. The viscosity profile is advantageous for the hybrid nanofluid's application even in conditions of variable shear rate.

Figure 4.11 (a) and (b) show that the viscosity profile of the ternary hybrid nanofluids. It decreases with the increase in the temperature of the fluid. The inter-particle and intermolecular adhesion forces weaken with the increase of temperature, thereby decreasing the viscosity. When the kinetic energy of the molecules increases with the increase in temperature, the particle closest reduces the contact. This gap reduction decreases the intermolecular forces leading to a decrease in the viscosity of the nanofluids (Sharma et al., 2018). The shear stress is linearly dependant on the shear rate, which shows the Newtonian behavior of the ternary-hybrid nanofluids. An increase in the slope of the line shows the increase in volumetric concentration and volumetric particle fraction of the ternary-hybrid nanofluids. The temperature dependency behavior of the ternary-hybrid nanofluid's viscosity is evident based on figure 4.11 (a) and (b).

The Rheological measurements of the hybrid nanofluids were carried out by varying the shear rate of the nanofluid samples under constant temperature. The shear stress in any fluids helps to determine if the fluid is Newtonian or non-Newtonian. Figure 4.11 (c) and (d) illustrate the measured shear stress versus shear rate exerted on the respective sample of the ternary-hybrid nanofluids. The measurements were carried out for various temperatures ranging from 25°C to 50°C with an increment of 5°C for a shear rate of 10 and 1000 1/s. Shear stress is linearly dependent on the shear strain for the ternary-hybrid nanofluids. The slope of the line increases linearly with the rise of volumetric concentration.

A sharp decrease in the viscosity was noticed with the increase in the temperature of the nanofluid. The viscosity of the nanofluids with various metallic, oxide, and carbon-based nanoparticles increases with particle loading or increase in the concentration of particles and decreases with the increase in temperature, as reported by many researchers (Ahammed et al., 2016). Various research illustrated that the viscosity increased with the increase in concentration volume (Ahammed et al., 2016). Prasher et al. reported an increase in viscosity with increased volume concentration (Prasher et al., 2006). The particle size also plays a crucial role in the increase in viscosity. Viscosity measurements by Murshed et al. (Murshed and Estellé, 2017) indicated an increase in viscosity with the increase in volumetric loading of nanoparticles, while Lee et al. (Lee et al., 2007) reported a decrease in viscosity with an increase in temperature.

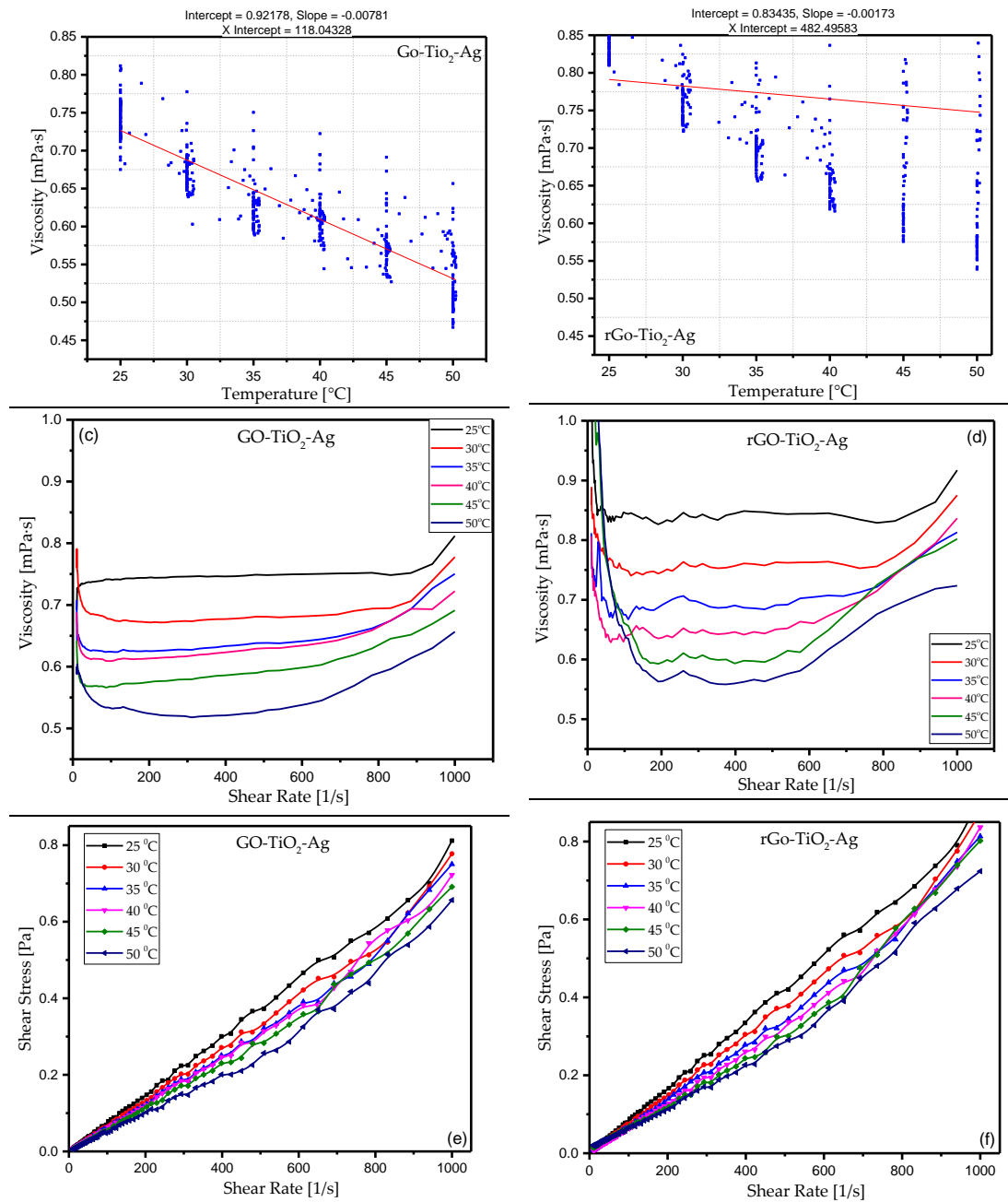


Figure 4.11 (a) Viscosity of THNp GO-TiO₂-Ag, (b) Viscosity of THNp rGO-TiO₂-Ag, (c) Viscosity Vs. The shear rate of THNp GO-TiO₂-Ag (d) Viscosity Vs. The shear rate of THNp rGO-TiO₂-Ag, (e) Shear stress Vs. Shear rate of THNp GO-TiO₂-Ag (f) Shear stress Vs. The shear rate of THNp rGO-TiO₂-Ag

This linear increase in shear stress validates that the viscosity of the nanofluid increases with the increase of volumetric concentration. The viscosity of the nanofluids is generally higher than that of their base fluids. The particle-to-particle interactions create a decrease in viscosity with an increase in shear rate. It is also influenced by the

concentration and the type of nanoparticles. An increase in nanoparticle concentration leads to an increase in the viscosity of nanofluids, as reported by many researchers (Sajid and Ali, 2018). The agglomeration of nanoparticles at higher concentrations can be one of the factors that influence viscosity. This agglomeration leads to the enhancement of internal shear stress in the nanofluids. Therefore, greater force is required for the dissipation of solid components in the dispersion, which leads to an increase in the viscosity of the nanofluids. Micro-aggregation of nanoparticles leads to higher volume fraction, which increases the viscosity (H. Chen et al., 2009). Figures 4.11(e) and (f) show that shear rate is a function of shear stress, which means that the shear stress of the ternary-hybrid nanofluids is directly dependent on the shear stress nanofluids when the viscosity is constant.

As the temperature of the nanofluids increases, the shear stress and the shear rate increase, which indicates the Newtonian behavior of the ternary-hybrid nanofluids. The shear viscosity at 25°C is approximately double that at 50°C, indicating a robust temperature-dependent nature of the ternary-hybrid nanofluids. The rheological behavior was further studied with the increase in temperature of the nanofluid. The results show similar Newtonian behavior with a further increase in temperature of the ternary-hybrid nanofluids. Similarly, Newtonian behaviors were reported by many other researchers for the hybrid nanofluids based on iron and copper nanoparticles (Bahrami et al., 2016), Fe₃O₄-MWCNTs/EG hybrid nanofluid (Ahmadi et al., 2018), MWCNT-SiO₂ (Motahari et al., 2018), and Al₂O₃-SiO₂/PAG (Zawawi et al., 2017), etc. As the temperature increases, the ternary-hybrid nanofluids behave as a shear-thinning fluid that lowers the shear viscosity and increases the shear rate.

The measurements show a similar trend of shear-thinning for both the ternary-hybrid nanofluids. There are a fair agreement and similarity between the two nanofluids,

which are presented in the figures repeatedly showing the measurements and stability of the temperatures. The shearing effects on the nanoparticles in the fluid can affect the particle orientation that causes the disintegration of the agglomeration of particles, as discussed above. Shear-thinning behavior can occur due to various situations and stresses applied to the fluid, which reduces the viscosity. When the temperature of nanofluids is increased, the Brownian motion, its average speed, and the molecules' thermal movement are increased. This process weakens the adhesion forces and the intermolecular interaction between the molecules.

The effects of the nanoparticle size, shape, pH, temperature and volumetric concentrations may increase or decrease the ternary-hybrid nanofluids' viscosity. Viscosity change may also be dependent on the type of base fluids used, particle volume fraction, particle size distribution, shear rate, surfactants, dispersion techniques, and particle aggregation (Mishra et al., 2014). Clustering is another factor that influences the viscosity of nanofluids. The effect is that very few nanoparticles collide with each other, while other nanoparticles may have an interfacial layer that is developed around them.

4.3.1.1 Effect of Ternary Hybrid Nanoparticle Type on Temperature

The viscosity of water, EG, and oil-based nanofluids decrease with the increase in temperature of the fluid is a known phenomenon. The rate of decrease in viscosity due to an increase in temperature depends on the fluid's intrinsic property or the intermolecular bond strength. Increasing the temperature of the fluid is supplying the molecules in the fluids with higher energy. In nanofluids, which have new particles, this increase of temperature leads to increased heating and heat transfer, which leads to

faster weakening of the intermolecular forces leading to a decrease in viscosity of the fluid (Lee et al., 2011).

The intermolecular interactions of the molecules of water-nanoparticle become weaker with the increase in the temperature of the fluid, leading to a decrease of the viscosity of the ternary hybrid nanofluid. The robust Van der Waals forces act on the particles in lower temperatures. Once the temperature is increased, the forces weaken, leading to a decrease in viscosity (Nabil et al., 2017). Figure 4.12 (a) and (b) below show the averaged plot of viscosity versus temperature in terms of concentration of GO and rGO based ternary hybrid nanofluids. It can be seen that the viscosity is almost similar except for a slight variation with the lower concentration fluid exhibit slightly higher viscosity at lower temperatures. (Hu et al., 2020). The rGO based ternary hybrid nanofluids show a similar trend that the viscosity decreases with the increase in temperature of the fluid for all concentrations. Concentration B shows a higher viscosity than the other concentration, while the lowest concentration has a lower viscosity.

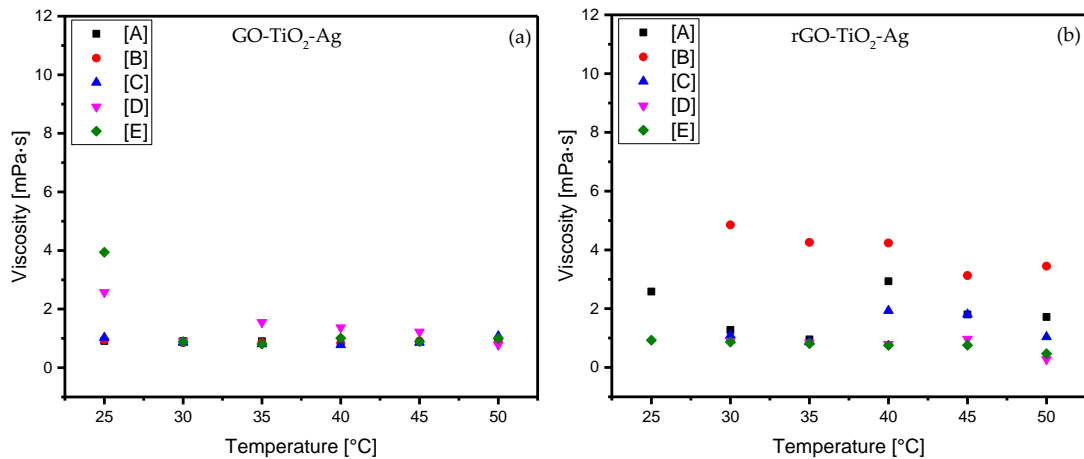


Figure 4.12 (a) and (b): Viscosity Vs. The temperature at different temperatures and concentrations of ternary hybrid nanoparticles. A, B, C, D, and E are serial dilutions

It shows that concentration plays a vital role in the change of viscosity with the temperature change. The viscosity varies with a temperature change. The addition of heat changes the nanoparticles in the fluid from surface force attraction to interatomic bonding (Ali et al., 2018). The change is evident between various concentration samples of the nanofluids. It may be due to the agglomeration of nanoparticles in higher temperatures (Koca et al., 2018). Similar results were observed by most researchers who study the effect of temperature on the viscosity of the nanofluids based on different levels of concentration. Shah. S. et al., in their study on rGO-Eg nanofluids, reported a viscosity decrease of 56.4% and 73.9% at 50°C and 70°C, respectively (Shah et al., 2020).

Hu, Xichen, et al. has reported an astronomical viscosity decrease of about 593% at 50°C for their study of graphite/engine oil nanofluids (Hu et al., 2020). Few researchers reported the effect of temperature on the viscosity of hybrid nanofluids. Esfe and Rostamian reported a 171% decrease of viscosity from 40 °C to 100 °C with a volume fraction of 0.05, 0.1, 0.2, 0.4, 0.8, and 1 vol% using CuO-MWCN hybrid nanofluids (Esfe et al., 2018). When the temperature is in all volume fractions of the nanofluids, viscosity decreases exponentially.

4.3.2 Viscosity Vs. Shear Rate

4.3.2.1 Effect of Ternary Hybrid Nanoparticle Type on Viscosity

The viscosity measurements were done for the two ternary hybrid nanoparticles based nanofluids of five different concentrations. Of the five measured samples, the concentration of 0.0005wt% (sample E (5×10^{-5})) wt% was chosen to study the effect of shear rate on viscosity concerning temperature. Figure 4.13 (a) and (b) below show that the nanofluids' viscosity decreases with the increase in the shear rate at different

temperatures. The ternary hybrid nanofluids behave like Newtonian fluids at lower temperatures. The viscosity decreases at higher temperatures and lower shear rates, indicating Shear thinning behavior, as reported by many studies (Sharma et al., 2016). It can be observed from both the ternary hybrid nanofluids, the fluid's viscosity is very high at 40°C and 50°C.

The possible explanations for this behavior could be that at higher temperatures and lower shear rates, the nanoparticles in the fluids aggregates with other particles similar to the formation of nano-clusters due to Van der Waal's forces between the nanoparticles. The resistance to flow is higher when the shear rate is lower. Agglomeration of nanoparticles at higher temperatures causes internal shear stress between particle-fluid interface interactions leading to an increase in the viscosity of hybrid nanofluids. The nanoparticles form clusters due to higher attractive forces at higher temperatures, leading to increased viscosity (Babar et al., 2019). Then as the shear rate increases, the attractive forces between the nanoparticles weaken, and the particles are dispersed, leading to a decrease in viscosity, called shear thinning behavior. She-thinning is synonymous with pseudoplastic behavior, which may affect minor structural changes in the fluid with microscale geometries of fluids rearranging themselves to facilitate shearing. Phase separation is another phenomenon that leads to shear thinning. Countless studies have measured the rheological properties of various nanofluids since the inception of the same. Studies have reported the effects of adding a nanoparticle on the rheological properties of the base fluid. Rheological studies are also done to determine the pressure drop, and the structure of nanoparticles can help predict the thermal conductivity of nanofluids (Sharma et al., 2016). Numerous theoretical models were also presented to date for various concentrations, along with experimental measurements of nanofluids (Koca et al., 2018). The majority of the

studies have been done based on single material nanoparticles, and theoretical models are also derived (Babu et al., 2017).

Rheological measurements by Masuda et al. (Masuda et al., 1993) have shown that the viscosity increased by 60% against water using single material nanoparticles of Aluminium oxide, silicon dioxide, and titanium dioxide at a concentration of 4.3%. Wang et al. observed Pseudo-plastic behavior in the fluid with the addition of graphite in oil. Viscosity was increased along with visco-elastic enhancement of about 1.36 vol% (Wang et al., 2012). Newtonian behavior was reported using hybrid nanofluid with Cu-Zn (1:1) alloy with vegetable oil, exhibiting the linear relationship between shear stress and shear rate with lower viscosity (Kumar et al., 2016).

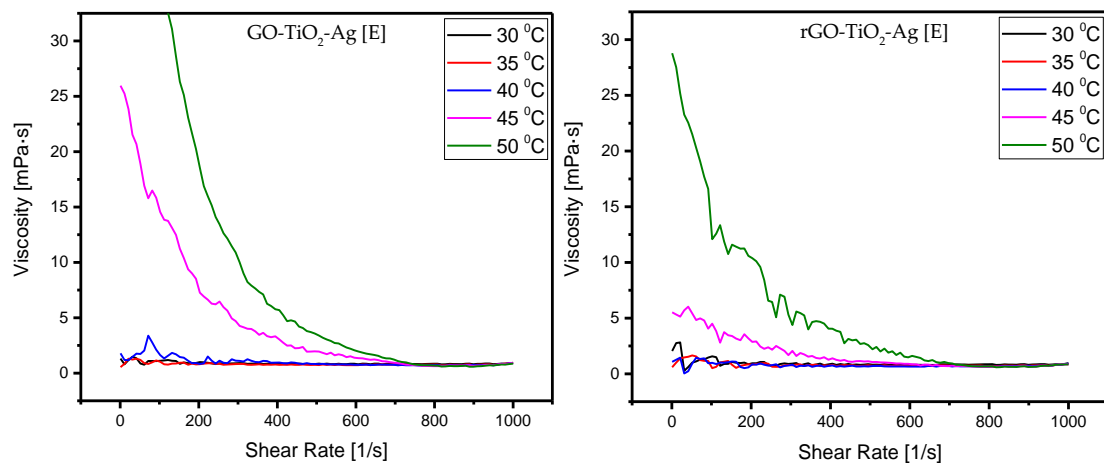


Figure 4.13 (a) and (b): Shear rate Vs. viscosity at different temperatures and at a concentration of 5×10^{-5} ternary hybrid nanoparticles

4.3.2.2 Effect of Ternary Hybrid Nanoparticle Type on Concentration

The measurement plots in figure 4.14 (a) and (b) show the variation of viscosity with the change in the concentration of nanofluids. The points A to E represents five levels of serial dilution of the nanofluids, with A as the highest concentration of 5×10^{-1} and E as the lowest concentration of 5×10^{-5} . The two-ternary hybrid nanofluids are inversely proportional in terms of their increase in viscosity. The viscosity of the GO-based

ternary hybrid nanofluid increases with the decrease in concentration. In contrast, it is otherwise in the rGO based ternary hybrid nanofluid in which the viscosity decreases with the decrease in concentration in various measured temperatures. It can be seen from the plots that in both GO and rGO based THNp, the viscosity of individual concentration increases gradually with the increase in temperature.

Generally, the viscosity of the water-based nanofluids decreases with lower concentrations. This was observed in the rGO based nanofluids. The GO-based ternary hybrid nanofluids behave otherwise. Observing the plots shows that at 35⁰C, the nanofluids spike in the viscosity, which can be considered an optimum operating temperature. The GO-based ternary hybrid nanofluid, the concentration D (5×10^{-4}), increases the viscosity by about 50% at almost all the temperatures measured. A similar hike in viscosity can be seen in the concentration C (5×10^{-3}) in the rGO based ternary hybrid nanofluids. GO-based ternary hybrid nanofluid has significantly higher viscosity at all concentrations and temperatures compared to rGO based ternary hybrid nanofluid, as evident from the plots. A change in the viscosity of the GO-based nanofluids is due to various factors. A slight variation of the concentration of the nanofluids tends to increase or decrease the rheological property of the nanofluids. Most studies on nanofluids have reported the same.

Substantial efforts have been applied to the research of concentrations or volume fractions of nanoparticles in nanofluids. There is a strong relationship between the increase in the concentration of nanoparticles and the increase in viscosity (Kumar et al., 2016). Few reports have studied the Newtonian behavior of water-based metallic nanofluids where the viscosity increased with the increase of nanoparticle concentration on the fluid (Das et al., 2003; Polidori et al., 2007; Putra et al., 2003). The viscosity increased can be as low as 4 to 15% (Godson et al., 2010), or it can be as high as 50%

(Lee et al., 2011; Nguyen et al., 2008). It can be seen that viscosity is detrimental to the increase of thermal conductivity in the nanofluids. Still, it cannot be generalized that the increase of nanoparticle concentration viscosity will increase. Figure 4.14 (a) and (b) below show the viscosity measurements of the two ternary hybrid nanoparticles.

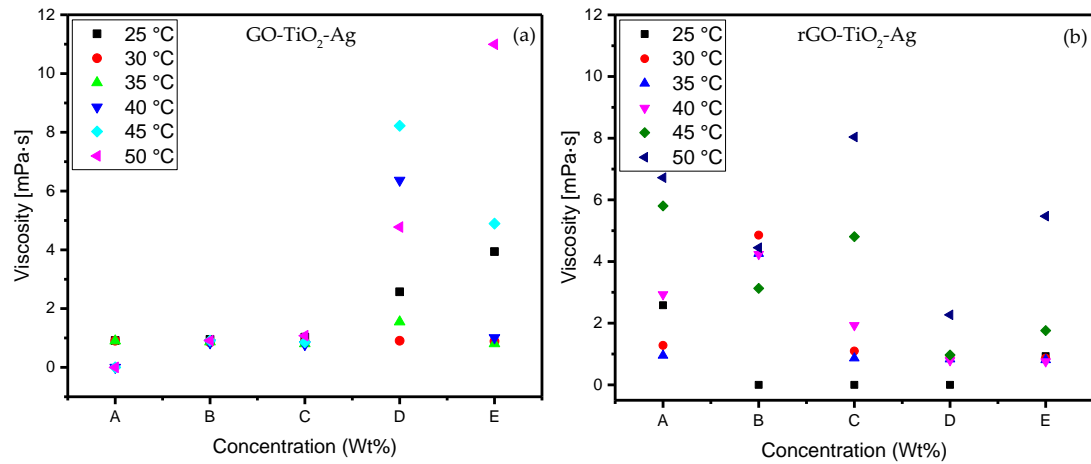


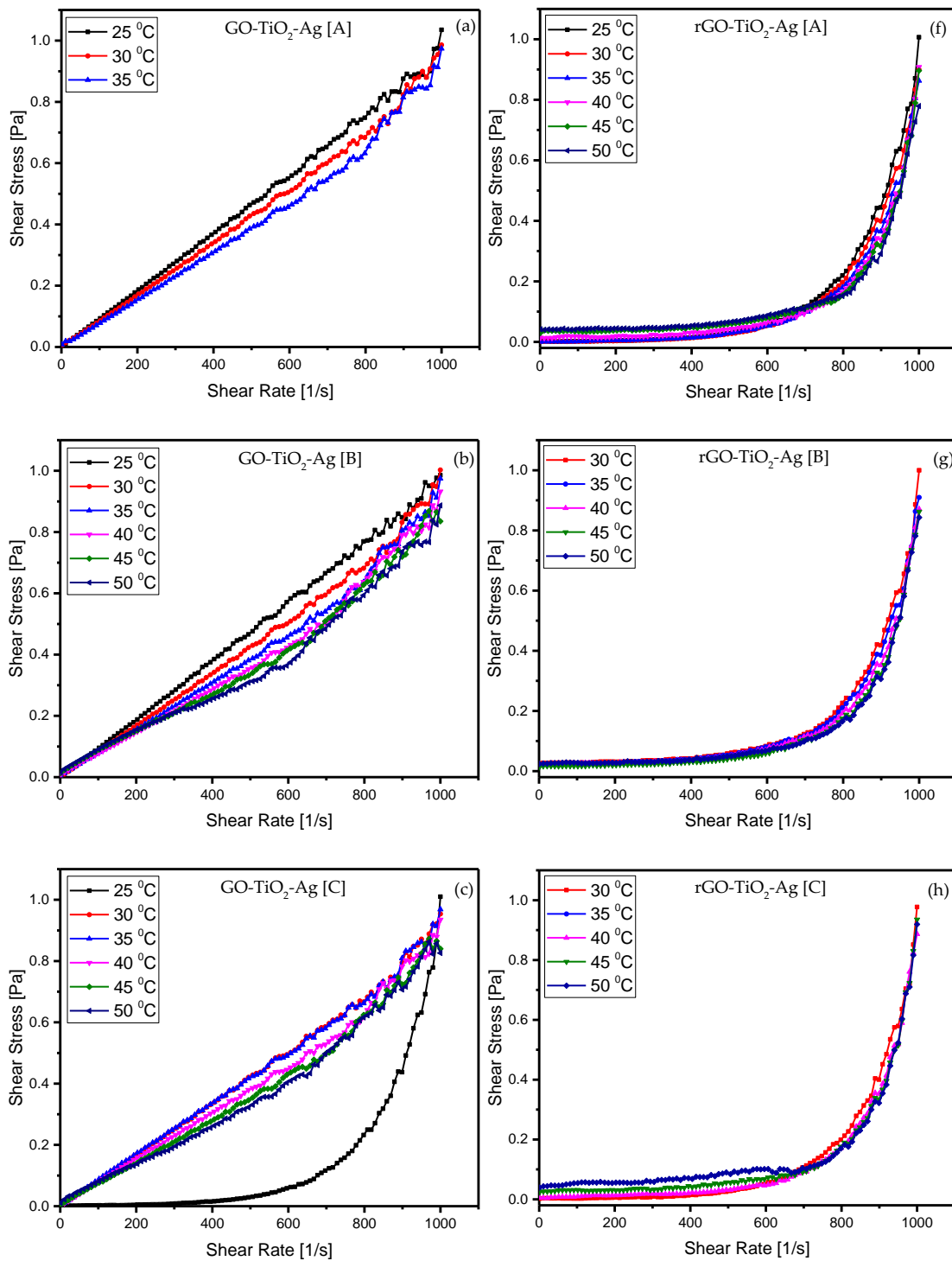
Figure 4.14 (a) and (b): Viscosity Vs. Concentration at different temperatures of ternary hybrid nanofluids. A, B, C, D, and E are serial dilutions

4.3.3 Shear stress Vs. Shear rate

4.3.3.1 Effect of Ternary Hybrid Nanoparticle Type on Shear Rate

Shear stress is the factor that determines whether the fluid is Newtonian or non-Newtonian. The control of the nanofluid suspension's flow property is crucial in many large-scale industries like paint, crude oil drilling, handling and transportation, food processing, and other consumer health products. The study of their rheological properties will give them the insight to control and for easy transportation of all manufactured products in the industries, as mentioned earlier. One of the methods to study their flow-based property is to determine the shear rate and shear stress of the flow in the fluids. Since nanofluids are widely used in many large-scale industries, it is essential to study their rheological flow properties. The water-based nanofluids generally behave as shear-thinning fluids at temperatures ranging from 30°C to 80°C

(Yang et al., 2020). Numerous researches have studied flow properties from the past few decades, and different characteristics were reported like the fluids are Newtonian, non-Newtonian or dilatant or pseudoplastic or thixotropic fluids, etc.



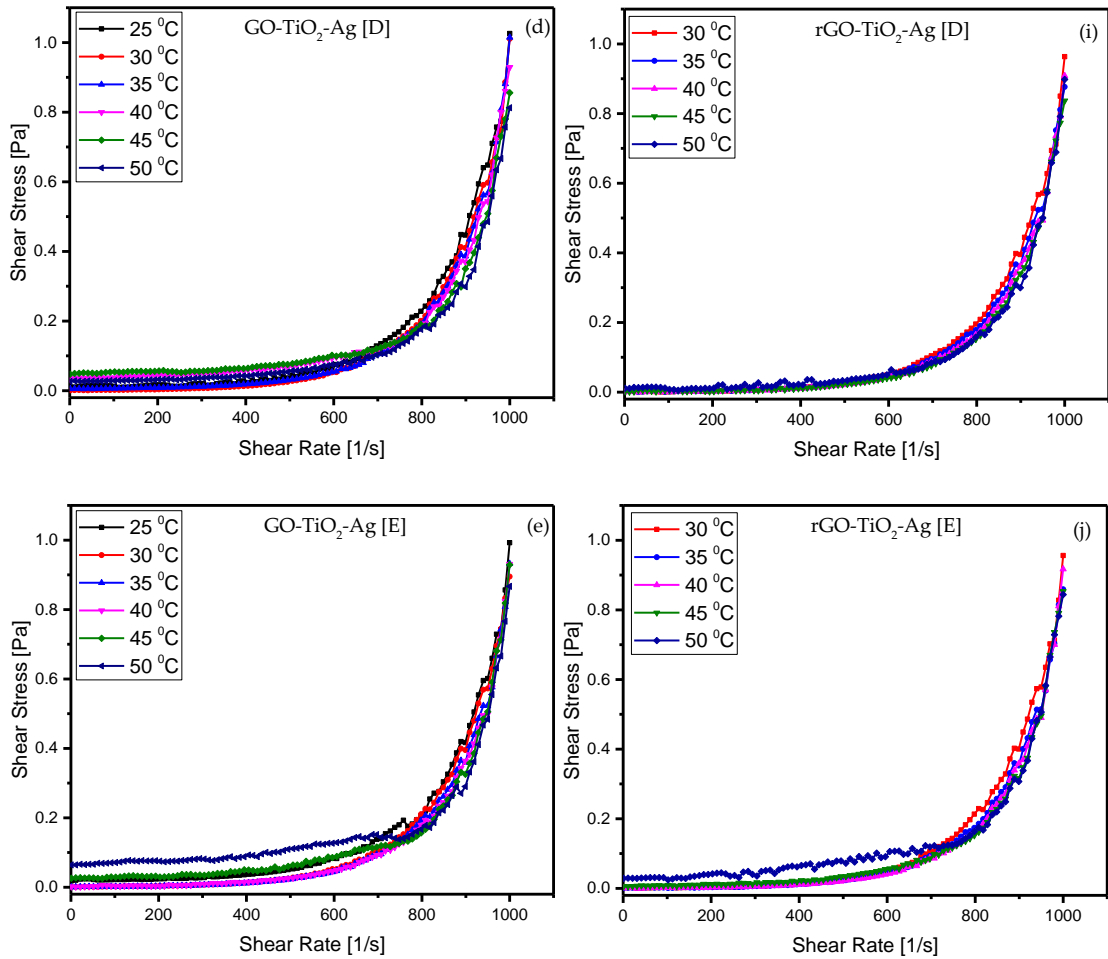


Figure 4.15 Shear Stress Vs. Shear rate. Plots a, b, c, d and e are GO- TiO₂-Ag samples of concentrations A(5×10^{-1})wt%, B(5×10^{-2})wt%, C(5×10^{-3})wt%, D(5×10^{-4})wt% ,and E(5×10^{-5})wt%, and f, g, h, I and j are rGO-TiO₂-Ag samples of concentrations A(5×10^{-1})wt%, B(5×10^{-2})wt%, C(5×10^{-3})wt%, D(5×10^{-4})wt%, and E(5×10^{-5})wt%

Figure 4.15 shows the shear rate versus shear stress for the two types of GO-based ternary hybrid nanofluids at various concentrations and temperatures. The GO-based ternary hybrid nanofluid behaves as a Newtonian fluid at higher concentrations, indicating that shear stress is linearly proportional to the shear strain in the fluids at all the measured temperatures. On the other hand, in the rGO based ternary hybrid nanofluids, the shear stress is not proportional to the shear strain. The GO-based ternary hybrid nanofluids, even though they behave as a Newtonian fluid at a higher concentration of nanoparticles, gradually behave as a shear-thinning or pseudoplastic

fluid as the concentration decreases. For instance, it can be seen from the plots that at a particular level of serial dilution (concentration C) and room temperature (25°C), it behaves like a shear-thinning or pseudoplastic fluid. In contrast, at a higher temperature (30°C to 50°C), it behaves as a Newtonian fluid where the shear stress and shear rate are linearly proportional.

4.3.3.2 Effect of Ternary Hybrid Nanoparticle Type on Concentration

The shear stress and shear strain are a function of concentration and temperature. Studies have revealed that the water-based nanofluids behave as a Newtonian fluid at a lower concentration of nanoparticles in the fluid (Halelfadl et al., 2013) and as a non-Newtonian fluid at higher concentrations (Kole and Dey, 2013). The nanofluids behaved as shear-thinning fluids when the concentration of the nanoparticles increased (Halelfadl et al., 2013).

A side-by-side comparison between the GO and rGO based ternary hybrid nanofluids is made. The GO-based ternary hybrid nanofluid behaves like a Newtonian fluid for sample A at temperatures ranging from 25°C to 50°C, while the rGO based Ternary hybrid nanofluids behave like a shear-thinning or plastic fluid for the same concentration for all temperatures. In the following plot for the second concentration (sample B), the GO-based Ternary hybrid nanofluids at lower temperatures of 25°C behave like a Newtonian fluid but start to show slight shear thinning behavior temperature is increased till the maximum measured temperature of 50°C. In contrast, rGO based Ternary hybrid nanofluids behave as a shear-thinning fluid from the starting range of 25°C till 50°C. The measurements on concentration (sample C), the GO-based Ternary hybrid nanofluids at 25°C behave like a shear-thinning fluid but tends to be a

Newtonian fluid once the temperature is increased from 30°C until the final measured temperature of 50°C.

The concentrations (sample D and E), the GO-based Ternary hybrid nanofluids behave like a shear-thinning fluid at all measured temperatures ranging from 25°C till 50°C, while the rGO based nanofluids follow the same trend and behave like a shear-thinning fluid at all measured temperatures and concentrations. There can be many reasons behind the nanofluid behavior as Newtonian fluids at higher concentrations and as a pseudoplastic behavior at lower concentrations. The particle-to-particle interactions at higher concentrations are more robust, and hence it retains as a Newtonian fluid. Once the shear rate and temperature increase, the particle-to-particle interactions become weaker, and the attractive forces diminish, forcing the nanofluids to behave as pseudoplastic fluid.

The GO-based ternary hybrid nanofluids ultimately behave as dilatant or shear thickening fluid on further reduction of concentration. This influence of the concentration of the nanoparticles in the fluid may be due to the higher inter-particle forces in higher concentrations (Ahammed et al., 2016). These higher inter-particle forces influence the nanofluids to remain Newtonian (Kaggwa and Carson, 2019). At the same time, the rGO based nanofluids remain consistently as shear thickening or dilatant fluids in all concentrations and temperatures. This may be due to the lesser number of oxygen molecules in the rGO nanoparticles. Agglomeration structures formed in the nanofluids during the shearing process get diminished to an orderly arrangement within the shear rate range, as has been observed by recent research (Murshed and Estellé, 2017). Studies by yang et al. on Al₂O₃-diamond hybrid on DI water and silicone oil showed that the nanofluids tend to be Newtonian but due to agglomeration, but once the shear rate is increased, it tends to be non-Newtonian shear-

thinning fluids similar to the behavior of the GO-based nanofluids in our study (Yang et al., 2012). It is also because of the agglomeration due to van der Waals forces' dominance at lower shear rates. The agglomeration breaks down at higher shear rates, leading to reduced viscosity, substantially making the fluid behave as a non-Newtonian shear-thinning fluid.

4.3.3.3 Effect of Ternary Hybrid Nanoparticle Type on Temperature

Nanofluids at lower shear rates exhibit Newtonian behavior and non-Newtonian behavior at higher shear rates, as seen from the plots in figure 4.15. Many studies have shown that the temperature is directly related to change in rheological properties and the thermal conductivity of nanofluids (Colangelo et al., 2016). The rheological measurements on the two GO-based ternary hybrid nanofluids were done at temperatures ranging from 25°C to 50°C. It can be seen that the shear stress increases with the increase in shear rate and decreases with temperature. The trend in the GO plots shows that at a particular concentration (sample C) and lower temperature (25°C), the fluid shows dilatant or shear-thinning behavior. Still, when the temperature increases (30°C to 50°C), the nanofluid exhibits Newtonian behavior. On further dilution at a concentration D, the nanofluids ultimately exhibit shear-thinning or pseudo plastic behavior irrespective of the temperature. The rGO profiles, on the other hand, exhibit shear thinning or pseudoplastic behavior on all concentrations and temperatures.

4.3.4 Amplitude sweep

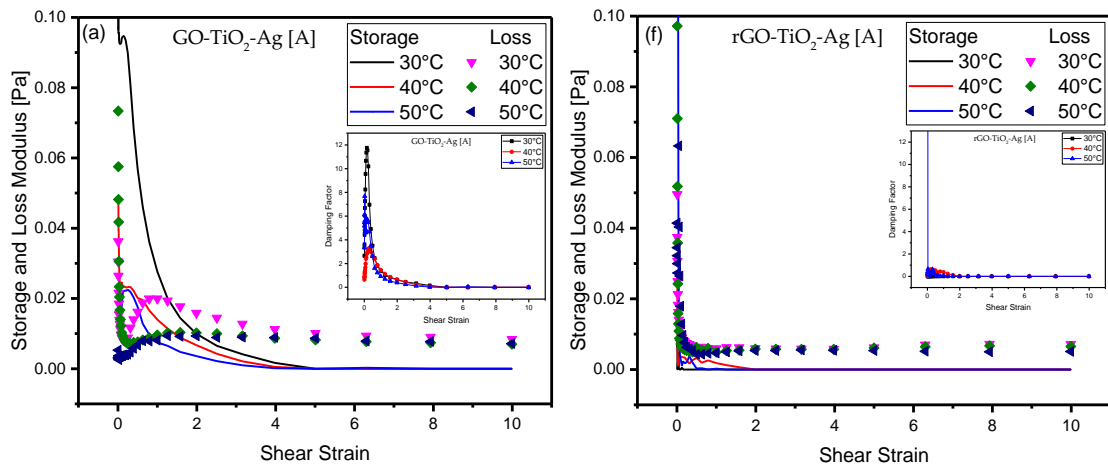
The linear viscoelastic (LVE) is a region that indicates the range in the fluid in which the stresses are tested without destroying the fluid structure. The LVE measurements are another set of rheological measurements that can be determined by measuring stresses divided into storage (G' - elastic) and loss (G'' - viscous) moduli. The loss and

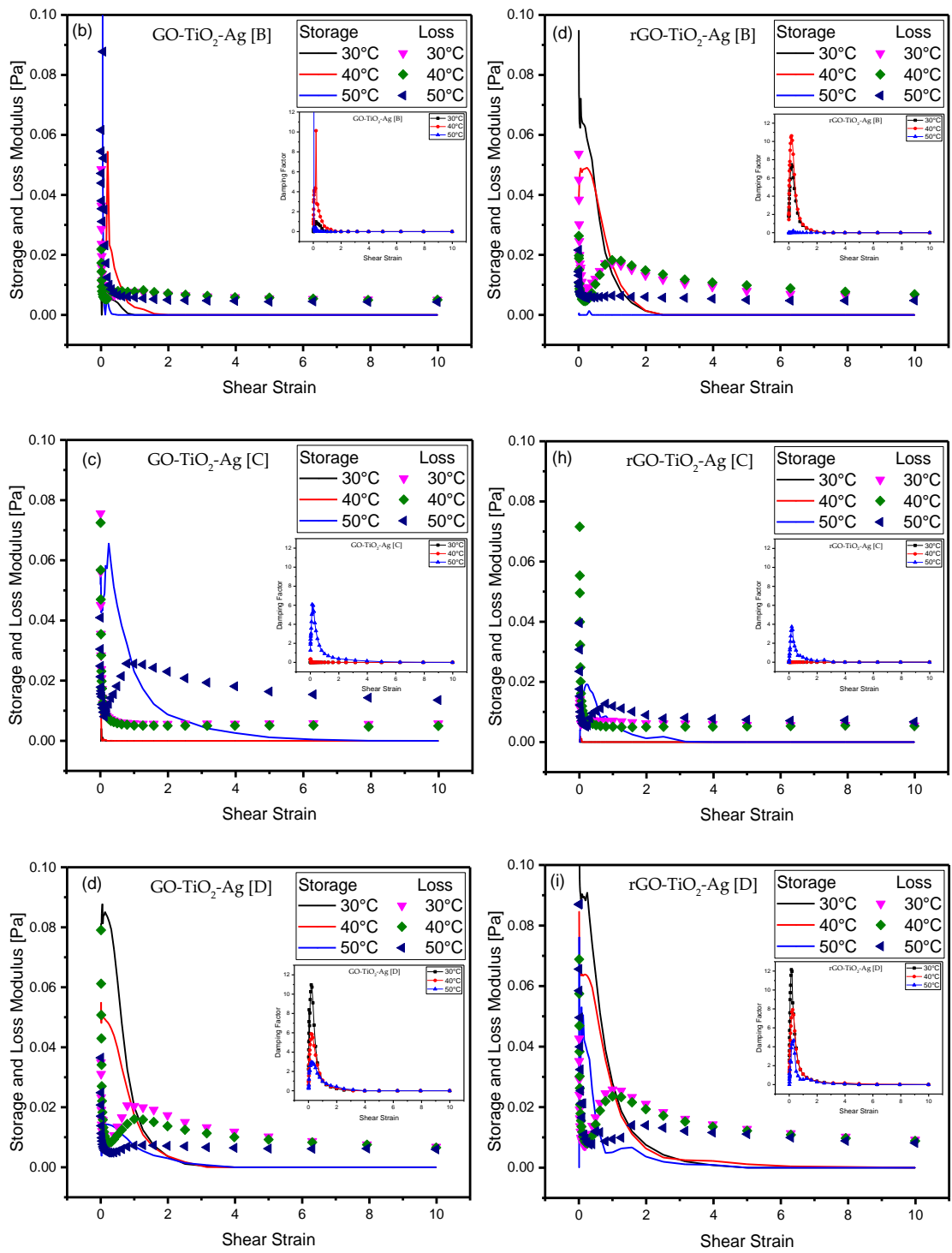
storage moduli show the mechanical properties of the nanoparticles under low oscillatory shear. It is the range with the lowest strain values. The G' in the LVE region shows a constant value, which is also called the plateau value. These measurements are done using the rheometer in which the spindle performs oscillatory motions of stress range between 0.01 and 10 Pa at a constant frequency of 1 Hz. If $G'' > G'$, then the fluid can be termed a viscoelastic liquid. When an external strain is applied to the fluids, the fluid-structure opposes the strains until a certain extent where the loss modulus G'' increases.

Then the fluid structure in LVE deforms, leading to the dismantling of the aggregations of the nanoparticles in the fluid. This will lead to nanoparticles in the fluids aligned to the flow field, which decreases the storage and loss of moduli in the fluid (Pastoriza-Gallego et al., 2011). The plots in figure 4.16 show the loss and storage moduli of the two GO-based ternary hybrid nanofluids. It can be seen that the curves demonstrate a similar qualitative feature with a sharp decline of high oscillating stresses and characterized by constant modulus or linear viscoelastic plateau. It can also be seen from the plots that the loss modulus is higher in the nanofluids with higher concentrations. There is a crossover area between the loss and storage moduli, which shows yield stress in the nanofluids, as mentioned by a few studies (Baek and Kim, 2011). At higher shear strain, the G' decreases indicating the loss of viscoelastic structure in the nanofluid. One striking feature is that at lower concentrations, both GO and rGO based ternary hybrid nanofluids, the loss modulus is almost similar, indicating the nanofluids lose the ability to lose or store stresses and remain constant at all measured temperatures. This indicates that the nanoparticles in the fluids enhance the rheological abilities like storage, damping, and loss moduli in the fluids. This may be

one of the reasons for the enhancement of thermal conductivity and other rheological properties.

Network structures are formed in the nanofluids at higher particle concentrations at lower stresses or frequencies, as reported by some studies (Jung et al., 2012). It is noted from the plots that the critical external strain is independent of all concentrations of the fluids. It should be noted that the base fluids exhibit a Newtonian behavior. Still, with the addition of ternary hybrid nanoparticles in the base fluids, it transitions to viscoelastic behavior, shear-thinning or pseudoplastic behavior in our case, and dilatant in other cases. A damping factor is a dimensionless unit that can be described as the ratio of loss over storage moduli (G''/G'), denoted by the term $\tan\delta$. The ideal value for the damping factor for a liquid in the viscoelastic region is always greater than unity ($\tan\delta = G''/G' > 1$) (Pastoriza-Gallego et al., 2011). The damping factor plots are shown in figure insets in each plot.





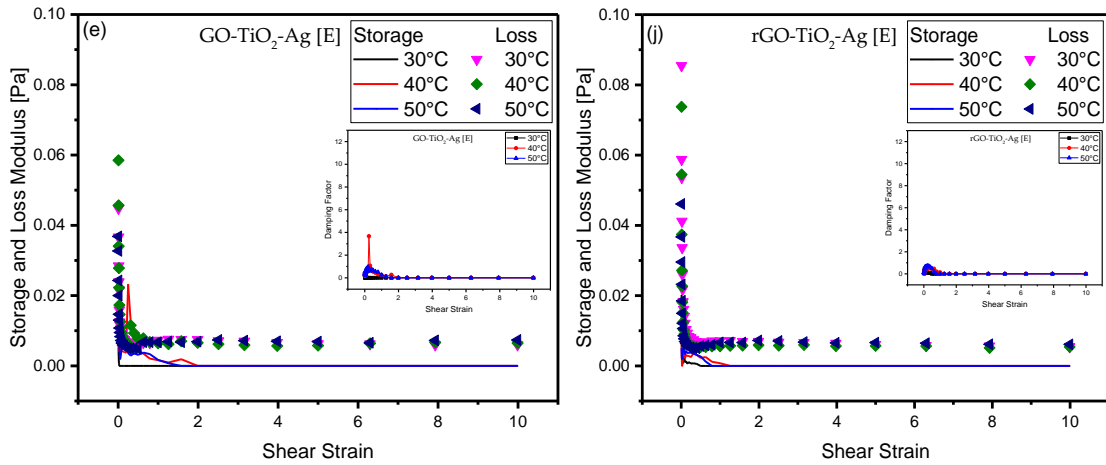


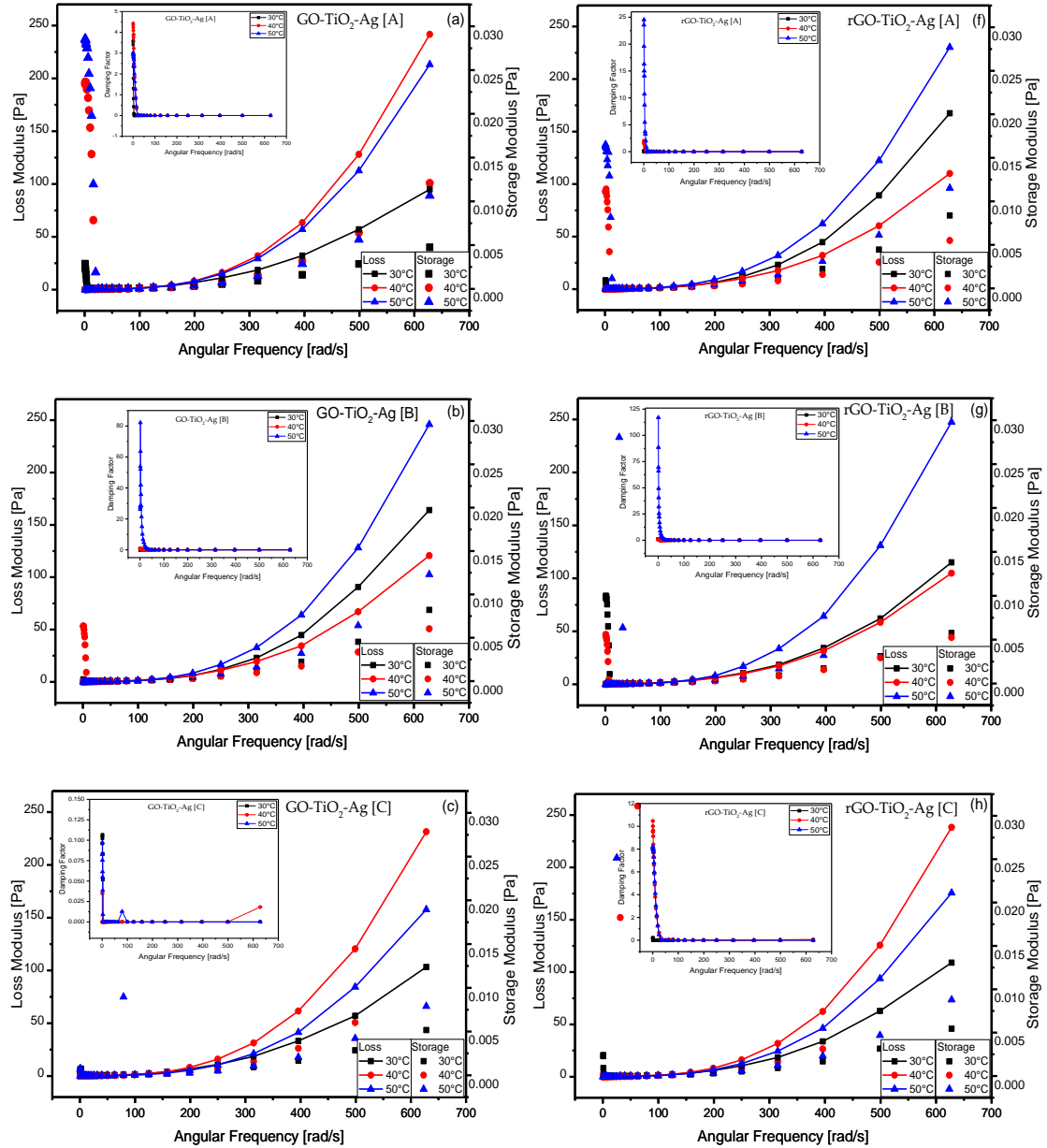
Figure 4.16 Amplitude sweep – Storage modulus and Loss Modulus Vs. Shear stress and their damping factor (Inset) at different temperatures Plots a, b, c, d, and e are GO-TiO₂-Ag samples of concentrations A(5×10^{-1})wt%, B(5×10^{-2})wt%, C(5×10^{-3})wt%, D(5×10^{-4})wt%, and E(5×10^{-5})wt%, and f, g, h, I and j are rGO-TiO₂-Ag samples of concentrations A(5×10^{-1})wt%, B(5×10^{-2})wt%, C(5×10^{-3})wt%, D(5×10^{-4})wt%, and E(5×10^{-5})wt%

4.3.5 Frequency sweep

Frequency sweep tests are carried out to measure the time-dependent behavior of the nanofluids in a non-destructive deformation range. It is a valuable tool to measure the stability of nanofluids. It helps to quantify zero shear viscosity for viscoelastic liquids. Frequency sweeps can be measured by using fast-moving high-frequency stimulation or slow-moving low-frequency stimulation (figure 4.17).

The frequency sweeps were measured in the LVE region with angular frequencies ranging from the frequency range of 0.1 Hz to 10 Hz (0.628 rad/s to 62.831 rad/s) by applying oscillatory stress of 0.05 Pa. The loss and storage moduli are similar and practically constant in all the concentrations of the measured ternary hybrid nanofluids. The measurements show that at higher frequencies, both the storage and the loss moduli increase. The damping factor is shown in figure insets. The damping factors are higher only in the viscoelastic region with low angular frequency. On increasing the frequency, the damping factor is minimum and uniform across all the concentrations and

independent of temperature. Both the GO and rGO based ternary hybrid nanofluids exhibit a similar trend for the damping factor. The damping factor decreases exponentially with the increase in angular frequency.



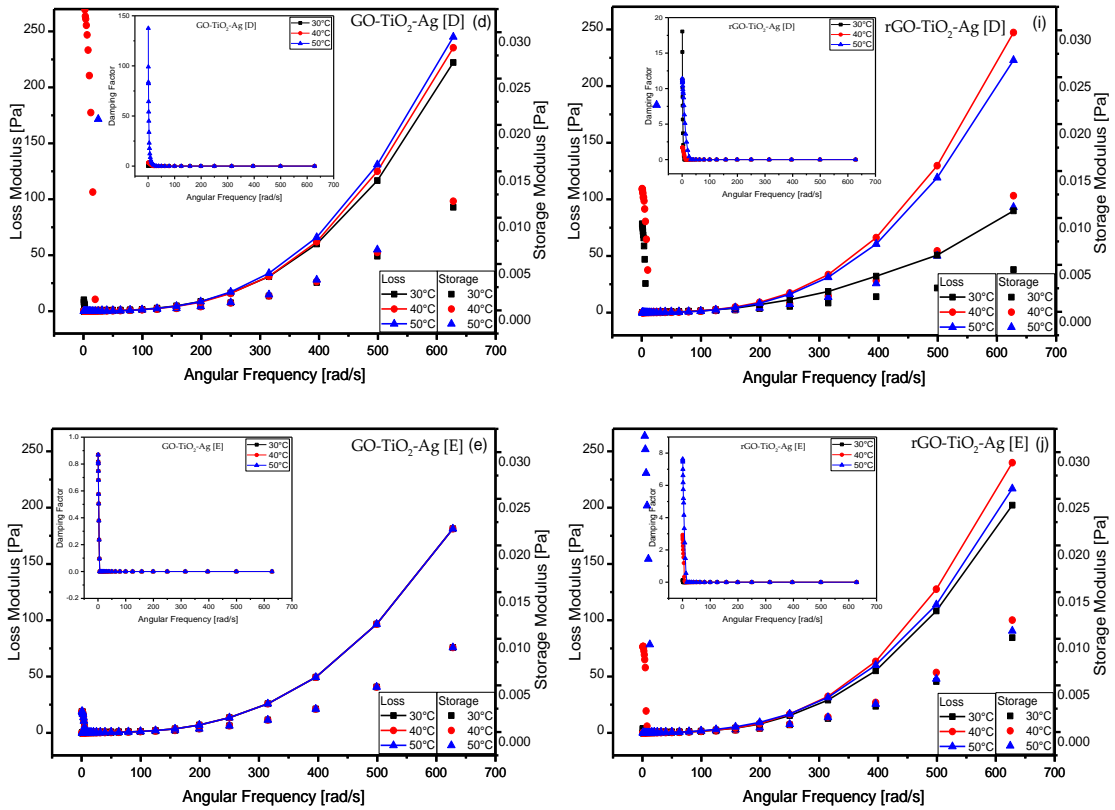


Figure 4.17 Frequency sweep – Storage modulus and Loss Modulus Vs. Angular frequency and their damping factor (Inset) at a different temperature at different temperatures Plots a, b, c, d, and e are GO-TiO₂-Ag samples of concentrations A(5×10^{-1})wt%, B(5×10^{-2})wt%, C(5×10^{-3})wt%, D(5×10^{-4})wt%, and E(5×10^{-5})wt% and f, g, h, I and j are rGO-TiO₂-Ag samples of concentrations A(5×10^{-1})wt% B(5×10^{-2})wt%, C(5×10^{-3})wt%, D(5×10^{-4})wt%, and E(5×10^{-5})wt%

4.4 EFFECT OF TERNARY HYBRID NANOPARTICLES ON DNA DENATURATION, PCR ENHANCEMENT, AND SEQUENCING

Different nanoparticle at various concentrations was used to enhance the PCR reactions (Ali et al., 2018; Aysan et al., 2017; Dantas et al., 2017; Gabriel et al., 2018; Liu et al., 2019; Zhang et al., 2013; Sang et al., 2017; Shen & Zhang, 2013; Upadhyay et al., 2020; Yuan et al., 2016). Since this section is the core objective of this study, which is to enhance the efficiency of PCR, the importance of nanoparticle-based PCR enhancement and its mechanisms areas addressed in introductory section 1.2. In this section, PCR experiments were conducted on a set of extracted DNAs with and without ternary hybrid nanoparticles to study the enhancement characteristics. The PCR products were then gel eluted to check the bands, and then the intensity of the band is studied through a digital camera. Quantification of the band intensity was done to quantify the intensity of the bands. The reactions were iterated several times to check the correctness and optimize the proper concentration of the DNA, giving us the most enhancements. The PCR product was then sent to sequencing, and the amplification was studied and detailed. The detailed methodology of this study is presented in section 3.6. Further, the DNA denaturation study was conducted using a spectrophotometer to study the effect of nanoparticles on the denaturation process at various temperatures and nanoparticle concentrations.

4.4.1 Effects of THNp in Reduction of PCR Reaction Times / PCR Efficiency

Graphene oxide is a mono-atomic layer of hybridized carbon atoms. It is widely used in PCR amplification owing to its high specific area, ability to conduct better heat transfer, and highly biocompatible. When synthesized into a ternary hybrid nanoparticle along with silver and titanium oxide, which have their unique characteristics, Graphene performs better as a nanoPCR material compared to using as a single nanoparticle.

Amplification was done on the plasmid DNA with different concentrations of nanofluids mixed with the PCR master mix. The two types of graphene-based nanofluids enhanced the PCR reaction and brought down the number of cycles from 40 to 30 cycles, reducing 10 cycles.

The concentration of nanoparticles in the nanofluid played a significant role in the reduction of cycles. Both GO, and rGO based nanofluids at a concentration of 5×10^{-3} wt% enhanced the PCR product while reducing the number of cycles from 40 to 30 without decreasing the amount of amplified product compared to the control reaction (without the addition of nanofluids in the PCR), achieving a reduction of 10 cycles or about 25% cycle reduction. This suggests that with the addition of ternary hybrid nanoparticles-based nanofluids, many cycles have been reduced, as seen from figure 4.19.

Further PCR experiment showed improvements more than the initial experiment. The two Graphene oxide (GO and rGO) based ternary hybrid nanoparticle performed better as a nanoPCR additive. The experiments were carried out using 25 and 35 cycles in the PCR gave almost equal quantification of enhancement, which shows that the nanoparticles reduce the reaction time considerably for similar output with a reduction of 10 cycles or 25%. Visible bands were observed in gel electrophoresis for both 25 and 35 cycles and the control group (master mix without nanoparticle) as seen from Figures 4.20 and 4.21. The robust amplification of PCR products suggested the efficiency of the nanofluids in the enhancement of PCR output improvement. It was also noted that the concentration of nanoparticles in the nanofluid played a significant role in reducing cycles. Lower concentrations of both GO and rGO based ternary hybrid nanofluids enhanced the PCR product while reducing the number of cycles without decreasing the amount of amplified product compared to the control reaction (without

nanofluids' addition the PCR). This suggests that with the addition of ternary hybrid nanoparticles-based nanofluids, a considerable number of cycles can be reduced without compromising the quantity of the PCR product.

4.4.2 Effects of THNp on PCR yield

Several parameters affect the enhancement of NanoPCR amplification and efficiency. The thermal conductivity of the nanofluids, the concentration of the particle in the nanofluids, shape of the nanoparticle, type of base fluids used, additives, and stabilizers used, the acidity of the nanofluids used, etc. (Sun et al., 2020). Even though not all these aspects are investigated in this study, few aspects showed promising results. The Plasmid DNA was amplified in the PCR along with two types of GO-based ternary hybrid nanofluids. The PCR product after the gel analysis and the quantification of the band intensity analysis showed that the nanoparticle concentration played a role in the enhancement of PCR reaction. The results indicated that the optimum mixture of the nanoparticles in the fluids yielded higher amplification than the control of DNA amplification.

Band intensities are quantified and plotted as shown in figure 4.18 illustrates that the concentration of 5×10^{-1} wt% and 5×10^{-2} wt% does not amplify as much as the concentration of 5×10^{-3} wt% of the GO-based ternary hybrid nanoparticles, which shows an increase of 12% along with a 40% reduction of the number of cycles. Repeated experiments confirmed the results and indicated that the ternary hybrid nanoparticles' optimum concentration was 5×10^{-3} wt% for both GO and rGO based ternary hybrids. The reaction was also carried out for DNA without the addition of ternary hybrid nanofluids to confirm that nanoparticles enhance the PCR reaction and not by any impurities in the reaction mixture. The reaction was carried out with a supernatant of

nanofluids without nanoparticles; no PCR enhancements were observed, as seen in Figure 4.18 (a) and (b).

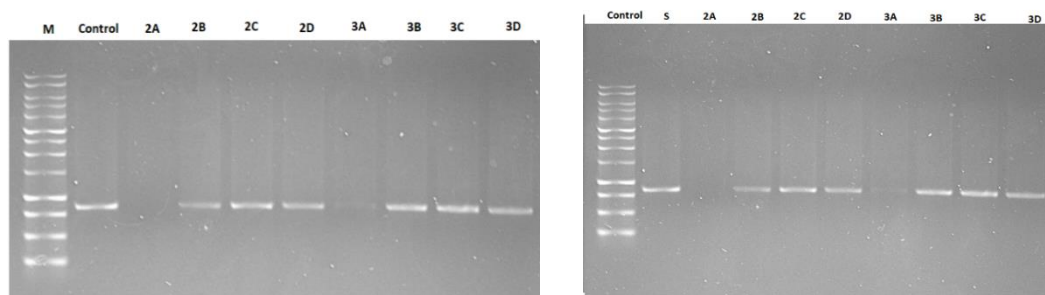


Figure 4.18 (a) and (b): The Lane control is for the marker, and the S is for positive control. The tag 2A to 2D represents the GO-TiO₂-Ag ternary hybrids mixture, while the 3A to 3D represents the rGO-TiO₂-Ag ternary hybrid mixture. The term A to D represents the concentration of the nanoparticles in the mixture.

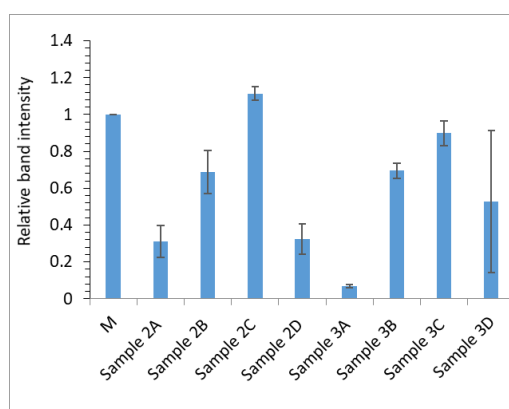


Figure 4.19: The Lane control is for the marker, and the S is for positive control. The tag 2A to 2D represents the GO-TiO₂-Ag ternary hybrids mixture, while the 3A to 3D represents the rGO-TiO₂-Ag ternary hybrid mixture. The term A to D represents the concentration of the nanoparticles in the mixture.

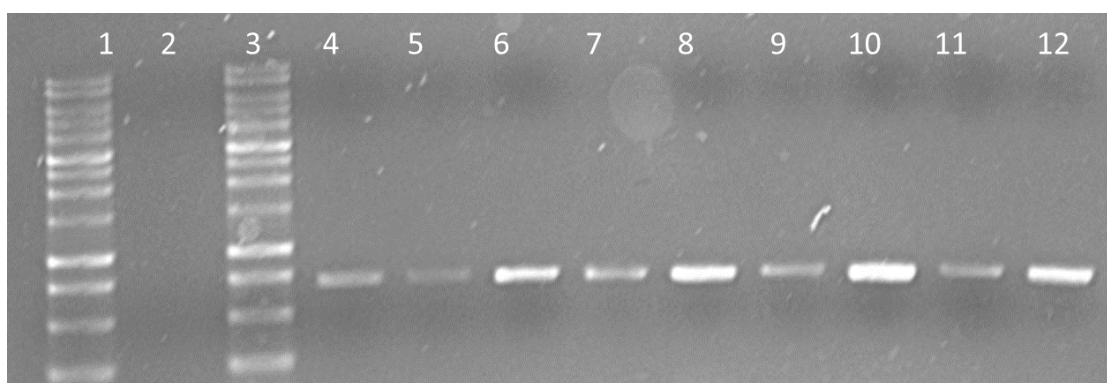


Figure 4.20 (a) lanes (1 and 3) 1kb ladder; (2,5,7,9, and 11) PCR amplicon amplified using 25 cycle for negative control, sample treated with GO-TiO₂-Ag nanofluid at

different concentration. (4,6,8,10,and 12) PCR amplicon amplified using 35 cycles for the negative control, the sample treated with GO-TiO₂-Ag nanofluid at different.

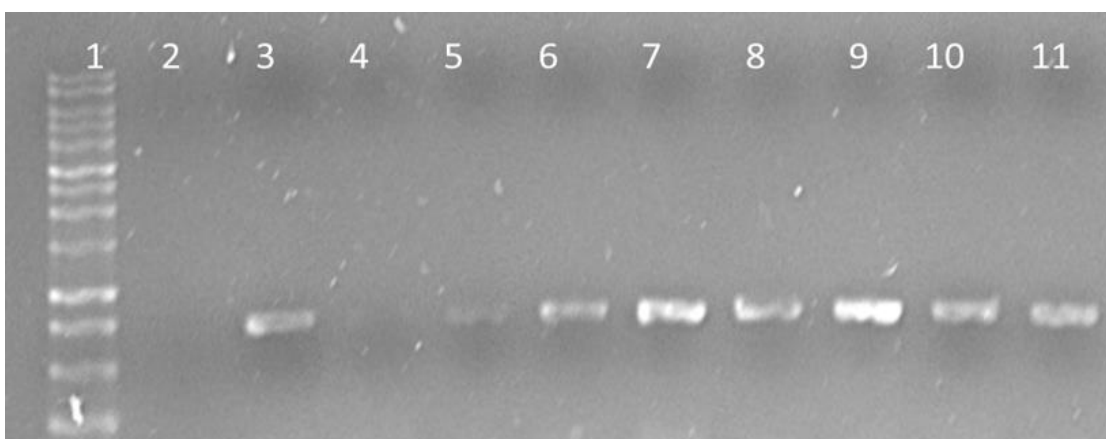


Figure 4.21 (b) lanes (1) 1kb ladder; (2,4,6,8, and 10) PCR amplicon amplified using 25 cycles for the negative control, the sample treated with rGO-TiO₂-Ag nanofluid at different. (3,5,7,9, and 11) PCR amplicon amplified using 35 cycles for the negative control, the sample treated with rGO-TiO₂-Ag nanofluid at different concentrations.

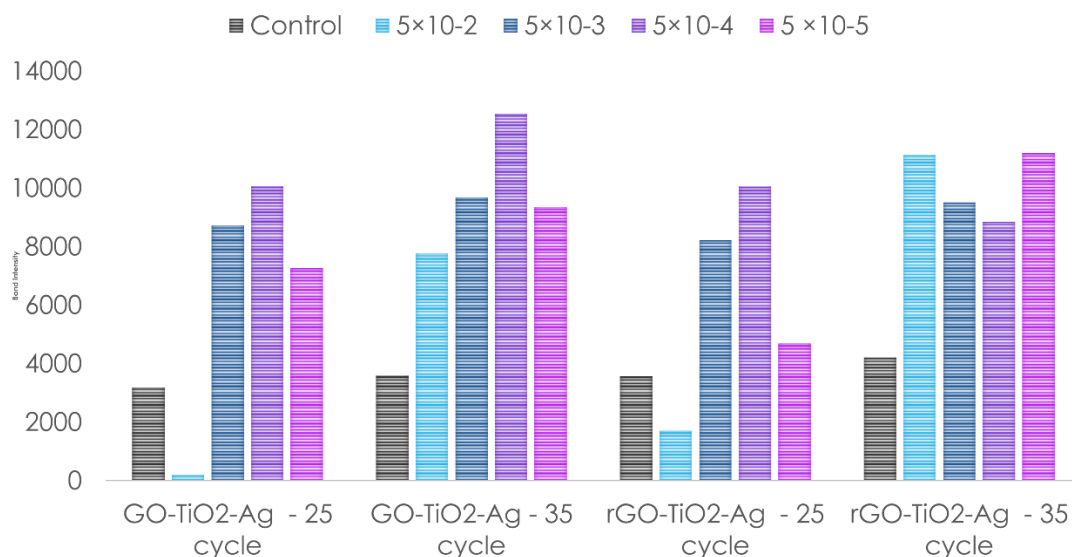


Figure 4.22: Quantification of band intensity of the gel electrophoresis of GO-TiO₂-Ag and rGO-TiO₂-Ag with 25 and 35 cycles.

There are two possibilities involved in a nanoPCR process regarding the interaction with the ternary hybrid nanoparticles in the mixture. THNp might interact with single-

strand DNA in the PCR or interaction between the THNp and the polymerase. Both these interactions should be taking place on the surface of the THNp. Several other nanoparticles were also found to be enhancing the PCR reactions like AuNP (Huang et al., 2008) and other additives such as non-ionic detergents, betaine, etc., to name a few. However, most of their enhancing mechanisms are still a hypothesis. The THNp in the PCR mixture will enhance the reaction mixture's thermal conductivity, which may also contribute to enhancing and optimizing the PCR reactions since the THNp is proved to be better thermal conducting fluids according to our own separate thermal conductivity measurements. The THNp in the mixture may assist the initial steps of PCR by enhancing the thermal conductivity of the reaction mixture, which might result in the earlier denaturation of the DNA. Then during the annealing step, the THNp may get attached to the DNA strands due to Van der Waal's forces facilitating the interaction between the PCR reagent mixture and during the extension step of the PCR cycle, the THNp may dissipate the heat, which will lead to early finishing off of the PCR cycle (Khaliq et al., 2012). It is still difficult to pinpoint the mechanism responsible for the enhancements since it involves many materials such as DNAs, Primers, Polymerase, dNTPs, or Proteins in the PCR mixture.

Contrary to the initial experiment, the following PCR experiment showed much higher enhancements. The experiments showed that the PCR yield had been enhanced with the nanofluids. The enhancement was mainly due to the addition of nanoparticles in the PCR mixture. For 35 cycles, GO-TiO₂-Ag nanofluid exhibited the highest increase in PCR yield, with maximal enhancement at a concentration of 5×10^{-4} wt%. From figure 4.20, the GO-TiO₂-Ag nanofluid band was 16.74-folds more intense than the negative control (PCR sample prepared with nuclease-free water without nanoparticles). Similarly, from figure 4.21, rGO-TiO₂-Ag nanofluid exhibited the

highest increase in PCR yield at the concentration of 5×10^{-4} wt% rGO-TiO₂-Ag nanofluids bands were 2.82- and 3.15-fold respectively, more intense than the negative control, even though the control band was 2.09- and 15.30- fold more intense than them at the concentration 5×10^{-2} wt. Figure 4.22 shows the quantified data of the amplification.

4.4.3 Effects of THNp on DNA/PCR Amplification

Single round PCR was performed to determine the effect of different concentrations of two GO-based THNp on the amplification of EGFP plasmid DNA. Gene-specific primers forward primer (5'-CCCACTGCTTACTGGCTTATC-3'), EGFP reverse primer (5'- CCATGTGATCGCGCTTCT -3') were used in this study resulted in inaccurate amplification of target DNA (800bp length). As shown in figure 4.18, the presence of THNp does not lead to nonspecific PCR product binding, and it was apparent when the PCR product was visualized in 1% agarose. Visual observation of band intensities is also prominent compared to control (sample with no nanoparticle) samples with different dilutions of nanoparticles in the fluid.

When the concentration of nanoparticles is decreased in the master mix at the rate of 10 times dilution starting from the stock solution (with the concentration of 5×10^{-1} wt %), there is a substantial increase in the band intensity observed regardless of different THNPs employed. However, a significant increase in band intensity was observed in samples 2C and 3C (representing 100 times dilution, 5×10^{-3}). Strikingly, the addition of THNPs with two other dilutions (stock and ten times dilution) did not interfere negatively in yielding PCR amplicon. This indicates that target sequence amplification was uninhibited when different concentrations of THNPs were employed to enhance the PCR efficiency. Similar observations were documented in earlier studies

when graphene oxide (GO) nanoparticle was used in different concentrations to amplify PEGFP-N1 vectors containing the coding sequence of the FOXL2 gene (Khaliq et al., 2010).

The optimum dilution observed in this study was the 100th dilution, and it indicates that the concentration of THNPs is crucial in obtaining optimal PCR results. Though PCR bands were observed in Sample 2D and 3D, the intensity gradually reduced compared to control and sample 2C and 3C, respectively. The results also showed the specificity of primer hybridization and extension did not influence the addition of different concentrations of THNPs used in PCR reaction. No hurdles were observed in primer extension or conditions such as primer mismatch, indicating that the addition of THNPs in the PCR master mix could enhance the PCR amplification without compromising the product yield and product specificity.

4.4.4 Effects of THNp on DNA Sequencing

Based on the existing literature, none of the studies to date has addressed the effect of adding nanoparticles at the DNA sequence level. In order to address this, the same gene (EGFP) was amplified using different concentrations of 2 THNPs in the conventional PCR setup. The chromatogram was inferred using a Bio-edit sequence alignment editor to identify noise during sequencing. Each sequence was truncated at 5' and 3' end to avoid initial and final noise during the sequencing process. However, noticeable baseline noise was observed in all the middle of the sequencing. This might probably be due to the affinity of THNPs towards the salt present in the sample. Earlier works have demonstrated high salt concentration, incubation time, and agitation rate has significantly improved nanoparticle (Au) synthesis rate (Bhargava et al., 2016). The presence of noise in the sequence might probably be due to various conditions.

- 1) The amount of DNA templet or primer in the reaction tube,
- 2) The presence of inhibitory contaminants such as salt and phenols,
- 3) Non-specificity of the primers, and
- 4) The presence of two alleles in the DNA that code for the same gene

From the PCR amplification and efficiency enhancement study, it is evident that there were no issues with the amount of DNA template used or specific primers adopted in this study. PCR purification kit was used before sequencing to eliminate impurities. The only possible reason for the presence of noise in the sequence is due to the affinity of THNPs towards the salt. Figure 4.23 and Figure 4.24 illustrate the inbound noise observed in the sequences and the consequential impact on base pair mismatch. The detailed sequence in FASTA format is presented in appendix 1.

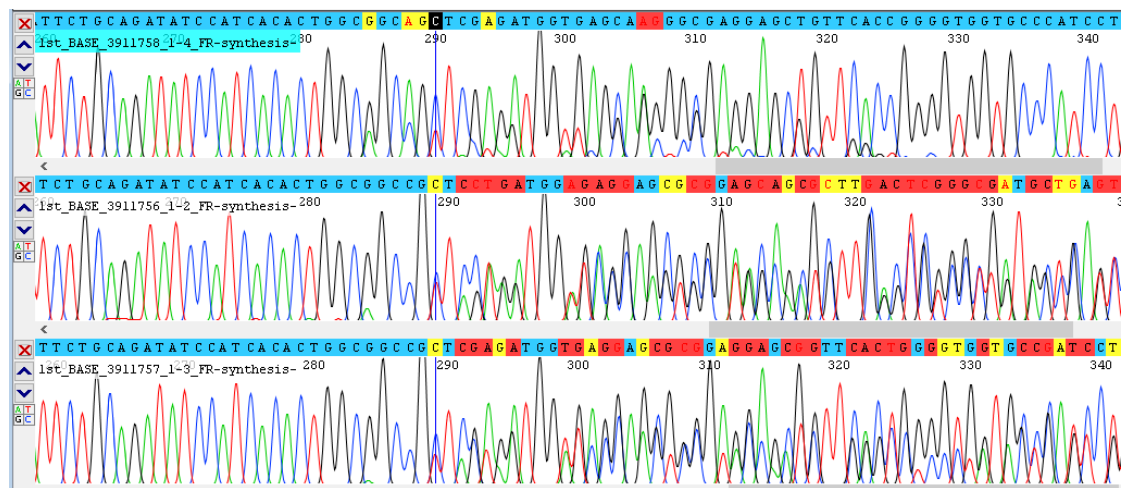


Figure 4.23 chromatogram noise observed in sequences

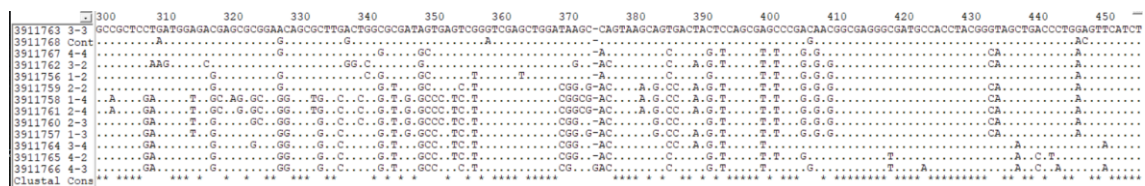


Figure 4.24 Bio-edit sequence alignment tool shows base pair mismatch after multiple pairwise sequence analysis using Clustal W v2.

The sequencing for the second PCR experiment showed a different result compared to the initial reaction. Manual screening of the raw sequence data was performed to identify chromatogram noise. Out of 34 sequences generated in this study, two samples showed deep chromatogram noise throughout the target sequence length (supplementary file 1). Hence, 32 sequences were further analyzed manually and aligned using the Clustal X2 (Larkin 2007). Multiple pairwise analysis (MPA) showed a well-conserved region of the target gene (partial COX1 gene of the mitochondrial DNA) with 630bp length. Analyzed sequences (n=32) were submitted to the NCBI genbank database and accessed through the submission ID: SUB8809298. Sequence analysis revealed no visible DNA damage in DNA break or single nucleotide polymorphism in the conserved region (Supplementary file 1).

Additionally, no sequence gaps were observed in the conserved cite indicating that THNp does not cause negative impact during the sequencing process. Studies have argued that ultrathin nanoparticles such as graphene could help achieve rapid DNA detection at single nucleotide resolution during the DNA sequencing because it can offer larger surface area and anchoring cites for the DNA to adsorb, shown in figure 4.25. To minimize the interaction of DNA molecules on GO and rGO during the sequencing, TiO₂ and Ag formed THNp, which exhibit high mechanical stability (Khaliq et al., 2010). In this study, we used two different concentrations of THNp (GO-TiO₂-Ag and rGO-TiO₂-Ag) as an additive to expedite the heating/cooling rate in the PCR in achieving the desired sequence quality and formation of no primer dimers in the sequencing process. Overall, the study demonstrated that adding different concentrations of THNps at least up to 0.05 wt% would not cause any observable DNA damage or mutation in the most commonly used cytochrome oxidase subunit 1 DNA

barcode reads. Many studies have argued the effect of different nanoparticles on enhancing the efficiency of different PCR techniques. However, to our knowledge, no studies were attempted to explore the impact of the addition of nanoparticles in post PCR applications such as genomic sequencing or cloning. From this experiment, we conclude that the THNP (GO-TiO₂-Ag and rGO-TiO₂-Ag) can be effectively used in PCR reactions to shorten the PCR reaction time without compromising the PCR amplicon quantity and qualitatively at the genome level. A graphical representation of nanoparticle interaction in the DNA sequencing is depicted in Figure 4.26.



Figure 4.25 Conserved region of cytochrome oxidase 1 gene showed in stars

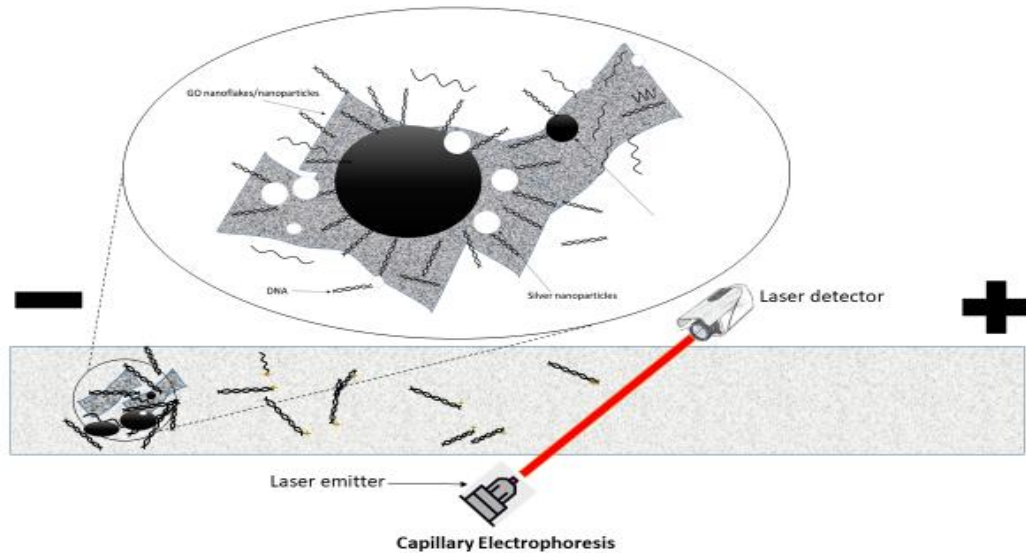


Figure 4.26 A graphical representation of nanoparticle interaction in the DNA sequencing is depicted.

DNA strands are cohesively attached to the ternary hybrid nanoparticles. Since the nanoparticle size is bigger than the DNA material, it can be said that the DNA material is not affected by unwanted reactions or damaged by the addition of nanoparticles. The presence of irregularly shaped graphene nanoparticles increases the surface area in the PCR master mix, which enhances the thermal conductivity of the reaction and, in turn, enhances the reaction's efficiency. The nanoparticles do not pass through the capillary tube towards the positively charged electrode in the capillary electrophoresis due to its positive or neutral charge (Lamminen, 2011).

4.4.5 Effects of THNp on DNA Denaturation

DNA denaturation refers to the melting or the opening of a double-stranded DNA into two single strands of DNA, which involves breaking the hydrogen bonds between the two strands of DNA in the duplex. In simple terms, it is the breaking down of DNA molecules for comparison or sequencing. This usually occurs at higher temperatures of around 92°C to 94°C, depending on the type of DNA used in the reaction. From the point of view of the heating aspect of the DNA strands and its stability is to stack the primer bases on top of the two DNA strands once it has un-winded. For the DNA to denature, the main complication is to overcome the binding energies of the hydrogens, which hold up the DNA in double strands of the base pairs. The bonding or the stacking energies are less for pyrimidine/purine (YR) steps and A: T-rich regions. The sequence of TATATA quickly melts in both the test tube and inside the cells (Ussery, 2013).

There are a few ways to denature DNA; the top methods include heating, chemical denaturation by adding NaOH and adding a high salt concentration. The three

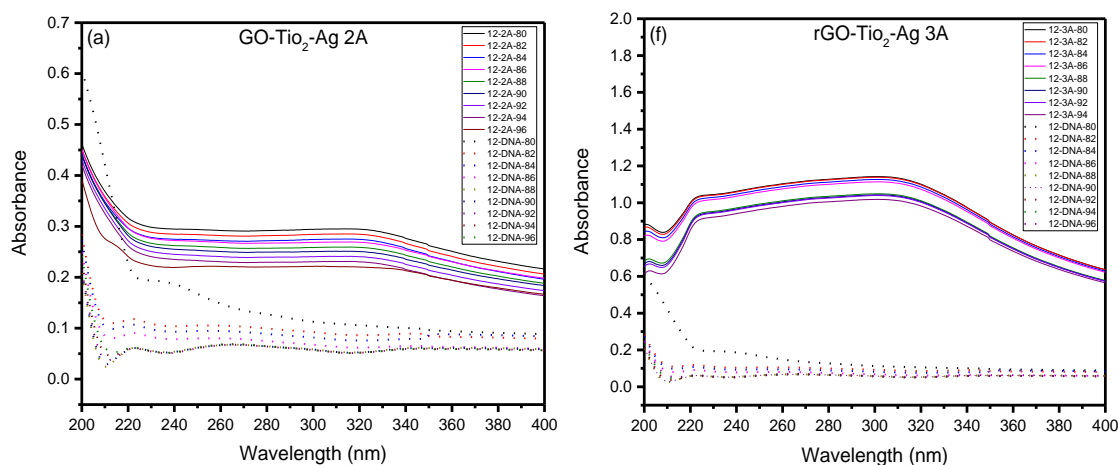
mentioned methods are used depending on the specific application. The most common method is to simply heat the DNA to a specific temperature above its melting point. The DNA unwinding the double strands of DNA can be monitored by using a spectrophotometer, which uses the principle of focusing UV light through a transparent cuvette and measuring the DNA's absorbance. The DNA usually has a strong absorbance at 260nm. The denaturation can determine once there is an increase in absorbance of UV light in the spectrophotometer until it has completely melted or unwinded to two single strands. Then the absorbance will remain constant even on a further increase of temperature or heating. The higher absorbance of UV light by the single-strand DNA is called the hypochromic effect, as it absorbs 50% more light than the dual strand before the melting point. The denaturation process is reversible, and it occurs once the temperature is lowered below the melting point, and it is known as renaturation. The time taken for renaturation can be used to determine the repetitive fractions and DNA base composition.

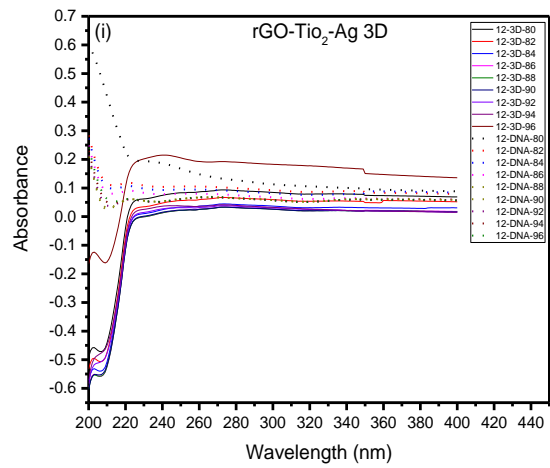
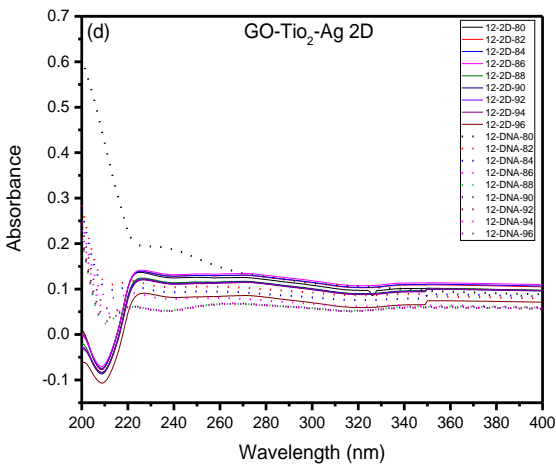
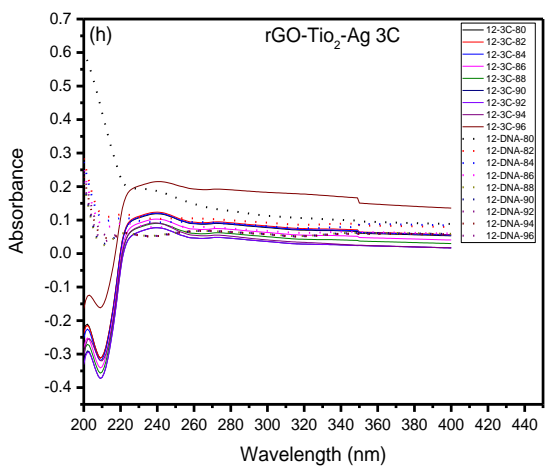
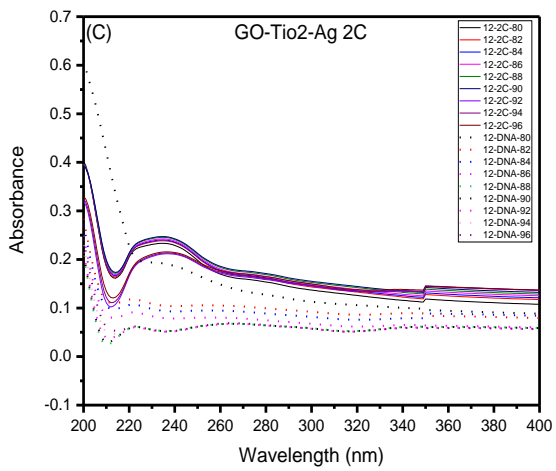
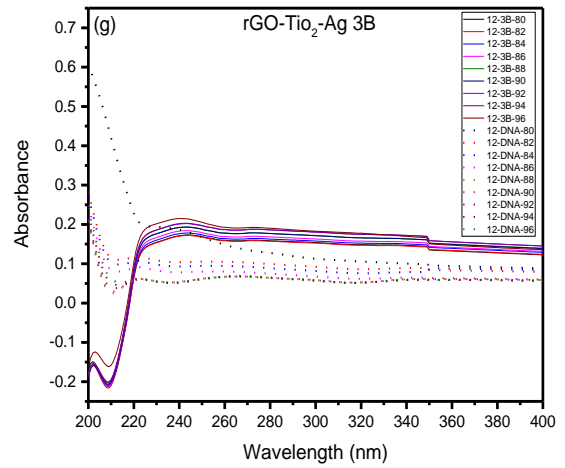
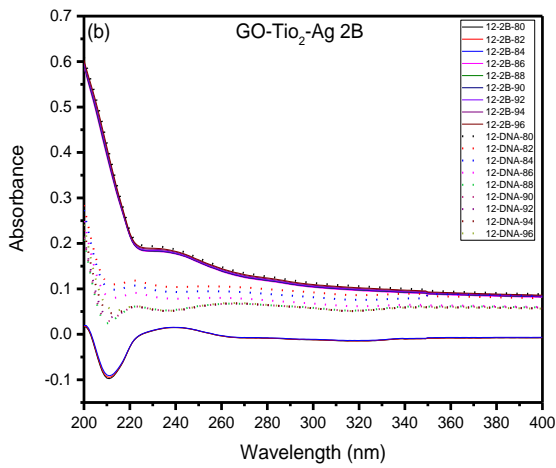
The melting point or the T_m will vary for different DNA based on many factors such as length of the DNA strand, base composition, topological condition of DNA, the composition of the buffer, etc. shorter strand of DNA will have a shorter melting time and will melt easily compared to a longer strand of DNA. Since the melting point of DNA has so many dependant variables, it is difficult to accurately predict the exact melting temperature of the given DNA sequence. DNA denaturation was done in a spectrophotometer with Two DNA samples (named 12 and 27) of concentration 1.793 and 1.895 along with the synthesized graphene-based ternary hybrid nanofluids (GO-TiO₂-Ag and rGO- TiO₂-Ag) with five levels of concentrations.

Figure 4.27 and 4.28 below shows a series of the absorption plots of the DNA samples with and without the addition of THNp. Thermal studies of DNA in the

presence of THNp using a spectrophotometer can give us a more in-depth insight into the behavior of DNA denaturation. The denaturation measurements were carried out in various temperatures starting from 80°C to 96°C. The measurements plots for GO-TiO₂-Ag and rGO-TiO₂-Ag are presented side by side based on the concentration. It will be helpful in the comparison between the two different THNp of the same concentration. From Figures 4.27 and 4.28, it is evident that the absorbance of the DNA in the presence of THNp is much higher than the DNA without THNp. The GO-based THNp peaks at a wavelength of 200nm, while the rGO based THNP peaks at around 300nm. The nanoparticles tend to aid the process of denaturation even at 80°C. Observations from the series of plots of DNA in the presence of both GO and rGO based THNp, it is evident that the absorbance is higher at the higher concentrations of nanoparticles in the fluids. When the concentration is decreased, the absorbance is decreased, making the absorbance peaks of the DNA flat after 240nm.

At the lowest concentration of the nanoparticles, the absorbance curves are almost in sync with that of the absorbance of plain DNA in the absence of THNp. Interestingly, at the lowest concentration of the THNp, their absorbance is negative, which indicates that the UV light passing through the DNA samples in the presence of THNp gives out a greater intensity of light. It may have important significance.





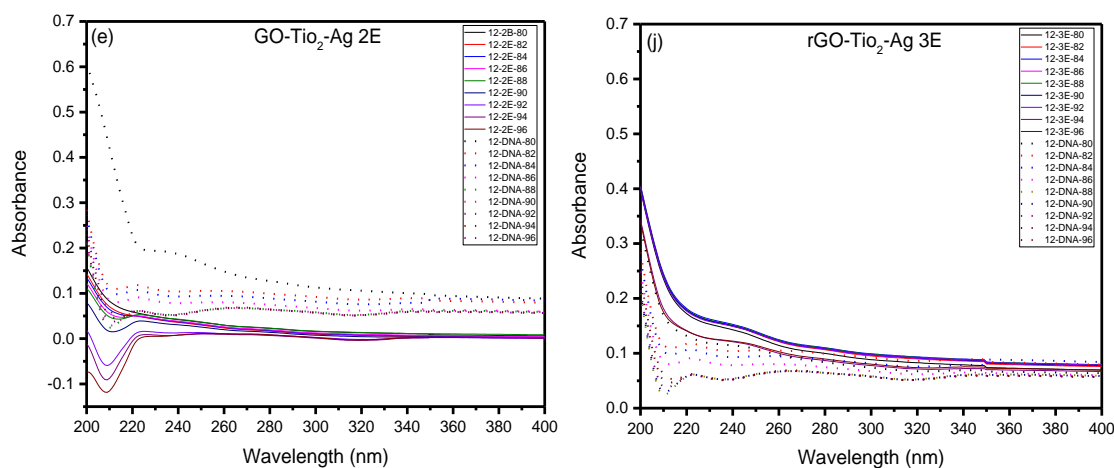
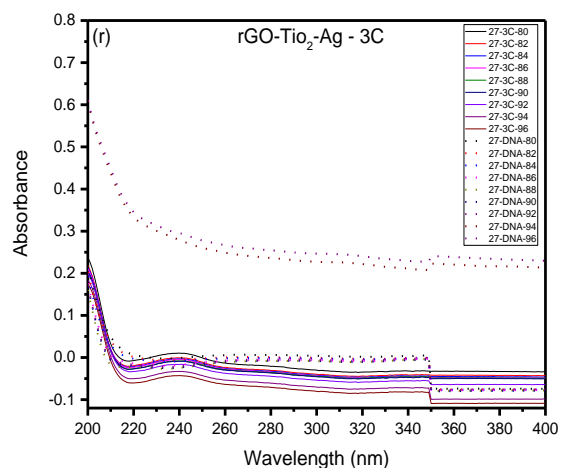
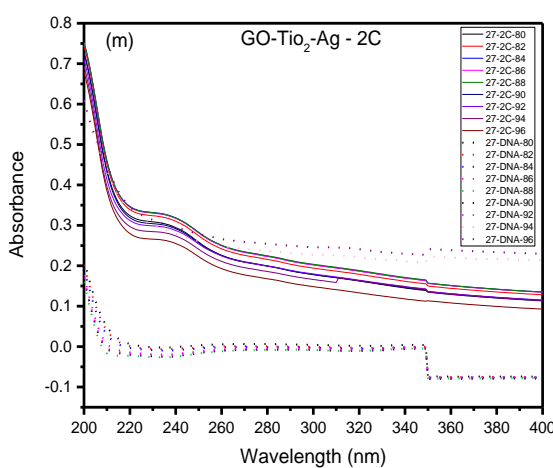
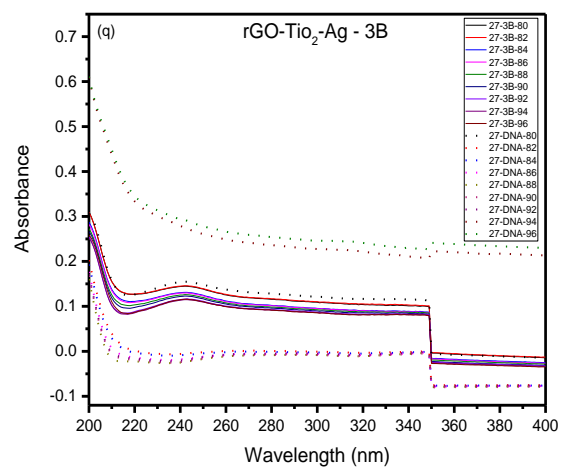
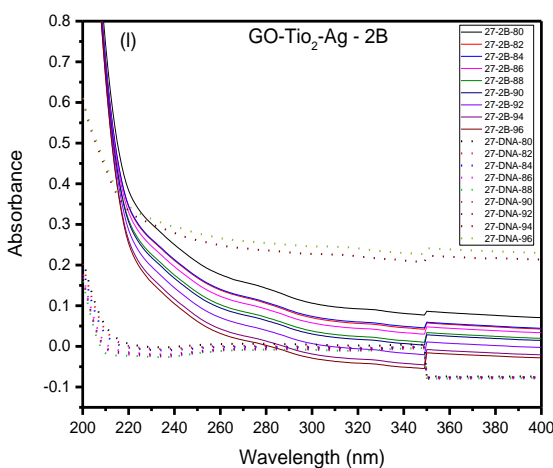
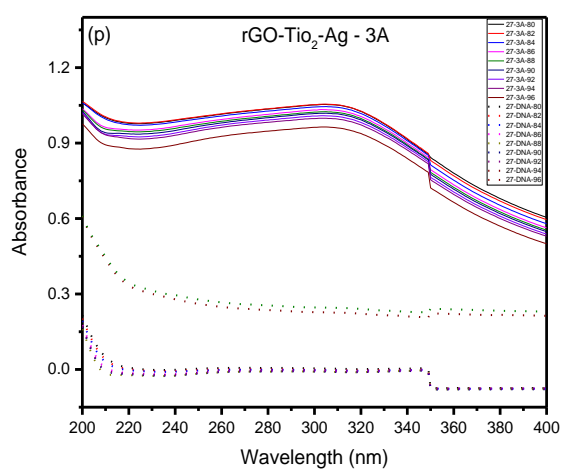
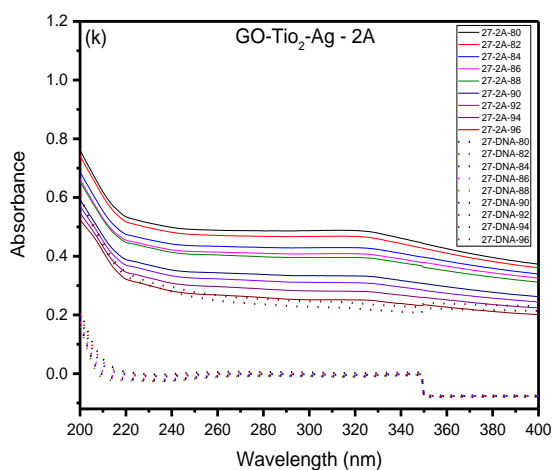


Figure 4.27 DNA – 12, plots a, b, c, d, e are GO-TiO₂-Ag samples of concentrations A(5×10^{-1})wt%, B(5×10^{-2})wt%, C(5×10^{-3})wt%, D(5×10^{-4})wt%, and E(5×10^{-5})wt%, and f, g, h, I, j are rGO-TiO₂-Ag samples of concentrations A(5×10^{-1})wt%, B(5×10^{-2})wt%, C(5×10^{-3})wt%, D(5×10^{-4})wt%, and E(5×10^{-5})wt%

The plots in Figure 4.27 and 4.28 shows the DNA samples with THNp of the different DNA samples. The DNA concentration of 6.493 ng/ μ l and is much lower than the previous measurements. Similar absorbance patterns can be seen in these plots, except that the absorbance of the rGO based THNp added to DNA samples shows higher absorbance for the same concentration of nanoparticles. The trend seems to be similar to a higher concentration of the nanoparticles in DNA samples, shows higher absorbance in all measured temperatures, and the absorbance is lower in the lower concentration of nanoparticles in the samples. Plot I has a higher absorbance at a wavelength of 220nm, which shows that the THNp induces earlier denaturation of DNA at significantly lower temperatures when compared to samples of DNA without the nanoparticles. With the reduction of nanoparticles in lower concentration samples, the absorbance shows a negative value, which indicates that there is more UV light emitted. The stark difference between the GO and rGO based THNp is that The GO-based

samples have higher absorbance even at lower concentrations, and negative absorbance is not observed in any of the samples, unlike rGO based samples.



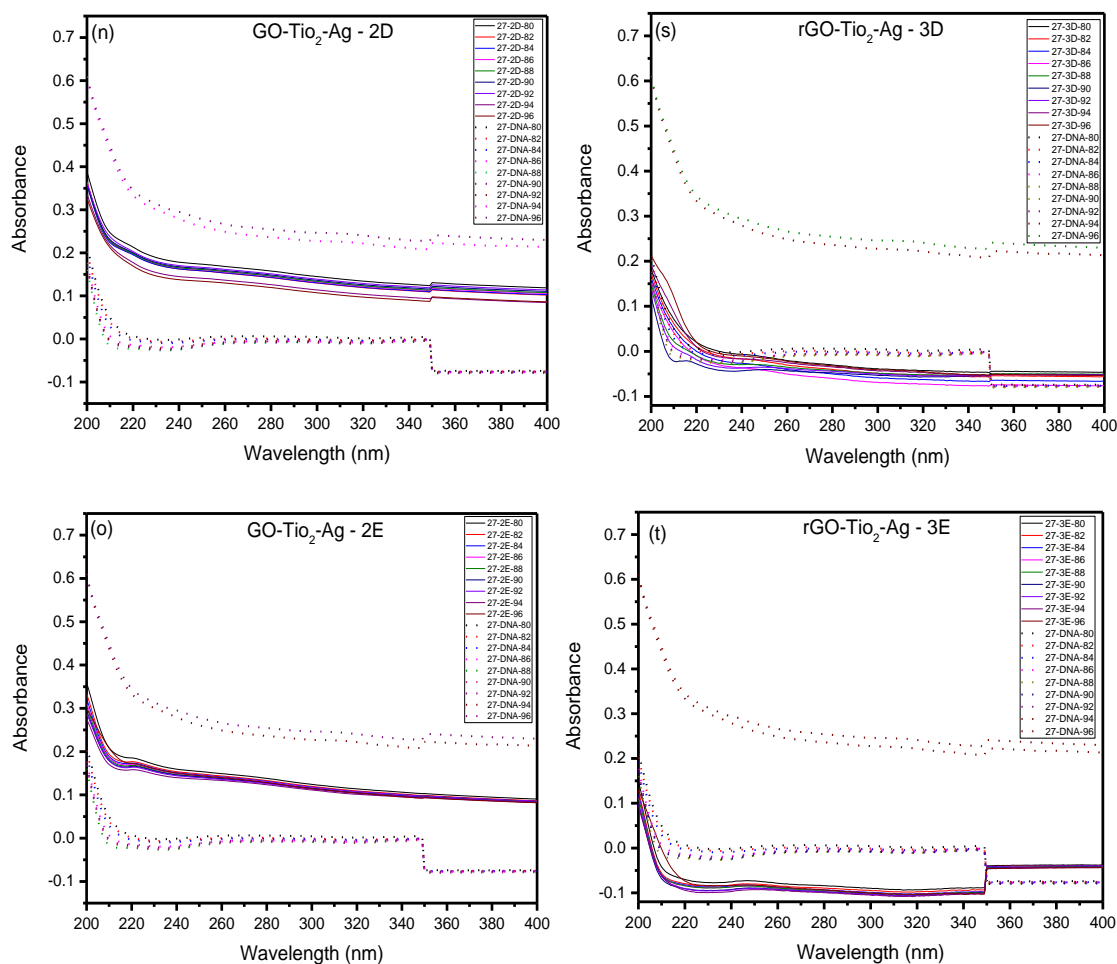


Figure 4.28 DNA – 27, plots k, l, m, n, and o are GO-TiO₂-Ag samples of concentrations A(5×10^{-1})wt%, B(5×10^{-2})wt%, C(5×10^{-3})wt%, D(5×10^{-4})wt%, and E(5×10^{-5})wt% and p, q, r, s, and t are rGO-TiO₂-Ag samples of concentrations A(5×10^{-1})wt%, B(5×10^{-2})wt%, C(5×10^{-3})wt%, D(5×10^{-4})wt%, and E(5×10^{-5})wt%

4.4.6 Absorbance at 260nm

Figure 4.29 shows the absorbance at 260nm for the two DNA samples measured along with the two types of GO-based ternary hybrid nanoparticles. The absorbance plots at 260 nm show that most samples have higher absorbance at various temperatures than the sample DNA measured without the nanoparticles. This plot signifies that the DNA denaturation occurs at an earlier temperature as the absorbance is much higher for the samples with the nanoparticles. The nanoparticles present in the fluids confront the DNA with increased thermal conductivity in the reaction mixture, which advances the

melting temperature of the DNA. It leads to the uncoiling of the double helix of the DNA to single strands. This results in higher absorbance of UV light from the spectrophotometer.

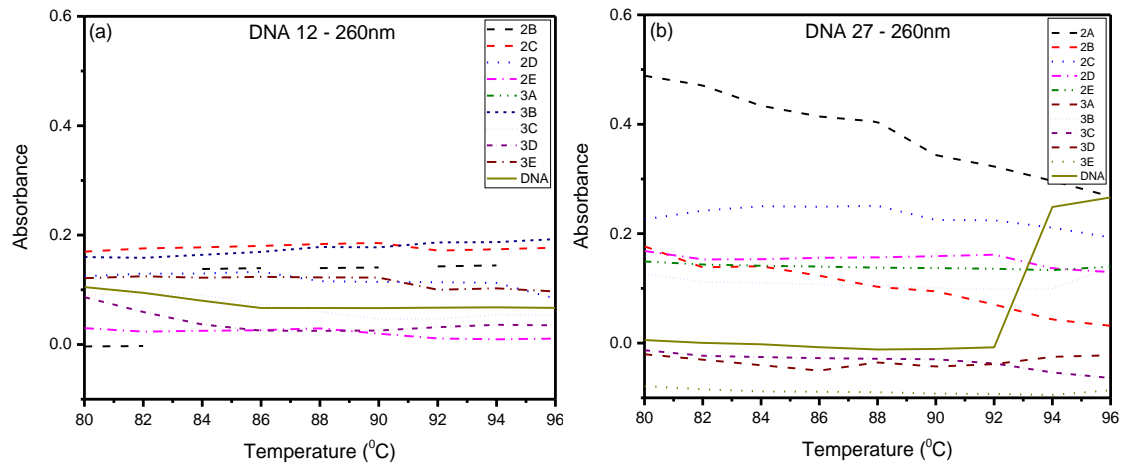


Figure 4.29 Absorbance at a wavelength of 260 nm for 2 samples of DNA (a) 12 (Wavelength 260) (b) 27 (Wavelength 260)

4.5 NUMERICAL SIMULATION OF PCR USING ANSYS

The PCR reaction was numerically simulated using ANSYS workbench© from ANSYS, Inc. The USA. Solid works© 3D modeling software was used to design the heating aluminum plate consisting of 96 wells for the PCR tubes. The model was designed based on the Bio-Rad thermos-cycler commonly used in PCR. The 3D model of the polypropylene 0.2 ml PCR tubes was also designed in solid works. The thermal transient model in the ANSYS workbench was used to simulate PCR conditions. The fluid inside the tube was well described with the same initial conditions as the PCR reaction agents and the addition of nanoparticles to the fluid. The simulation was run with and without the addition of nanoparticles in the tube, and then post-processing was done with contours of the heat transfer.

4.5.1 Finite Element Method

The finite elements system is a computational tool for finding possible solutions to a broad range of engineering problems. Owing to its versatility and simplicity as a means of analysis, the finite element approach gains substantial attention in engineering education and industry. The need to obtain approximate numerical solutions for complex industrial problems is ever-growing as numerical simulations reduce the cost and time exponentially in contrast to making an entire model or obtain a complete exact experimental solution that is difficult to a closed-form. The refrigeration of computer devices (or chips) offers an example of a complicated situation where an FEA is highly necessary to study the behavior even before the actual production. A few examples of these dynamic issues are the dispersion of contaminants in non-uniform ambient settings, metal wall temperatures in gas turbine blades where the inlet gas temperatures reach the melting point of the blade material, cooling issues in electric motors, multiple

phase-change problems, and so on. While they can be extracted, it is difficult to obtain an analytical solution to these problems by controlling equations and border conditions from the first principles. The complexity is because there is irregular or arbitrary geometry or other feature of the problem.

The most widely used approaches include finite difference, finite volume, and finite element methods, among the numerous computational methods developed over the years. The finite difference is a well-established and conceptually simple method that needs an approximation of the governing equations pointwise.

The models are shaped like a set of grid points by writing the differential equations, which can be strengthened by increasing the number of points. Although many thermal transfer problems may be resolved using the finite difference methods (Ozisik, 1994), the finite difference technique becomes challenging to use when irregular geometries or unusual boundary conditions are found. The finite volume method is a simplified version of the finite differences method and has been popular with the dynamics of computational fluids. The finite volume technology of vertex-centered is very similar to the finite element method of the linear element (Malan et al., 2002).

In the present study, a synthetic combination of polypropylene and aluminum nanopowders released in the molten liquid is known to be isotropic, single-phase gas, Newtonian fluid. The equivalent thermal properties Density, thermal conductivity, Specific heat capacity, and viscosity of hybrid nanofluids have been calculated using mathematical formulas developed (Sharma, 2014) as indicated:

$$\rho_{\text{eff}} = \left(\frac{\varphi}{100}\right) \rho_p + \left(1 - \frac{\varphi}{100}\right) \rho_f \quad (4.1)$$

$$\frac{k_{eff}}{k_f} = 1.2035 \left[\left(0.001 + \frac{\varphi}{100}\right)^{0.0098} \left(0.01 + \frac{T_{nf}}{90}\right)^{0.1331} \left(0.001 + \frac{d_p}{170}\right)^{-0.0001} \left(0.01 + \frac{\alpha_p}{\alpha_f}\right)^{0.0153} \right] \quad (4.2)$$

$$C_{eff} = \frac{\left(\frac{\varphi}{100}\right)(\rho C)_p + \left(1 - \frac{\varphi}{100}\right)(\rho C)_f}{\rho_{eff}} \quad (4.3)$$

$$\frac{\mu_{eff}}{\mu_f} = 0.3659 \times C1 \times \exp \left[\left(1 + \frac{\varphi}{100}\right)^{10.83} \left(\frac{T_{nf}}{90}\right)^{0.1331} \left(0.001 + \frac{d_p}{170}\right)^{-0.0239} \left(1 + \frac{\alpha_p}{\alpha_f}\right)^{-0.1609} \right] \quad (4.4)$$

Where φ is the hybrid nanofluid volume fractions and the symbols subscript f , p and eff are referred to fluid, solid nanoparticles and hybrid nanofluid part respectively (see Table 4.1).

4.5.1.1 Finite Element Modelling

The simple 3D modeling of the 0.2mL PCR tube was modeled in solid works with reference from Bio-rad© PCR tubes. It has a total height of 15.06 mm, as shown in Figure 4.3030. The tube was designed along with a proper lid to close. The material chosen was polypropylene. The aluminum plate with 96 wells was also designed using the Bio-Rad thermocycler plate design with an area of 127.76x85.48mm², as shown in Figure 4.31. The plate and the tube were then assembled to enumerate real PCR conditions, as shown in Figure 4.32. The material characteristics of the chosen Aluminum and Polypropylene are as illustrated in Table 4.1.

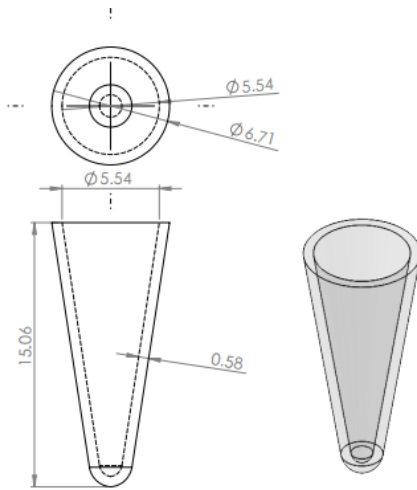


Figure 4.30 3D model of a 0.2mL PCR tube

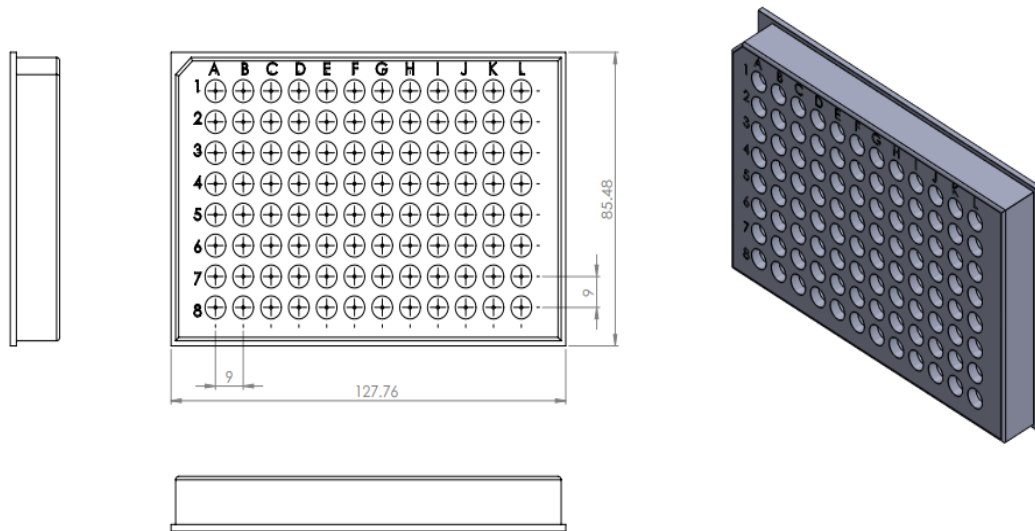


Figure 4.31 3D model of the thermo-cycler Aluminum plate

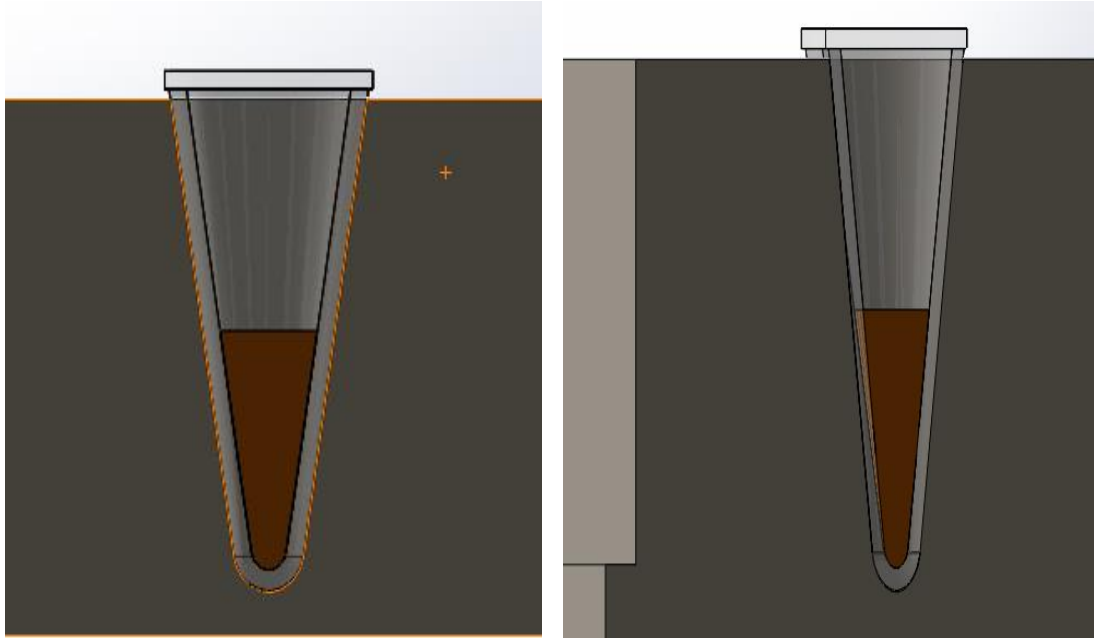


Figure 4.32 Section view of the PCR tube inside the Aluminum well set up with the PCR reaction mixture.

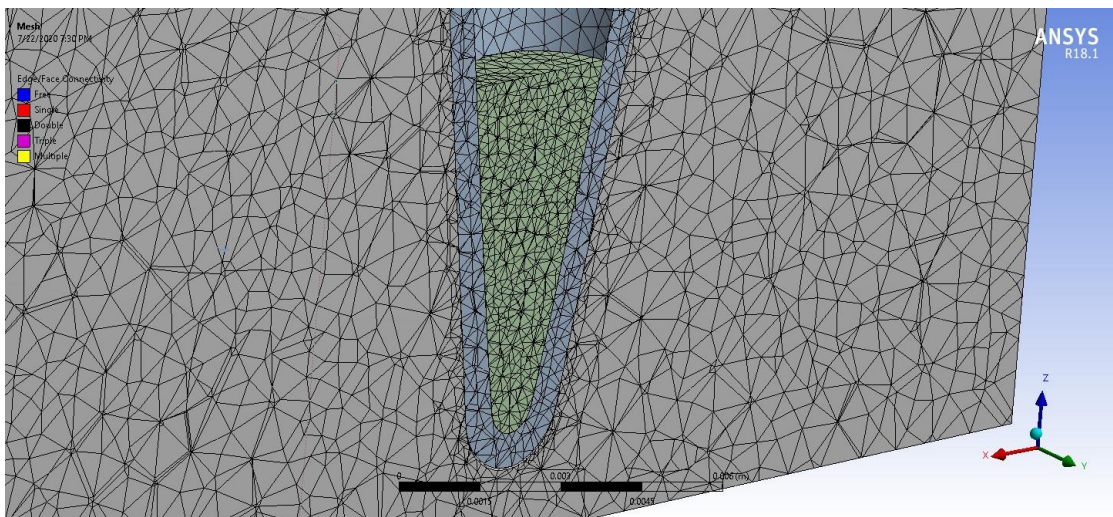
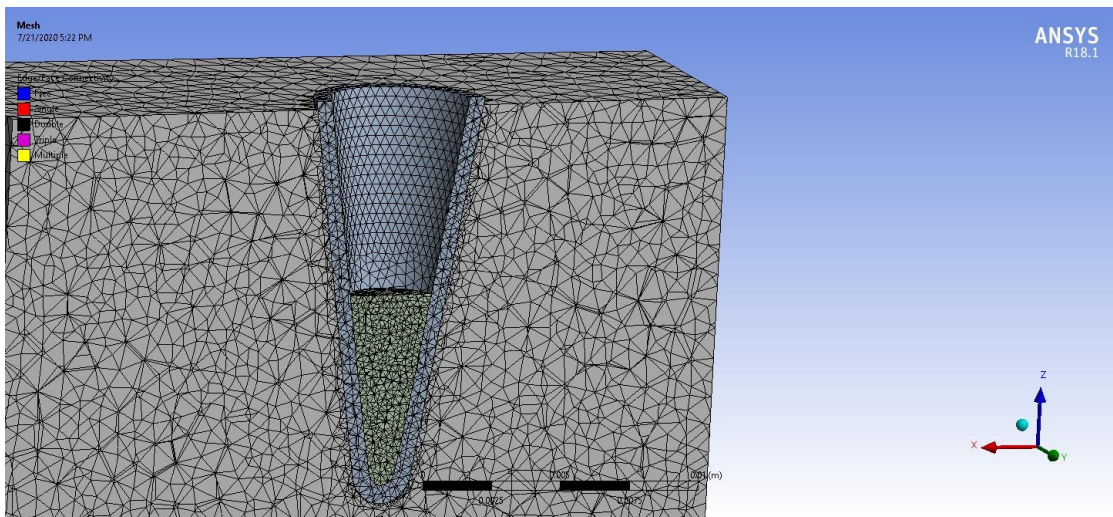
Table 4.1 Material properties

Material	Polypropylene	Aluminium
Density	910 kg/m ³	2700 kg/m ³
Tensile Strength	150 – 200 n/mm ²	205 n/mm ²
Thermal Coefficient of expansion	1.5 – 4 x 10 ⁻⁴ /k	2.34 x 10 ⁻⁵
Specific heat capacity	1180 – 1500 J/(kg·K)	887 - 963 J/(kg·K)
Thermal conductivity	0.3 W/(m·K)	170 - 220 W/(m·K)

4.5.1.2 Meshing and Boundary Conditions

The simple meshing of the assembled aluminum and 0.2mL polypropylene PCR tube was done on ANSYS using unstructured tetrahedral mesh. The boundary conditions were set with the bottom base of the aluminum plate as a heating and cooling side. The skin contact between the aluminum plate and the PCR tube was set as convection where the heat transfer takes place. The contact point of the PCR tube and the PCR mixture

was set as convection, where there is a heat transfer taking place between the PCR mixture and the inner side of the PCR tube. The faces and the body of any particular geometry were merged to make it one solid body. Meshing was done with a course adaptive sizing function. The inflation transition ratio was set as 0.272, with a maximum of 5 layers. The element size was set at 3.10^{-4} m, with the total number of nodes and elements generated were 187574 and 125472, respectively. The detailed cross-section of the mesh generated is as shown in Figure 4.33.



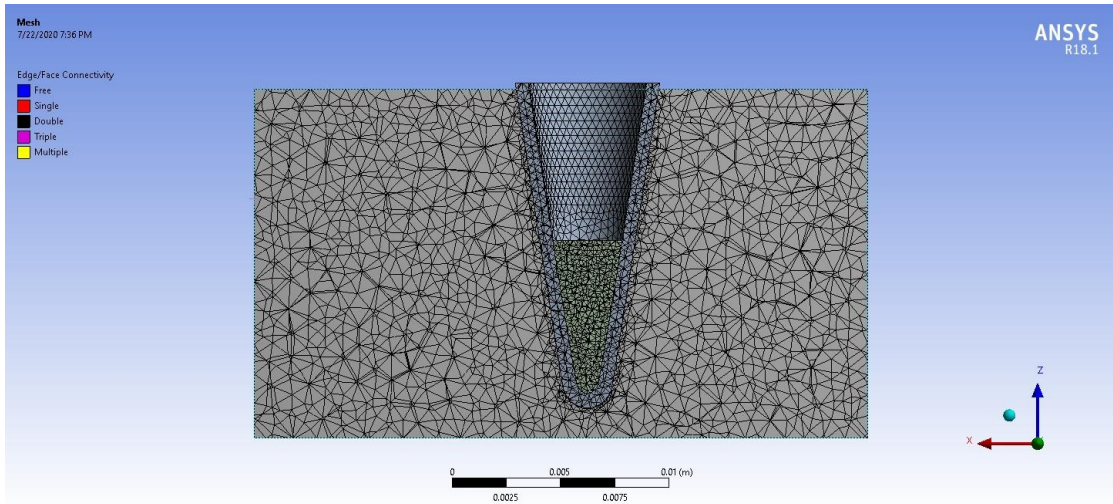


Figure 4.33 Sectioned view of meshing in the assembly

4.5.2 Results

The PCR mechanism was simulated in and ANSYS to investigate the thermal enhancement of reaction by adding ternary hybrid nanoparticles. The simulation was performed with a three-dimensional model. The analysis was done on the aluminum plate and PCR tube by selecting only one tube/well of the aluminum plate of the Thermocycler to reduce the simulation size and the computing memory. Adiabatic conditions were set for the top surface. The bottom surface was set as a heating side. As mentioned in the above section, the typical PCR reaction tube and the reaction were set in geometry. The boundary conditions were set as actual PCR conditions. Temperature sensors were set at different heights inside the PCR tube to check the temperature. Two cases were performed, the first was simulated without nanoparticles on a simple PCR reaction mixture (using the following values: $\rho = 998.2 \text{ kg m}^{-3}$; $C_p = 4182 \text{ J kg}^{-1} \text{ K}^{-1}$; $k = 0.6 \text{ W m}^{-1} \text{ K}^{-1}$; $\mu = 0.001003 \text{ kg ms}^{-1}$). Then the case 2 was simulated with similar values except for the effective thermal conductivity and specific heat, which was calculated using. In contrast, the effective thermal conductivity was determined based on the Hamilton–Crosser and Bergman equation on a mass-averaged expression.

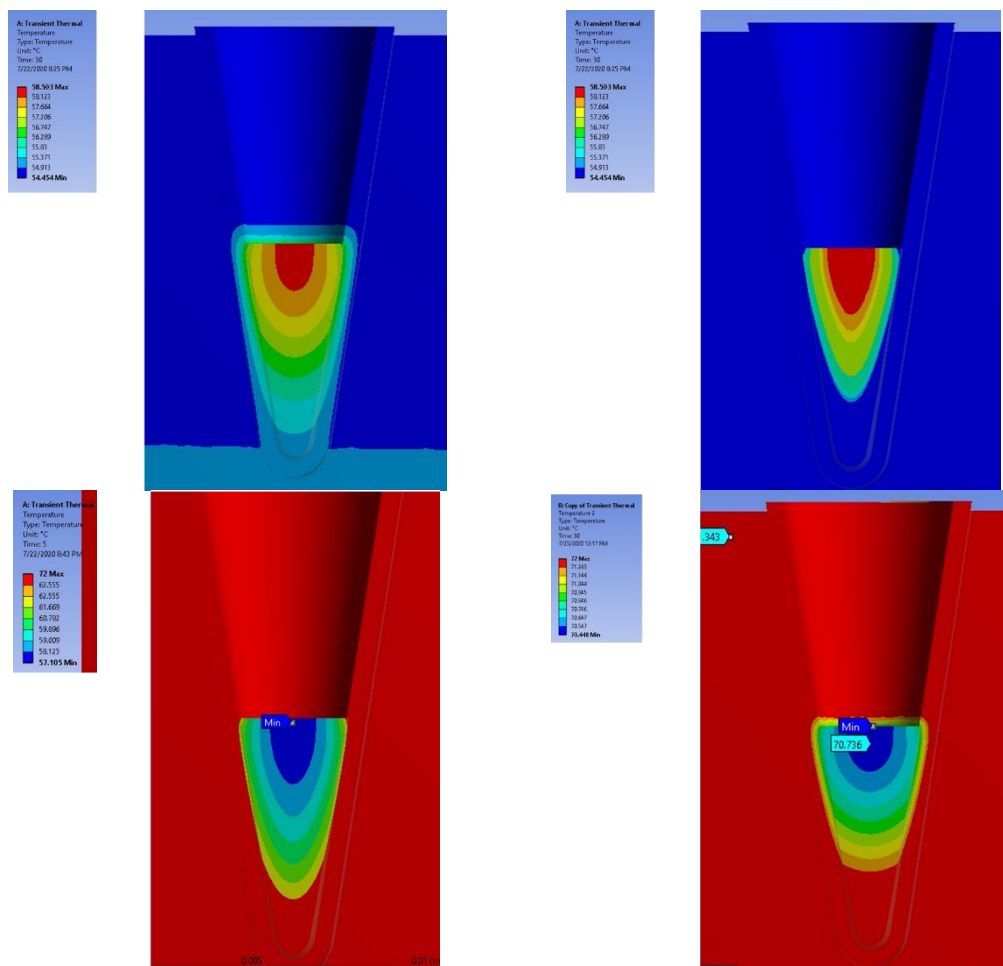


Figure 4.34 Temperature contours of the simulation, with three different PCR steps (a) 28°C–92°C (denaturation), (b) 92°C–55°C, (annealing), and (C) 55°C–72°C (extension) using the ANSYS.

4.6 CHAPTER SUMMARY

The ternary-hybrid nanoparticles (THN_p) were synthesized and characterized using SEM, FTIR, Raman spectroscopy, and XRD. The SEM results show that graphene has bonded with the silver and titanium nanoparticles to form a ternary-hybrid nanoparticle. The FTIR plots show that the transmittance is highest at a wavelength of about 1000 cm⁻¹ for the THN_p, while the lowest transmittance is 1300 cm⁻¹. Raman spectra results show that a highly intense G band occurs at 750⁻² for the rGO-TiO₂-Ag, whereas it is 1300⁻² for GO-TiO₂-Ag. According to the XRD pattern, the THN_p shows

a peak at 25°, and the particle size distribution analysis shows that the GO-based ternary hybrid has a particle size peak at 750nm while the rGO based ternary hybrid peaks at 1750 nm.

Two GO-based ternary hybrid nanoparticles (GO- TiO₂-Ag and rGO-TiO₂-Ag) were synthesized and dispersed in deionized water with a concentration of about 0.05 wt%. The nanofluids are then serially diluted for about five levels. The stability of the concentrated stock solution is checked by measuring the Zeta potential. It showed that the measured value was in a range between 25 mV to 5 mV, which is considered stable. Anton-Paar MCR302 modular compact rheometer was used for rheological measurements. The measurements were carried out in controlled stress and temperature, with the temperatures ranging from 25°C to 50°C at 5°C increments. The GO-based ternary hybrid nanofluids exhibited Newtonian behavior with higher concentrations, whereas the nanofluids exhibit non-Newtonian shear thinning behavior or Pseudoplastic at lower concentrations. The ternary hybrid nanofluids behave like Newtonian fluids at lower temperatures. At higher temperatures and lower shear rates, the viscosity decreases, indicating Shear thinning behavior. Phase separation is believed to be the reason for the nanofluid's shear thinning behavior. The viscosity of GO and rGO based THN fluids behave opposite to each other. The viscosity of GO-based nanofluid increases while the viscosity of rGO based nanofluid decreases with the decrease of concentration of nanoparticles in the fluid. Concentration plays a vital role in the change of viscosity with the temperature change. Van der Waals forces act on the particles in lower temperatures, whereas there is a weak force of attraction at higher temperatures, leading to a decrease in viscosity. Agglomeration plays a crucial at higher temperatures. The GO-based nanofluid behaves as a Newtonian fluid at higher concentrations, while the rGO behaves as a dilatant fluid or shear thickening. The GO-based nanofluids at

lower concentrations follow similar trends as rGO based ternary hybrid nanofluids. The effects of concentration, temperature, and stresses applied to the non-linear viscoelastic reveal the presence of the linear viscoelastic (LVE) region. Non-destructive stress tests were conducted using oscillating angular sweep.

The PCR reaction was conducted with the addition of two types of graphene oxide-based ternary hybrid nanoparticles. The plasmid DNA was isolated from bacterial samples. PCR reactions were carried out with and without the addition of GO-based ternary hybrid nanoparticles in various concentrations. Agarose gel electrophoresis was performed on the PCR product to check the band intensity of the PCR product. Visual observations using fluorescence ultraviolet light showed substantial enhancements on a particular concentration of 5×10^{-3} wt% of the nanoparticles in the fluids in both the GO and rGO based ternary hybrid nanoparticles. The band quantification of the agarose gel confirmed the results. The PCR product was sent for sequencing analysis. It showed that a higher concentration of the ternary hybrid nanoparticles inhibits the PCR reaction, which does not lead to enhancement, but at a lower concentration, it gives better enhancements. DNA denaturation test on the spectrophotometer showed that samples with ternary hybrid nanoparticles had higher absorbance of UV light at various concentrations and temperatures when compared to DNA samples without the use of nanoparticles. The PCR product DNA was sent for sequencing. The sequence analysis was done using Clustal W v2. It showed the presence of noise. We highly suspect it to be due to the affinity of Ternary hybrid nanoparticles towards the salt molecules present in the PCR reaction mixture.

The PCR tube and the thermocycler aluminum plate were modeled and assembled in Solid works and then simulated with ANSYS using a thermal transient model. The

simulations were performed similarly to PCR conditions with three steps, such as denaturation (28°C–92°C), annealing (92°C–55°C), and extension (55°C–72°C). The simulations were performed as two cases of PCR with and without nanoparticles. It was found that the samples with ternary hybrid nanoparticles have enhanced thermal conductivity when compared to samples without the ternary hybrid nanoparticles. It also showed a considerable reduction in time for the thermal enhancement in a sample consisting of ternary hybrid nanoparticles.

CHAPTER FIVE

CONCLUSION AND RECOMMENDATIONS

5.1 CONCLUSION

In this study, two types of novel ternary hybrid nanoparticles (THNp) or tri-hybrid nanoparticles (GO-TiO₂-Ag and rGO-TiO₂-Ag) were synthesized using three of the highly reputable nanoparticles, namely graphene oxide, titanium dioxide, and silver. The nanoparticles were selected based on the merits after studying the literature thoroughly and based on the feasibility to synthesize them, keeping in mind the ease of manufacturability and costs and the suitability of application. Graphene oxide (GO) sheets and reduced graphene oxide (rGO) was decorated by two types of nanoparticles, namely, TiO₂ and Ag. The two ternary hybrid nanoparticles were then characterized using Scanning electron microscopy (SEM), which showed that the GO-TiO₂-Ag ternary hybrid nanoparticle was crumpled and rippled. Whereas the rGO appeared more as layered and wrinkled nano-sheets decorated with the TiO₂ and the Ag.

It was observed that the flakes are not as scattered as in GO-TiO₂-Ag. A non-uniform distribution pattern of the flakes can be observed. Laser Raman spectroscopy (LRS) was used to measure Raman Spectroscopy at room temperature in the 200-3000 cm⁻¹ region through a UV excitation at 325 nm. The spectra of the GO-TiO₂-Ag and rGO-TiO₂-Ag showed structural defects in the sp²-hybridized carbon system are determined mainly by analyzing the D- and G- bands in Raman spectra. The peak intensity ratio I_D/I_G of rGO-TiO₂-Ag increased to 1.41 compared to the GO-TiO₂-Ag (0.96). It could be to the presence of higher defects in its graphitic domains during the chemical reduction of the GO. Fourier transform infrared spectroscopy (FTIR) showed peaks at 1,620 cm⁻¹, and 1,223 cm⁻¹, together with a small peak at 596 cm⁻¹, which may

also attribute to the stretching vibration of (NH) C=O group of silver nanoparticles. The essential peak of Ag and TiO₂ is present in the FTIR of rGO-TiO₂-Ag, which indicates the successful manifestation of the silver and titanium nanoparticles on the rGO. X-ray powder diffraction (XRD) showed a series of reflections which peaks at 24.5° (101), 38.9° (004), 49.5° (200), 55.4° (105), and 64.2° (204) corresponding to the anatase phase of titanium. The peaks at 70.5° (220) and 79.5° (311) belong to silver nanoparticles. Diffraction peaks of the GO-TiO₂-Ag are not distinguishable with the rGO-TiO₂-Ag due to the lower crystallinity degree of the GO and the rGO compared to the TiO₂, which resulted in the shielding of the peaks. The scattering of particle size distribution ranged from 0.2 μm to 500 μm. The GO-based-ternary hybrid has particle size peaks at 750nm, while the rGO- based-ternary hybrid is at the peak of 1750 nm.

Nanofluids were prepared using the synthesized THNp and lab-grade double distilled water at a concentration of 5×10^{-1} wt% known as stock solution. They were then sonicated with probe and water bath sonication till the nanoparticles are completely dissolved without sedimentation. Zeta potential measurements were performed on the stock solution to check the stability of the ternary hybrid nanofluids. The zeta potential measurements showed that the peaks are in the range of 25 mV to 35 mV, which are considered stable. The prepared nanofluids stock solution was then serially diluted to about five levels (5×10^{-2} wt%, 5×10^{-3} wt%, 5×10^{-4} wt%, and 5×10^{-5} wt %).

Thermal conductivity measurements were performed on the stock and the serially diluted nanofluids using a KD2 pro device at temperatures ranging from 25°C to 50°C at 5°C increments. The thermal conductivity measurements showed an enhanced thermal conductivity of the base fluids in the presence of THNp in the fluids. The measurements showed a significant enhancement of about 66% and 83% for both GO-TiO₂-Ag and rGO-TiO₂-Ag, respectively. The enhancement of thermal

conductivity may be due to various factors such as agglomeration, inter-particle adhesion, liquid layering, phonon transport, and others, as discussed in detail in the discussion chapter.

Anton-Paar MCR302 modular compact rheometer was used for rheological measurements. The measurements were carried out in controlled stress and temperature, with the temperatures ranging from 25°C to 50°C at 5°C increments. The nanofluids' dynamic viscosity measurements show that the ternary hybrid nanofluids behave as Newtonian and non-Newtonian fluids where the viscosity decreases with the increase in temperature. Rheological investigations showed that GO-based ternary hybrid nanofluids were observed to exhibit Newtonian behavior with higher concentrations. In contrast, the nanofluids exhibit non-Newtonian shear thinning behavior or pseudo-plastic at lower concentrations. The ternary hybrid nanofluids behave like Newtonian fluids at lower temperatures. At higher temperatures and lower shear rates, the viscosity decreases, indicating Shear thinning behavior. Phase separation is believed to be the reason for the nanofluid's shear thinning behavior. At higher temperatures and lower shear rates, the viscosity decreases, indicating Shear thinning behavior. The concentration of nanoparticles in the nanofluids played a vital role in the change of viscosity in variation to temperature. The viscosity of GO and rGO based THNf behave opposite to each other. The viscosity of GO-based nanofluid increases while the viscosity of rGO based nanofluid decreases with the decrease of concentration of nanoparticles in the fluid. Agglomeration is believed to be the reason for such behavior.

Van der Waals forces act on the particles in lower temperatures, whereas there is a weak force of attraction at higher temperatures, leading to a decrease in viscosity. The results indicate that thermo-physical properties of nanofluids rise with an increase of the nanoparticle volume fraction and also noted that with the reduction in

nanoparticle diameter, there is an increase in the surface area of the particle. It is understood that viscosity and thermal conductivity depend on volume fractions and nanoparticle concentration. Effects of concentration, temperature, and stresses applied to the non-linear viscoelastic revealed linear viscoelastic (LVE) region through oscillating amplitude and frequency sweep tests.

The PCR reaction was conducted with and without the addition of two types of graphene oxide-based ternary hybrid nanoparticles. PCR tests were performed with extracted plasmid DNA isolated from bacterial samples. Initial PCR results from the agarose gel electrophoresis analysis showed that a higher concentration of ternary hybrid nanoparticles inhibits PCR, while lower concentration (5×10^{-3} wt.%) of both GO-TiO₂-Ag and rGO-TiO₂-Ag contribute a significant enhancement of PCR product and 40% reduction of the number of cycles compared to PCR without nanoparticles. Agarose gel electrophoresis was performed on the PCR product to check the band intensity of the PCR product. Visual observations of the eluted gel using fluorescence ultraviolet light showed substantial enhancements on a particular concentration of 5×10^{-3} wt% of the nanoparticles in the fluids in both the GO and rGO based ternary hybrid nanoparticles.

Quantification results derived from the band intensity study using ImageJ software corroborated the same. Sequencing results of the initial experiment analyzed with Clustal W v2 showed noise in the PCR product. It may be due to the affinity of THNp to salts present in the product or the presence of more than one allele in the EGFP coding gene. Further PCR experiments were done, and the results from the agarose gel electrophoresis analysis showed that there is a significant enhancement of the DNA for about 16.74-folds more intense than the negative control for GO-TiO₂-Ag and about 15.30- fold increase for rGO-TiO₂-Ag. The addition of nanoparticles reduced the

number of cycles considerably. The reduction was about 28.5% of the number of cycles from 35 to 25 cycles. This may be attributed to the effective thermal conductivity of the ternary hybrid nanoparticles in the PCR master mix, which enhanced the reaction. In the consecutive experiments, the addition of nanoparticles does not cause any DNA damage or mutation, or nonspecific binding of primers during sequencing. The analysis did not show the presence of noise in the sequencing of subsequent experiments. Hence, SNPs (GO-TiO₂-Ag and rGO-TiO₂-Ag) can be effectively used as an additive to achieve higher PCR efficiency at the genome level. Separately DNA denaturation tests were performed with a spectrophotometer with and without ternary hybrid nanofluids of all the prepared concentrations. The results showed a significant absorbance of UV light in the samples with THNp, indicating earlier denaturation.

Numerical simulations using ANSYS thermal transient model were performed for a PCR setup with and without THNp. The PCR tube and the thermocycler aluminum plate were modeled and assembled in Solidworks. The simulations were performed similarly to PCR conditions with three steps, such as denaturation (28°C–92°C), annealing (92°C–55°C), and extension (55°C–72°C). The simulations were performed as two cases of PCR with and without nanoparticles. It was found that the samples with ternary hybrid nanoparticles have enhanced thermal conductivity when compared to samples without the ternary hybrid nanoparticles. It also showed a considerable reduction in time for the thermal enhancement in a sample consisting of ternary hybrid nanoparticles. The temperature contours showed a significant enhancement of the heat transfer in the PCR reaction with THNp, with a significant reduction of time taken for the thermal enhancements corroborating our experimental results. Overall, the ternary hybrid nanoparticles prove to be an excellent thermal enhancer for PCR as desired in our objectives.

5.2 RECOMMENDATIONS FOR FUTURE

It was observed that the thermal conductivity of the base fluid and the PCR assay was significantly enhanced with the prepared ternary hybrid nanofluids. In the next phase of the study, it is desired to study the characteristics of the THNp characterization using the Atomic Force Microscope (AFM) to imagine the surface topography of the THNp and study its physical, mechanical, functional, and electrical properties. It is also desired to characterize the nanofluids for other higher concentrations using Liquid cell transmission electron microscopy (TEM) to check the interactions of the base fluids.

The Characterized THNp can also be applied to other biological applications other than conventional PCR like Gene editing, targeted drug delivery, Bio detection of pathogens, detection of proteins, tissue engineering, tumor destruction via heating (hyperthermia), Separation and purification of biological molecules and cells, MRI contrast enhancement, Phagokinetic studies etc.

REFERENCES

- Abdul Khaliq, R., Sonawane, P. J., Sasi, B. K., Sahu, B. S., Pradeep, T., Das, S. K., & Mahapatra, N. R. (2010). Enhancement in the efficiency of polymerase chain reaction by TiO₂ nanoparticles: the crucial role of enhanced thermal conductivity. *Nanotechnology*, 21(25), 255704. <https://doi.org/10.1088/0957-4484/21/25/255704>
- Ahmed, N., Asirvatham, L. G., & Wongwises, S. (2016). Effect of volume concentration and temperature on viscosity and surface tension of graphene-water nanofluid for heat transfer applications. *Journal of Thermal Analysis and Calorimetry*, 123(2), 1399–1409. <https://doi.org/10.1007/s10973-015-5034-x>
- Ahmadi Nadooshan, A., Eshgarf, H., & Afrand, M. (2018). Measuring the viscosity of Fe₃O₄-MWCNTs/EG hybrid nanofluid for evaluation of thermal efficiency: Newtonian and non-Newtonian behavior. *Journal of Molecular Liquids*, 253, 169–177. <https://doi.org/10.1016/j.molliq.2018.01.012>
- Al-Dhabaan, F. A., Yousef, H., Shoala, T., Shaheen, J., El Sawi, Y., & Farag, T. (2018). Enhancement of fungal DNA templates and PCR amplification yield by three types of nanoparticles. *Journal of Plant Protection Research*, 58(1), 66–72. <https://doi.org/10.24425/119119>
- Aleksenskii, A. E., Baidakova, M. V., Vul, A. Y., & Siklitskii, V. I. (1999). The structure of diamond nanoclusters. *Physics of the Solid State*, 41(4), 668–671.
- Ali, N., Teixeira, J. A., & Addali, A. (2018). A Review on Nanofluids: Fabrication, Stability, and Thermophysical Properties. *Journal of Nanomaterials*, 2018. <https://doi.org/10.1155/2018/6978130>
- Ali, Z., Jin, G., Hu, Z., Wang, Z., Khan, M. A., Dai, J., & Tang, Y. (2018). A Review on NanoPCR: History, Mechanism and Applications. *Journal of Nanoscience and Nanotechnology*, 18(12), 8029–8046. <https://doi.org/10.1166/jnn.2018.16390>
- Aysan, A. B., Knejzlík, Z., Ulbrich, P., Šoltys, M., Zadražil, A., & Štěpánek, F. (2017). Effect of surface functionalisation on the interaction of iron oxide nanoparticles with polymerase chain reaction. *Colloids and Surfaces B: Biointerfaces*, 153, 69–76. <https://doi.org/10.1016/j.colsurfb.2017.02.005>
- Allardyce, C. S., & Dyson, P. J. (2001). Ruthenium in medicine: current clinical uses and future prospects. *Platinum Metals Reviews*, 45(ARTICLE), 62.
- Amini, F., Miry, S. Z., Karimi, A., & Ashjaee, M. (2019). Experimental Investigation of Thermal Conductivity and Viscosity of SiO₂/Multiwalled Carbon Nanotube Hybrid Nanofluids. *Journal of Nanoscience and Nanotechnology*, 19(6), 3398–3407. <https://doi.org/10.1166/jnn.2019.16127>
- Aravind, S. S. J., & Ramaprabhu, S. (2013). Graphene-multiwalled carbon nanotube-

- based nanofluids for improved heat dissipation. *RSC Advances*, 3(13), 4199–4206. <https://doi.org/10.1039/c3ra22653k>
- Arshad, A., Jabbar, M., Yan, Y., & Reay, D. (2019). A review on graphene based nanofluids: Preparation, characterization and applications. *Journal of Molecular Liquids*, 279, 444–484. <https://doi.org/10.1016/j.molliq.2019.01.153>
- Aschberger, K., Johnston, H. J., Stone, V., Aitken, R. J., Tran, C. L., Hankin, S. M., ... Christensen, F. M. (2010). Review of fullerene toxicity and exposure—appraisal of a human health risk assessment, based on open literature. *Regulatory Toxicology and Pharmacology*, 58(3), 455–473.
- Avouris, P., & Dimitrakopoulos, C. (2012). Graphene: synthesis and applications. *Materials Today*, 15(3), 86–97.
- Aybar, H., Sharifpur, M., Azizian, M. R., Mehrabi, M., & Meyer, J. P. (2015). A review of thermal conductivity models for nanofluids. *Heat Transfer Engineering*, 36(13), 1085–1110. <https://doi.org/10.1080/01457632.2015.987586>
- Aysan, A. B., Knežlík, Z., Ulbrich, P., Šoltys, M., Zdražil, A., & Štěpánek, F. (2017). Effect of surface functionalisation on the interaction of iron oxide nanoparticles with polymerase chain reaction. *Colloids and Surfaces B: Biointerfaces*, 153, 69–76. <https://doi.org/10.1016/j.colsurfb.2017.02.005>
- Azmi, W. H., Sharma, K. V., Mamat, R., Najafi, G., & Mohamad, M. S. (2016). The enhancement of effective thermal conductivity and effective dynamic viscosity of nanofluids - A review. *Renewable and Sustainable Energy Reviews*. <https://doi.org/10.1016/j.rser.2015.09.081>
- Babar, H., & Ali, H. M. (2019). Towards hybrid nanofluids: Preparation, thermophysical properties, applications, and challenges. *Journal of Molecular Liquids*, 281, 598–633. <https://doi.org/10.1016/j.molliq.2019.02.102>
- Babar, H., Sajid, M., & Ali, H. (2019). Viscosity of hybrid nanofluids: A critical review. *Thermal Science*, 23(3 Part B), 1713–1754. <https://doi.org/10.2298/tsci181128015b>
- Baek, G., & Kim, C. (2011). Rheological properties of Carbopol containing nanoparticles. *Journal of Rheology*, 55(2), 313–330. <https://doi.org/10.1122/1.3538092>
- Bahrami, M., Akbari, M., Karimipour, A., & Afrand, M. (2016). An experimental study on rheological behavior of hybrid nanofluids made of iron and copper oxide in a binary mixture of water and ethylene glycol: Non-Newtonian behavior. *Experimental Thermal and Fluid Science*, 79, 231–237. <https://doi.org/10.1016/j.expthermflusci.2016.07.015>
- Balandin, A. A., Ghosh, S., Bao, W., Calizo, I., Teweldebrhan, D., Miao, F., & Lau, C. N. (2008). Superior thermal conductivity of single-layer graphene. *Nano Letters*, 8(3), 902–907. <https://doi.org/10.1021/nl0731872>

- Barranco, V., Lillo-Rodenas, M. A., Linares-Solano, A., Oya, A., Pico, F., Ibañez, J., ... Rojo, J. M. (2010). Amorphous carbon nanofibers and their activated carbon nanofibers as supercapacitor electrodes. *The Journal of Physical Chemistry C*, *114*(22), 10302–10307.
- Bergamo, A., & Sava, G. (2011). Ruthenium anticancer compounds: myths and realities of the emerging metal-based drugs. *Dalton Transactions*, *40*(31), 7817–7823.
- Bhargava, A., Jain, N., Khan, M. A., Pareek, V., Dilip, R. V., & Panwar, J. (2016). Utilizing metal tolerance potential of soil fungus for efficient synthesis of gold nanoparticles with superior catalytic activity for degradation of rhodamine B. *Journal of Environmental Management*, *183*, 22–32.
- Bhaskar, S., Tian, F., Stoeger, T., Kreyling, W., de la Fuente, J. M., Grazú, V., ... Razansky, D. (2010). Multifunctional Nanocarriers for diagnostics, drug delivery and targeted treatment across blood-brain barrier: perspectives on tracking and neuroimaging. *Particle and Fibre Toxicology*, *7*(1), 3. <https://doi.org/10.1186/1743-8977-7-3>
- Bhatia, E., & Banerjee, R. (2020). Hybrid silver-gold nanoparticles suppress drug resistant polymicrobial biofilm formation and intracellular infection. *Journal of Materials Chemistry B*, *8*(22), 4890–4898. <https://doi.org/10.1039/d0tb00158a>
- Bruzzone, S., Malvaldi, M., Arrighini, G. P., & Guidotti, C. (2005). Theoretical study of electromagnetic scattering by metal nanoparticles. *Journal of Physical Chemistry B*, *109*(9), 3807–3812. <https://doi.org/10.1021/jp045451a>
- Bumataria, R. K., Chavda, N. K., & Panchal, H. (2019). Current research aspects in mono and hybrid nanofluid based heat pipe technologies. *Heliyon*, *5*(5), e01627. <https://doi.org/10.1016/j.heliyon.2019.e01627>
- Cao, J., Wang, Y., Yu, J., Xia, J., Zhang, C., Yin, D., & Häfeli, U. O. (2004). Preparation and radiolabeling of surface-modified magnetic nanoparticles with rhenium-188 for magnetic targeted radiotherapy. *Journal of Magnetism and Magnetic Materials*, *277*(1–2), 165–174.
- Cao, X., Chen, J., Wen, S., Peng, C., Shen, M., & Shi, X. (2011). Effect of surface charge of polyethyleneimine-modified multiwalled carbon nanotubes on the improvement of polymerase chain reaction. *Nanoscale*. <https://doi.org/10.1039/c0nr00833h>
- Cao, X., Shen, M., Zhang, X., Hu, J., Wang, J., & Shi, X. (2012). Effect of the surface functional groups of dendrimer-entrapped gold nanoparticles on the improvement of PCR. *Electrophoresis*. <https://doi.org/10.1002/elps.201200061>
- Cao, X., Shi, X., Yang, W., Zhang, X., Fan, C., & Hu, J. (2009). Enhanced specificity and efficiency of polymerase chain reactions using poly(amidoamine) dendrimers and derivatives. *The Analyst*, *134*(1), 87–92. <https://doi.org/10.1039/b812176a>
- Chakraborty, S., & Panigrahi, P. K. (2020). Stability of nanofluid: A review. *Applied Thermal Engineering*, *174*(December 2019).

<https://doi.org/10.1016/j.applthermaleng.2020.115259>

- Chao, J.-I., Perevedentseva, E., Chung, P.-H., Liu, K.-K., Cheng, C.-Y., Chang, C.-C., & Cheng, C.-L. (2007). Nanometer-sized diamond particle as a probe for biolabeling. *Biophysical Journal*, *93*(6), 2199–2208.
- Che Sidik, N. A., Mahmud Jamil, M., Aziz Japar, W. M. A., & Muhammad Adamu, I. (2017). A review on preparation methods, stability and applications of hybrid nanofluids. *Renewable and Sustainable Energy Reviews*, *80*(January 2016), 1112–1122. <https://doi.org/10.1016/j.rser.2017.05.221>
- Chen, A., & Holt-Hindle, P. (2010). Platinum-based nanostructured materials: synthesis, properties, and applications. *Chemical Reviews*, *110*(6), 3767–3804.
- Chen, H., Ding, Y., & Tan, C. (2007). Rheological behaviour of nanofluids. *New Journal of Physics*, *9*. <https://doi.org/10.1088/1367-2630/9/10/367>
- Chen, H., Witharana, S., Jin, Y., Kim, C., & Ding, Y. (2009). Predicting thermal conductivity of liquid suspensions of nanoparticles (nanofluids) based on rheology. *Particuology*, *7*(2), 151–157. <https://doi.org/10.1016/j.partic.2009.01.005>
- Chen, L., & Xie, H. (2010). Properties of carbon nanotube nanofluids stabilized by cationic gemini surfactant. *Thermochimica Acta*, *506*(1–2), 62–66. <https://doi.org/10.1016/j.tca.2010.04.016>
- Chernousova, S., & Epple, M. (2013). Silver as antibacterial agent: ion, nanoparticle, and metal. *Angewandte Chemie International Edition*, *52*(6), 1636–1653.
- Chisholm, S. A., Teare, E. L., Patel, B., & Owen, R. J. (2002). Determination of *Helicobacter pylori* vacA allelic types by single-step multiplex PCR. *Letters in Applied Microbiology*, *35*(1), 42–46. <https://doi.org/10.1046/j.1472-765X.2002.01129.x>
- Choi, B.-K., Choi, W.-K., Park, S.-J., & Seo, M.-K. (2018). One-Pot Synthesis of Ag-TiO₂ /Nitrogen-Doped Graphene Oxide Nanocomposites and Its Photocatalytic Degradation of Methylene Blue . *Journal of Nanoscience and Nanotechnology*, *18*(9), 6075–6080. <https://doi.org/10.1166/jnn.2018.15616>
- Choi, S. U.S., Zhang, Z. G., Yu, W., Lockwood, F. E., & Grulke, E. A. (2001). Anomalous thermal conductivity enhancement in nanotube suspensions. *Applied Physics Letters*, *79*(14), 2252–2254. <https://doi.org/10.1063/1.1408272>
- Choi, Stephen U.S. (1995). *Enhancing thermal conductivity of fluids with nanoparticles*. American Society of Mechanical Engineers, Fluids Engineering Division (Publication) FED (Vol. 231). Argonne National Lab., IL (United States).
- CHRYSALIS, G. (1882). *A Treatise on Electricity and Magnetism An Elementary Treatise on Electricity*. Nature (Vol. 25). Clarendon press. <https://doi.org/10.1038/025237a0>

- Colangelo, G., Favale, E., Miglietta, P., Milanese, M., & de Risi, A. (2016). Thermal conductivity, viscosity and stability of Al₂O₃-diathermic oil nanofluids for solar energy systems. *Energy*, 95, 124–136. <https://doi.org/10.1016/j.energy.2015.11.032>
- Collins, P. G., & Avouris, P. (2000). Nanotubes for electronics. *Scientific American*, 283(6), 62–69.
- Cooper, D. R., D’Anjou, B., Ghattamaneni, N., Harack, B., Hilke, M., Horth, A., ... Whiteway, E. (2012). Experimental review of graphene. *ISRN Condensed Matter Physics*, 2012.
- Cui, D., & al., E. (2004). Effects of single-walled carbon nanotubes on the polymerase chain reaction. *Nanotechnology*, 15(1), 154.
- Cui, Daxiang, Tian, F., Kong, Y., Titushikin, I., & Gao, H. (2004). Effects of single-walled carbon nanotubes on the polymerase chain reaction. *Nanotechnology*, 15(1), 154–157. <https://doi.org/10.1088/0957-4484/15/1/030>
- Dantas, P. V. P., Melo, C. F., Houllou, L. M., & Machado, G. (2017). Nanoparticle-assisted Polymerase Chain Reaction (NanoPCR): Optimization of PCR detection of *Leifsonia xyli* subsp. *xyli* by the addition of nanoparticles. *Journal of Applied and Advanced Research*, 2(1), 13. <https://doi.org/10.21839/jaar.2017.v2i1.47>
- Das, M., Shim, K. H., An, S. S. A., & Yi, D. K. (2011). Review on gold nanoparticles and their applications. *Toxicology and Environmental Health Sciences*, 3(4), 193–205. <https://doi.org/10.1007/s13530-011-0109-y>
- Das, Sarit K., Putra, N., & Roetzel, W. (2003). Pool boiling characteristics of nanofluids. *International Journal of Heat and Mass Transfer*, 46(5), 851–862. [https://doi.org/10.1016/S0017-9310\(02\)00348-4](https://doi.org/10.1016/S0017-9310(02)00348-4)
- Das, Sarit Kumar, Choi, S. U. S., & Patel, H. E. (2006). Heat transfer in nanofluids - A review. *Heat Transfer Engineering*, 27(10), 3–19. <https://doi.org/10.1080/01457630600904593>
- DeCarli, P. S., & Jamieson, J. C. (1961). Formation of diamond by explosive shock. *Science*, 133(3467), 1821–1822.
- Deprez, N., & McLachlan, D. S. (1988). The analysis of the electrical conductivity of graphite conductivity of graphite powders during compaction. *Journal of Physics D: Applied Physics*, 21(1), 101.
- Devendiran, D. K., & Amirtham, V. A. (2016). A review on preparation, characterization, properties and applications of nanofluids. *Renewable and Sustainable Energy Reviews*. <https://doi.org/10.1016/j.rser.2016.01.055>
- Dhanekar, S., & Jain, S. (2013). Porous silicon biosensor: Current status. *Biosensors and Bioelectronics*, 41(1), 54–64. <https://doi.org/10.1016/j.bios.2012.09.045>
- Du, J., & Cheng, H. M. (2012). The fabrication, properties, and uses of

- graphene/polymer composites. *Macromolecular Chemistry and Physics*, 213(10–11), 1060–1077. <https://doi.org/10.1002/macp.201200029>
- Dwyer, C., Guthold, M., Falvo, M., Washburn, S., Superfine, R., & Erie, D. (2002). DNA-functionalized single-walled carbon nanotubes. *Nanotechnology*, 13(5), 601–604. <https://doi.org/10.1088/0957-4484/13/5/311>
- Eastman, J. A., Choi, S. U. S., Li, S., Yu, W., & Thompson, L. J. (2001). Anomalously increased effective thermal conductivities of ethylene glycol-based nanofluids containing copper nanoparticles. *Applied Physics Letters*, 78(6), 718–720. <https://doi.org/10.1063/1.1341218>
- Eastman, J. A., Choi, U. S., Li, S., Thompson, L. J., & Lee, S. (1996). Enhanced thermal conductivity through the development of nanofluids. *MRS Online Proceedings Library Archive*, 457.
- Elder, A., Yang, H., Gwiazda, R., Teng, X., Thurston, S., He, H., & Oberdörster, G. (2007). Testing nanomaterials of unknown toxicity: an example based on platinum nanoparticles of different shapes. *Advanced Materials*, 19(20), 3124–3129.
- Esfahani, M. R., Languri, E. M., & Nunna, M. R. (2016). Effect of particle size and viscosity on thermal conductivity enhancement of graphene oxide nanofluid. *International Communications in Heat and Mass Transfer*, 76, 308–315. <https://doi.org/10.1016/j.icheatmasstransfer.2016.06.006>
- Fadhil, A. M. A. (2014). Improving and enhancement of PCR amplification by using ZnO and TiO₂ nanoparticles. *International Journal of Current Microbiology and Applied Sciences*, 3(11), 549–557.
- Fan, B., Guo, H., Shi, J., Shi, C., Jia, Y., Wang, H., ... Zhang, R. (2016). Facile one-pot preparation of silver/reduced graphene oxide nanocomposite for cancer photodynamic and photothermal therapy. *Journal of Nanoscience and Nanotechnology*, 16(7), 7049–7054. <https://doi.org/10.1166/jnn.2016.11327>
- Field, J. E. (2012). The mechanical and strength properties of diamond. *Reports on Progress in Physics*, 75(12), 126505.
- Gao, C. H., Mortimer, M., Zhang, M., Holden, P. A., Cai, P., Wu, S., ... Huang, Q. (2019). Impact of metal oxide nanoparticles on in vitro DNA amplification. *PeerJ*, 2019(6), 1–17. <https://doi.org/10.7717/peerj.7228>
- Gabriel, S., Rasheed, A. K., Siddiqui, R., Appaturi, J. N., Fen, L. B., & Khan, N. A. (2018). Development of nanoparticle-assisted PCR assay in the rapid detection of brain-eating amoebae. *Parasitology Research*, 117(6), 1801–1811. <https://doi.org/10.1007/s00436-018-5864-0>
- Garibyan, L., & Avashia, N. (2013). Research techniques made simple: polymerase chain reaction (PCR). *The Journal of Investigative Dermatology*, 133(3), e6.
- Ghadimi, A., & Metselaar, I. H. (2013). The influence of surfactant and ultrasonic processing on improvement of stability, thermal conductivity and viscosity of

- titania nanofluid. *Experimental Thermal and Fluid Science*, 51, 1–9. <https://doi.org/10.1016/j.expthermflusci.2013.06.001>
- Ghosh, M. M., Roy, S., Pabi, S. K., & Ghosh, S. (2011). A molecular dynamics-stochastic model for thermal conductivity of nanofluids and its experimental validation. *Journal of Nanoscience and Nanotechnology*, 11(3), 2196–2207. <https://doi.org/10.1166/jnn.2011.3557>
- Giljohann, D. A., Seferos, D. S., Prigodich, A. E., Patel, P. C., & Mirkin, C. A. (2009). Gene regulation with polyvalent siRNA– nanoparticle conjugates. *Journal of the American Chemical Society*, 131(6), 2072–2073.
- Giovannini, T., & Concilio, L. (2002). PCR detection of genetically modified organisms: A review. *Starch/Staerke*, 54(8), 321–327. [https://doi.org/10.1002/1521-379X\(200208\)54:8<321::AID-STAR2222321>3.0.CO;2-J](https://doi.org/10.1002/1521-379X(200208)54:8<321::AID-STAR2222321>3.0.CO;2-J)
- Godson, L., Raja, B., Lal, D. M., & Wongwises, S. (2010). Experimental investigation on the thermal conductivity and viscosity of silver-deionized water nanofluid. *Experimental Heat Transfer*, 23(4), 317–332. <https://doi.org/10.1080/08916150903564796>
- Gole, A., Dash, C., Ramakrishnan, V., Sainkar, S. R., Mandale, A. B., Rao, M., & Sastry, M. (2001). Pepsin– gold colloid conjugates: preparation, characterization, and enzymatic activity. *Langmuir*, 17(5), 1674–1679.
- Goodman, M. F., Creighton, S., & Btoom, L. (1993). Biochemical Basis of DNA Replication. *Critical Reviews in Biochemistry and Molecular Biology*, 28(2), 83–126.
- Graf, C., Vossen, D. L. J., Imhof, A., & van Blaaderen, A. (2003). A general method to coat colloidal particles with silica. *Langmuir*, 19(17), 6693–6700.
- Greshnyakov, V. A., & Belenkov, E. A. (2017). Investigation on the formation of lonsdaleite from graphite. *Journal of Experimental and Theoretical Physics*, 124(2), 265–274. <https://doi.org/10.1134/S1063776117010125>
- Gupta, R. a, Shah, N., Wang, K. C., Kim, J., Horlings, H. M., David, J., ... Chang, H. Y. (2010). Long noncoding RNA HONTAIR reprograms chromatin state to promote cancer metastasis. *Nature*, 464(7291), 1071–1076. <https://doi.org/10.1038/nature08975>.Long
- Gurunathan, S., Han, J. W., Park, J. H., Kim, E., Choi, Y. J., Kwon, D. N., & Kim, J. H. (2015). Reduced graphene oxide-silver nanoparticle nanocomposite: A potential anticancer nanotherapy. *International Journal of Nanomedicine*, 10, 6257–6276. <https://doi.org/10.2147/IJN.S92449>
- Haber, A. L., Griffiths, K. R., Jamting, Å. K., & Emslie, K. R. (2008). Addition of gold nanoparticles to real-time PCR: Effect on PCR profile and SYBR Green i fluorescence. *Analytical and Bioanalytical Chemistry*. <https://doi.org/10.1007/s00216-008-2358-4>

- Halefadi, S., Estellé, P., Aladag, B., Doner, N., & Maré, T. (2013). Viscosity of carbon nanotubes water-based nanofluids: Influence of concentration and temperature. *International Journal of Thermal Sciences*, *71*, 111–117. <https://doi.org/10.1016/j.ijthermalsci.2013.04.013>
- Hall, T. A. (1999). BioEdit: a user-friendly biological sequence alignment editor and analysis program for Windows 95/98/NT. In *Nucleic acids symposium series* (Vol. 41, No. 41, pp. 95-98). [London]: Information Retrieval Ltd., c1979-c2000..
- Hamzah, M. H., Sidik, N. A. C., Ken, T. L., Mamat, R., & Najafi, G. (2017). Factors affecting the performance of hybrid nanofluids: A comprehensive review. *International Journal of Heat and Mass Transfer*, *115*, 630–646. <https://doi.org/10.1016/j.ijheatmasstransfer.2017.07.021>
- Han, G., Ghosh, P., & Rotello, V. M. (2007). Functionalized gold nanoparticles for drug delivery.
- Harris, P. J. F. (1986). Sulphur-induced faceting of platinum catalyst particles. *Nature*, *323*(6091), 792–794.
- Haynes, W. M., Lide, D. R., & Bruno, T. J. (2011). Properties of solids in CRC Handbook of chemistry and Physics. CRC Press/Taylor and Francis, Boca Raton, FL, 91st edition (internet version
- HE, Q. Di, HUANG, D. P., HUANG, G., & CHEN, Z. G. (2016). Advance in Research of Microfluidic Polymerase Chain Reaction Chip. *Chinese Journal of Analytical Chemistry*, *44*(4), 542–550. [https://doi.org/10.1016/S1872-2040\(16\)60921-0](https://doi.org/10.1016/S1872-2040(16)60921-0)
- Hemmat Esfe, M., Alirezaie, A., & Rejvani, M. (2017). An applicable study on the thermal conductivity of SWCNT-MgO hybrid nanofluid and price-performance analysis for energy management. *Applied Thermal Engineering*, *111*, 1202–1210. <https://doi.org/10.1016/j.applthermaleng.2016.09.091>
- Hemmat Esfe, M., Zabihi, F., Rostamian, H., & Esfandeh, S. (2018). Experimental investigation and model development of the non-Newtonian behavior of CuO-MWCNT-10w40 hybrid nano-lubricant for lubrication purposes. *Journal of Molecular Liquids*, *249*, 677–687. <https://doi.org/10.1016/j.molliq.2017.11.020>
- Henke, W. (2008). Betaine improves the PCR amplification of GC-rich DNA sequences. *Nucleic Acids Research*, *25*(19), 3957–3958.
- Hotze, E. M., Phenrat, T., & Lowry, G. V. (2010). Nanoparticle Aggregation: Challenges to Understanding Transport and Reactivity in the Environment. *Journal of Environment Quality*, *39*(6), 1909. <https://doi.org/10.2134/jeq2009.0462>
- Hu, X., Yin, D., Xie, J., Chen, X., & Bai, C. (2020). Experimental study of viscosity characteristics of graphite/engine oil (5 W-40) nanofluids. *Applied Nanoscience (Switzerland)*, *10*(6), 1743–1756. <https://doi.org/10.1007/s13204-019-01240-w>
- Huang, H., Pierstorff, E., Osawa, E., & Ho, D. (2007). Active nanodiamond hydrogels

- for chemotherapeutic delivery. *Nano Letters*, 7(11), 3305–3314.
- Huang, J., Zhang, X., Wang, C., Wang, L., Li, H., Cao, X., ... Hu, J. (2008). Size and surface effect of gold nanoparticles (AuNPs) in nanogold-assisted PCR. *Surface Review and Letters*, 15(6), 757–762. <https://doi.org/10.1142/S0218625X08012189>
- Huang, S. H., Yang, T. C., Tsai, M. H., Tsai, I. S., Lu, H. C., Chuang, P. H., ... Lin, C. W. (2008). Gold nanoparticle-based RT-PCR and real-time quantitative RT-PCR assays for detection of Japanese encephalitis virus. *Nanotechnology*. <https://doi.org/10.1088/0957-4484/19/40/405101>
- Hussien, A. A., Abdullah, M. Z., Yusop, N. M., Al-Nimr, M. A., Atieh, M. A., & Mehrali, M. (2017). Experiment on forced convective heat transfer enhancement using MWCNTs/GNPs hybrid nanofluid and mini-tube. *International Journal of Heat and Mass Transfer*, 115, 1121–1131. <https://doi.org/10.1016/j.ijheatmasstransfer.2017.08.120>
- Hwang, K. S., Lee, J. H., & Jang, S. P. (2007). Buoyancy-driven heat transfer of water-based Al₂O₃ nanofluids in a rectangular cavity. *International Journal of Heat and Mass Transfer*. <https://doi.org/10.1016/j.ijheatmasstransfer.2007.01.037>
- Hwang, S. H., Im, S. G., Hah, S. S., Cong, V. T., Lee, E. J., Lee, Y. S., ... Son, S. J. (2013). Effects of Upconversion Nanoparticles on Polymerase Chain Reaction. *PLoS ONE*, 8(9), 855–859. <https://doi.org/10.1371/journal.pone.0073408>
- Jabbari, F., Rajabpour, A., & Saedodin, S. (2017). Thermal conductivity and viscosity of nanofluids: A review of recent molecular dynamics studies. *Chemical Engineering Science*, 174(June 2018), 67–81. <https://doi.org/10.1016/j.ces.2017.08.034>
- Jeong, H. Y., Baek, S. H., Chang, S. J., Yang, M., Lee, S. J., Lee, K. G., & Park, T. J. (2015). A hybrid composite of gold and graphene oxide as a PCR enhancer. *RSC Advances*, 5(113), 93117–93121. <https://doi.org/10.1039/c5ra12932j>
- Jia, F., Shan, C., Li, F., & Niu, L. (2008). Carbon nanotube/gold nanoparticles/polyethylenimine-functionalized ionic liquid thin film composites for glucose biosensing. *Biosensors and Bioelectronics*, 24(4), 945–950. <https://doi.org/10.1016/j.bios.2008.07.057>
- Jung, J. H., Cheon, D. S., Liu, F., Lee, K. B., & Seo, T. S. (2010). A Graphene Oxide Based Immuno-biosensor for Pathogen Detection. *Angewandte Chemie International Edition*, 49(33), 5708–5711. <https://doi.org/10.1002/anie.201001428>
- Jung, J. Y., Kim, E. S., & Kang, Y. T. (2012). Stabilizer effect on CHF and boiling heat transfer coefficient of alumina/water nanofluids. *International Journal of Heat and Mass Transfer*, 55(7–8), 1941–1946. <https://doi.org/10.1016/j.ijheatmasstransfer.2011.11.049>
- Kadish, K. M., & Ruoff, R. S. (2000). *Fullerenes: chemistry, physics, and technology*.

John Wiley & Sons.

- Kaggwa, A., & Carson, J. K. (2019). Developments and future insights of using nanofluids for heat transfer enhancements in thermal systems: a review of recent literature. *International Nano Letters*, 9(4), 277–288. <https://doi.org/10.1007/s40089-019-00281-x>
- Kambli, P., & Kelkar-Mane, V. (2016). Nanosized Fe₃O₄ an efficient PCR yield enhancer-Comparative study with Au, Ag nanoparticles. *Colloids and Surfaces B: Biointerfaces*, 141, 546–552. <https://doi.org/10.1016/j.colsurfb.2016.02.024>
- Kang, Y. S., Risbud, S., Rabolt, J. F., & Stroeve, P. (1996). Synthesis and characterization of nanometer-size Fe₃O₄ and γ -Fe₂O₃ particles. *Chemistry of Materials*, 8(9), 2209–2211.
- Katz, E. A. (2006). Fullerene thin films as photovoltaic material. In *Nanostructured materials for solar energy conversion* (pp. 361–443). Elsevier.
- Khaliq R, A., Kafafy, R., Salleh, H. M., & Faris, W. F. (2012). Enhancing the efficiency of polymerase chain reaction using graphene nanoflakes. *Nanotechnology*, 23(45), 455106. <https://doi.org/10.1088/0957-4484/23/45/455106>
- Kikugawa, G., Ohara, T., Kawaguchi, T., Torigoe, E., Hagiwara, Y., & Matsumoto, Y. (2009). A molecular dynamics study on heat transfer characteristics at the interfaces of alkanethiolate self-assembled monolayer and organic solvent. *Journal of Chemical Physics*, 130(7). <https://doi.org/10.1063/1.3077315>
- Kim, T., & Hyeon, T. (2013). Applications of inorganic nanoparticles as therapeutic agents. *Nanotechnology*, 25(1), 12001.
- Kleppe, K., Ohtsuka, E., Kleppe, R., Molineux, I., & Khorana, H. G. (1971). Studies on polynucleotides. XCVI. Repair replication of short synthetic DNA's as catalyzed by DNA polymerases. *Journal of Molecular Biology*, 56(2), 341–361. [https://doi.org/10.1016/0022-2836\(71\)90469-4](https://doi.org/10.1016/0022-2836(71)90469-4)
- Koca, H. D., Doganay, S., Turgut, A., Tavman, I. H., Saidur, R., & Mahbulul, I. M. (2018). Effect of particle size on the viscosity of nanofluids: A review. *Renewable and Sustainable Energy Reviews*, 82(February), 1664–1674. <https://doi.org/10.1016/j.rser.2017.07.016>
- Kole, M., & Dey, T. K. (2013). Investigation of thermal conductivity, viscosity, and electrical conductivity of graphene based nanofluids. *Journal of Applied Physics*. <https://doi.org/10.1063/1.4793581>
- Krüger, A., Liang, Y., Jarre, G., & Stegk, J. (2006). Surface functionalisation of detonation diamond suitable for biological applications. *Journal of Materials Chemistry*, 16(24), 2322–2328.
- Kumar, M. S., Vasu, V., & Gopal, A. V. (2016). Thermal conductivity and rheological studies for Cu–Zn hybrid nanofluids with various basefluids. *Journal of the Taiwan Institute of Chemical Engineers*, 66, 321–327.

<https://doi.org/10.1016/j.jtice.2016.05.033>

- Kumar, V., & Sarkar, J. (2019). Numerical and experimental investigations on heat transfer and pressure drop characteristics of Al₂O₃-TiO₂ hybrid nanofluid in minichannel heat sink with different mixture ratio. *Powder Technology*. <https://doi.org/10.1016/j.powtec.2019.01.061>
- Kwek, D., Crivoi, A., & Duan, F. (2010). Effects of temperature and particle size on the thermal property measurements of Al₂O₃ - Water nanofluids. *Journal of Chemical and Engineering Data*, 55(12), 5690–5695. <https://doi.org/10.1021/jc1006407>
- Lalwani, G., & Sitharaman, B. (2013). Multifunctional fullerene-and metallofullerene-based nanobiomaterials. *Nano Life*, 3(03), 1342003.
- Lamminen, E. (2011). Accurate measurement of nanoparticle charge, number and size with the ELPI+TM instrument. *Journal of Physics: Conference Series*, 304(1), 1–13. <https://doi.org/10.1088/1742-6596/304/1/012064>
- Larkin, M. A., Blackshields, G., Brown, N. P., Chenna, R., McGettigan, P. A., McWilliam, H., & Thompson, J. D. (2007). Clustal W and Clustal X version 2.0. *bioinformatics*, 23(21), 2947-2948.
- Lee, S. W., Park, S. D., Kang, S., Bang, I. C., & Kim, J. H. (2011). Investigation of viscosity and thermal conductivity of SiC nanofluids for heat transfer applications. *International Journal of Heat and Mass Transfer*, 54(1–3), 433–438. <https://doi.org/10.1016/j.ijheatmasstransfer.2010.09.026>
- Leong, K. H., Sim, L. C., Bahnemann, D., Jang, M., Ibrahim, S., & Saravanan, P. (2015). Reduced graphene oxide and Ag wrapped TiO₂ photocatalyst for enhanced visible light photocatalysis. *APL Materials*, 3(10), 104503. <https://doi.org/10.1063/1.4926454>
- Li, H., & Rothberg, L. (2004). Colorimetric detection of DNA sequences based on electrostatic interactions with unmodified gold nanoparticles. *Proceedings of the National Academy of Sciences*, 101(39), 14036–14039. <https://doi.org/10.1073/pnas.0406115101>
- Li, Haikuo, Huang, J., Lv, J., An, H., Zhang, X., Zhang, Z., Hu, J. (2005). Nanoparticle PCR: Nanogold-assisted PCR with enhanced specificity. *Angewandte Chemie - International Edition*, 44(32), 5100–5103. <https://doi.org/10.1002/anie.200500403>
- Li, M. (2005). Enhancing the efficiency of a PCR using gold nanoparticles. *Nucleic Acids Research*, 33(21), e184–e184. <https://doi.org/10.1093/nar/gni183>
- Li, X., Chen, Y., Mo, S., Jia, L., & Shao, X. (2014). Effect of surface modification on the stability and thermal conductivity of water-based SiO₂-coated graphene nanofluid. *Thermochimica Acta*. <https://doi.org/10.1016/j.tca.2014.09.006>
- Liang, Y., Luo, F., Lin, Y., Zhou, Q. F., & Jiang, G. Bin. (2009). C₆₀affects DNA replication in vitro by decreasing the melting temperature of DNA templates.

Carbon, 47(6), 1457–1465. <https://doi.org/10.1016/j.carbon.2009.01.038>

- Liu, H., Duan, C., Su, X., Dong, X., Huang, Z., Shen, W., & Zhu, Z. (2014). A hemoglobin encapsulated Titania nanosheet modified reduced graphene oxide nanocomposite as a mediator-free biosensor. *Sensors and Actuators, B: Chemical*, 203(7), 303–310. <https://doi.org/10.1016/j.snb.2014.07.006>
- Liu, Q., Cui, Q., Li, X. J., & Jin, L. (2014). The applications of buckminsterfullerene C60 and derivatives in orthopaedic research. *Connective Tissue Research*, 55(2), 71–79. <https://doi.org/10.3109/03008207.2013.877894>
- Liu, Z., Tabakman, S., Welsher, K., & Dai, H. (2009). Carbon nanotubes in biology and medicine: in vitro and in vivo detection, imaging and drug delivery. *Nano Research*, 2(2), 85–120.
- Liu, Z., Li, J., Liu, Z., Li, J., Li, Z., Wang, C., ... Guo, L. (2019). Development of a nanoparticle-assisted PCR assay for detection of bovine respiratory syncytial virus. *BMC Veterinary Research*, 15(1), 1–6. <https://doi.org/10.1186/s12917-019-1858-0>
- Lou, X., & Zhang, Y. (2013). Mechanism studies on nanoPCR and applications of gold nanoparticles in genetic analysis. *ACS Applied Materials and Interfaces*, 5(13), 6276–6284. <https://doi.org/10.1021/am4013209>
- Maleki, M. J., Ghasemi, Y., Pourhassan-Moghaddam, M., Asadi, N., Dadashpour, M., Abolghasem Mohammadi, S., Zarghami, N. (2019). Effect of green GO/Au nanocomposite on in-vitro amplification of human DNA. *IET Nanobiotechnology*, 13(9), 887–890. <https://doi.org/10.1049/iet-nbt.2018.5082>
- Marie, R., Thaysen, J., Christensen, C. B. V., & Boisen, A. (2003). A cantilever-based sensor for thermal cycling in buffer solution. *Microelectronic Engineering*, 67–68, 893–898. [https://doi.org/10.1016/S0167-9317\(03\)00152-7](https://doi.org/10.1016/S0167-9317(03)00152-7)
- Markwell, J. (2009). *Fundamental laboratory approaches for biochemistry and biotechnology, 2nd edition. Biochemistry and Molecular Biology Education* (Vol. 37). Fitzgerald Science Press Bethesda, MD. <https://doi.org/10.1002/bmb.20321>
- Masuda, H., Ebata, A., Teramae, K., & Hishinuma, N. (1993). Alteration of Thermal Conductivity and Viscosity of Liquid by Dispersing Ultra-Fine Particles. Dispersion of Al₂O₃, SiO₂ and TiO₂ Ultra-Fine Particles. *Netsu Bussei*, 7(4), 227–233. <https://doi.org/10.2963/jjtp.7.227>
- Ma, X., Cui, Y., Qiu, Z., Zhang, B., & Cui, S. (2013). A nanoparticle-assisted PCR assay to improve the sensitivity for rapid detection and differentiation of wild-type pseudorabies virus and gene-deleted vaccine strains. *Journal of Virological Methods*. <https://doi.org/10.1016/j.jviromet.2013.07.018>
- McMahon, S. J., Hyland, W. B., Muir, M. F., Coulter, J. A., Jain, S., Butterworth, K. T. O'sullivan, J. M. (2011). Biological consequences of nanoscale energy deposition near irradiated heavy atom nanoparticles. *Scientific Reports*, 1, 18.

- McNaught, A. D., & Wilkinson, A. (1997). *Compendium of chemical terminology* (Vol. 1669). Blackwell Science Oxford.
- Mekheimer, K. S., Hasona, W. M., Abo-Elkhair, R. E., & Zaher, A. Z. (2018). Peristaltic blood flow with gold nanoparticles as a third grade nanofluid in catheter: Application of cancer therapy. *Physics Letters, Section A: General, Atomic and Solid State Physics*, 382(2–3), 85–93. <https://doi.org/10.1016/j.physleta.2017.10.042>
- Meyer, J. P., Adio, S. A., Sharifpur, M., & Nwosu, P. N. (2016). The Viscosity of Nanofluids: A Review of the Theoretical, Empirical, and Numerical Models. *Heat Transfer Engineering*, 37(5), 387–421. <https://doi.org/10.1080/01457632.2015.1057447>
- Mi, L., Zhu, H., Zhang, X., Hu, J., & Fan, C. (2007). Mechanism of the interaction between Au nanoparticles and polymerase in nanoparticle PCR. *Chinese Science Bulletin*, 52(17), 2345–2349. <https://doi.org/10.1007/s11434-007-0327-5>
- Mihov, D., & Katerska, B. (2010). Some biocompatible materials used in medical practice. *Trakia Journal of Sciences*, 8(2), 119–125.
- Mintmire, J. W., Dunlap, B. I., & White, C. T. (1992). Are fullerene tubules metallic? *Physical Review Letters*, 68(5), 631.
- Mishra, P. C., Mukherjee, S., Nayak, S. K., & Panda, A. (2014). A brief review on viscosity of nanofluids. *International Nano Letters*, 4(4), 109–120. <https://doi.org/10.1007/s40089-014-0126-3>
- Mittal, A. K., Chisti, Y., & Banerjee, U. C. (2013). Synthesis of metallic nanoparticles using plant extracts. *Biotechnology Advances*, 31(2), 346–356.
- Mochalin, V. N., Shenderova, O., Ho, D., & Gogotsi, Y. (2012). The properties and applications of nanodiamonds. *Nature Nanotechnology*, 7(1), 11–23. <https://doi.org/10.1038/nnano.2011.209>
- Motahari, K., Abdollahi Moghaddam, M., & Moradian, M. (2018). Experimental investigation and development of new correlation for influences of temperature and concentration on dynamic viscosity of MWCNT-SiO₂ (20-80)/20W50 hybrid nano-lubricant. *Chinese Journal of Chemical Engineering*, 26(1), 152–158. <https://doi.org/10.1016/j.cjche.2017.06.011>
- Mukherjee, A., Mohammed Sadiq, I., Prathna, T. C., & Chandrasekaran, N. (2011). Antimicrobial activity of aluminium oxide nanoparticles for potential clinical applications. *Science against Microbial Pathogens: Communicating Current Research and Technological Advances*, 1, 245–251.
- Mullis, K., Faloona, F., Scharf, S., Saiki, R., Horn, G., & Erlich, H. (1986). Specific enzymatic amplification of DNA in vitro: The polymerase chain reaction. In *Cold Spring Harbor Symposia on Quantitative Biology* (Vol. 51, pp. 263–273). Cold Spring Harbor Laboratory Press. <https://doi.org/10.1101/SQB.1986.051.01.032>

- Murshed, S. M. S., & Estellé, P. (2017). A state of the art review on viscosity of nanofluids. *Renewable and Sustainable Energy Reviews*, 76(March), 1134–1152. <https://doi.org/10.1016/j.rser.2017.03.113>
- Nabil, M. F., Azmi, W. H., Abdul Hamid, K., Mamat, R., & Hagos, F. Y. (2017). An experimental study on the thermal conductivity and dynamic viscosity of TiO₂-SiO₂ nanofluids in water: Ethylene glycol mixture. *International Communications in Heat and Mass Transfer*, 86, 181–189. <https://doi.org/10.1016/j.icheatmasstransfer.2017.05.024>
- Nakamuta, Y., & Toh, S. (2013). Transformation of graphite to lonsdaleite and diamond in the Goalpara ureilite directly observed by TEM. *American Mineralogist*, 98(4), 574–581.
- Naphon, P., & Thongjng, C. (2014). Pool boiling heat transfer characteristics of refrigerant-nanoparticle mixtures. *International Communications in Heat and Mass Transfer*, 52, 84–89. <https://doi.org/10.1016/j.icheatmasstransfer.2014.01.014>
- Narang, J., Narang, J., Malhotra, N., Narang, S., Singhal, C., Kansal, R., ... Pundir, C. (2016). Replacement of magnesium chloride with magnesium nanoparticles in polymerase chain reaction. *Protocol Exchange*, 1–5. <https://doi.org/10.1038/protex.2016.021>
- Nejdl, L., Kudr, J., Moulick, A., Hegerova, D., Ruttkay-Nedecky, B., Gumulec, J., ... Adam, V. (2017). Platinum nanoparticles induce damage to DNA and inhibit DNA replication. *PLoS ONE*, 12(7), 1–19. <https://doi.org/10.1371/journal.pone.0180798>
- Németh, P., Garvie, L. A. J., Aoki, T., Dubrovinskaia, N., Dubrovinsky, L., & Buseck, P. R. (2014). Lonsdaleite is faulted and twinned cubic diamond and does not exist as a discrete material. *Nature Communications*, 5(1), 1–5.
- Nguyen, C. T., Desgranges, F., Galanis, N., Roy, G., Maré, T., Boucher, S., & Angue Mintsas, H. (2008). Viscosity data for Al₂O₃-water nanofluid-hysteresis: is heat transfer enhancement using nanofluids reliable? *International Journal of Thermal Sciences*, 47(2), 103–111. <https://doi.org/10.1016/j.ijthermalsci.2007.01.033>
- Niidome, T., Yamagata, M., Okamoto, Y., Akiyama, Y., Takahashi, H., Kawano, T., ... Niidome, Y. (2006). PEG-modified gold nanorods with a stealth character for in vivo applications. *Journal of Controlled Release*, 114(3), 343–347.
- Pan, D., Mi, L., Huang, Q., Hu, J., & Fan, C. (2012). Genetic analysis with nanoPCR. *Integrative Biology (United Kingdom)*, 4(10), 1155–1163. <https://doi.org/10.1039/c2ib20076g>
- Pan, Z., Sun, H., Zhang, Y., & Chen, C. (2009). Harder than diamond: Superior indentation strength of wurtzite BN and lonsdaleite. *Physical Review Letters*, 102(5), 1–4. <https://doi.org/10.1103/PhysRevLett.102.055503>
- Park, J. Y., Back, S. H., Chang, S. J., Lee, S. J., Lee, K. G., & Park, T. J. (2015a).

- Dopamine-Assisted Synthesis of Carbon-Coated Silica for PCR Enhancement. *ACS Applied Materials and Interfaces*, 7(28), 15633–15640. <https://doi.org/10.1021/acsami.5b04404>
- Park, J. Y., Back, S. H., Chang, S. J., Lee, S. J., Lee, K. G., & Park, T. J. (2015b). Dopamine-Assisted Synthesis of Carbon-Coated Silica for PCR Enhancement. *ACS Applied Materials and Interfaces*, 7(28), 15633–15640. <https://doi.org/10.1021/acsami.5b04404>
- Park, S. S., & Kim, N. J. (2014). Influence of the oxidation treatment and the average particle diameter of graphene for thermal conductivity enhancement. *Journal of Industrial and Engineering Chemistry*. <https://doi.org/10.1016/j.jiec.2013.09.011>
- Pastoriza-Gallego, M. J., Lugo, L., Legido, J. L., & Piñeiro, M. M. (2011). Rheological non-newtonian behaviour of ethylene glycol-based Fe₂O₃ nanofluids. *Nanoscale Research Letters*, 6, 1–7. <https://doi.org/10.1186/1556-276X-6-560>
- Pelka, J., Gehrke, H., Esselen, M., Türk, M., Crone, M., Bräse, S., ... Zibat, V. (2009). Cellular uptake of platinum nanoparticles in human colon carcinoma cells and their impact on cellular redox systems and DNA integrity. *Chemical Research in Toxicology*, 22(4), 649–659.
- Peng, H., Ding, G., & Hu, H. (2011). Effect of surfactant additives on nucleate pool boiling heat transfer of refrigerant-based nanofluid. *Experimental Thermal and Fluid Science*, 35(6), 960–970. <https://doi.org/10.1016/j.expthermflusci.2011.01.016>
- Perera, S. D., Mariano, R. G., Vu, K., Nour, N., Seitz, O., Chabal, Y., & Balkus, K. J. (2012). Hydrothermal synthesis of graphene-TiO₂ nanotube composites with enhanced photocatalytic activity. *ACS Catalysis*, 2(6), 949–956. <https://doi.org/10.1021/cs200621c>
- Pérez-Pérez, F. J., & Hanson, N. D. (2002). Detection of plasmid-mediated Amp^C beta-lactamase genes in clinical isolates by using multiplex PCR. *Journal of Clinical Microbiology*, 40(6), 2153–2162. <https://doi.org/10.1128/JCM.40.6.2153>
- Petralia, S., Barbuzzi, T., & Ventimiglia, G. (2012). Polymerase chain reaction efficiency improved by water soluble β -cyclodextrins capped platinum nanoparticles. *Materials Science and Engineering C*. <https://doi.org/10.1016/j.msec.2012.01.036>
- Pinto, R. V., & Fiorelli, F. A. S. (2016). Review of the mechanisms responsible for heat transfer enhancement using nanofluids. *Applied Thermal Engineering*, 108, 720–739. <https://doi.org/10.1016/j.applthermaleng.2016.07.147>
- Ponce, M. R., & Micol, J. L. (1992). PCR amplification of long DNA fragments. *Nucleic Acids Research*, 20(3), 623–623. <https://doi.org/10.1093/nar/20.3.623>
- Prasher, R., Song, D., Wang, J., & Phelan, P. (2006). Measurements of nanofluid viscosity and its implications for thermal applications. *Applied Physics Letters*, 89(13), 133108–3. <https://doi.org/10.1063/1.2356113>

- Putra, N., Roetzel, W., & Das, S. K. (2003). Natural convection of nano-fluids. *Heat and Mass Transfer/Waerme- Und Stoffuebertragung*, 39(8–9), 775–784. <https://doi.org/10.1007/s00231-002-0382-z>
- Qian, X., Zhou, X., & Nie, S. (2008). Surface-enhanced Raman nanoparticle beacons based on bioconjugated gold nanocrystals and long range plasmonic coupling. *Journal of the American Chemical Society*, 130(45), 14934–14935.
- Ranga Babu, J. A., Kumar, K. K., & Srinivasa Rao, S. (2017). State-of-art review on hybrid nanofluids. *Renewable and Sustainable Energy Reviews*, 77(March), 551–565. <https://doi.org/10.1016/j.rser.2017.04.040>
- Rao, C. N. R., Seshadri, R., Govindaraj, A., & Sen, R. (1995). Fullerenes, nanotubes, onions and related carbon structures. *Materials Science and Engineering: R: Reports*, 15(6), 209–262.
- Rasheed, A. K., Khalid, M., Rashmi, W., Gupta, T. C. S. M., & Chan, A. (2016). Graphene based nanofluids and nanolubricants - Review of recent developments. *Renewable and Sustainable Energy Reviews*, 63(September), 346–362. <https://doi.org/10.1016/j.rser.2016.04.072>
- Robertson, J. (2002). Diamond-like amorphous carbon. *Materials Science and Engineering: R: Reports*, 37(4–6), 129–281. [https://doi.org/10.1016/s0927-796x\(02\)00005-0](https://doi.org/10.1016/s0927-796x(02)00005-0)
- Rodríguez-Lázaro, D., Lombard, B., Smith, H., Rzezutka, A., D'Agostino, M., Helmuth, R., Cook, N. (2007). Trends in analytical methodology in food safety and quality: monitoring microorganisms and genetically modified organisms. *Trends in Food Science and Technology*, 18(6), 306–319. <https://doi.org/10.1016/j.tifs.2007.01.009>
- Rosen, Y., & Elman, N. M. (2009). Carbon nanotubes in drug delivery: focus on infectious diseases. *Expert Opinion on Drug Delivery*, 6(5), 517–530.
- Roy, P., Berger, S., & Schmuki, P. (2011). TiO₂ nanotubes: synthesis and applications. *Angewandte Chemie International Edition*, 50(13), 2904–2939.
- Rudge, S., Peterson, C., Vessely, C., Koda, J., Stevens, S., & Catterall, L. (2001). Adsorption and desorption of chemotherapeutic drugs from a magnetically targeted carrier (MTC). *Journal of Controlled Release*, 74(1–3), 335–340.
- Sailapu, S. K., Dutta, D., Sahoo, A. K., Ghosh, S. S., & Chattopadhyay, A. (2018). Single Platform for Gene and Protein Expression Analyses Using Luminescent Gold Nanoclusters. *ACS Omega*, 3(2), 2119–2129. <https://doi.org/10.1021/acsomega.7b01739>
- Sajid, M. U., & Ali, H. M. (2018). Thermal conductivity of hybrid nanofluids: A critical review. *International Journal of Heat and Mass Transfer*, 126, 211–234. <https://doi.org/10.1016/j.ijheatmasstransfer.2018.05.021>
- Sanchez, C., Lebeau, B., Chaput, F., & Boilot, J.-P. (2003). Optical Properties of

- Functional Hybrid Organic–Inorganic Nanocomposites. *Advanced Materials*, 15(23), 1969–1994. <https://doi.org/10.1002/adma.200300389>
- Sang, F. M., LI, X., & LIU, J. (2017). Development of Nano-Polymerase Chain Reaction and Its Application. *Chinese Journal of Analytical Chemistry*, 45(11), 1745–1753. [https://doi.org/10.1016/S1872-2040\(17\)61051-X](https://doi.org/10.1016/S1872-2040(17)61051-X)
- Sang, F., Yang, Y., Yuan, L., Ren, J., & Zhang, Z. (2015). Development of a high-throughput real time PCR based on a hot-start alternative for Pfu mediated by quantum dots. *Nanoscale*, 7(38), 15852–15862. <https://doi.org/10.1039/c5nr03596a>
- Schmid-Burgk, J. L., Schmidt, T., Kaiser, V., Höning, K., & Hornung, V. (2013). A ligation-independent cloning technique for high-throughput assembly of transcription activator-like effector genes. *Nature Biotechnology*, 31(1), 76–81. <https://doi.org/10.1038/nbt.2460>
- Schrand, A. M., Hens, S. A. C., & Shenderova, O. A. (2009). Nanodiamond particles: Properties and perspectives for bioapplications. *Critical Reviews in Solid State and Materials Sciences*, 34(1–2), 18–74. <https://doi.org/10.1080/10408430902831987>
- Schrand, A. M., Huang, H., Carlson, C., Schlager, J. J., Ōsawa, E., Hussain, S. M., & Dai, L. (2007). Are diamond nanoparticles cytotoxic? *The Journal of Physical Chemistry B*, 111(1), 2–7.
- Sellner, L. N., Coelen, R. J., & Mackenzie, J. S. (1992). Reverse transcriptase inhibits taq polymerase activity. *Nucleic Acids Research*, 20(7), 1487–1490. <https://doi.org/10.1093/nar/20.7.1487>
- Shah, S. N. A., Shahabuddin, S., Sabri, M. F. M., Salleh, M. F. M., Ali, M. A., Hayat, N., ... Saidur, R. (2020). Experimental investigation on stability, thermal conductivity and rheological properties of rGO/ethylene glycol based nanofluids. *International Journal of Heat and Mass Transfer*, 150, 118981. <https://doi.org/10.1016/j.ijheatmasstransfer.2019.118981>
- Sharma, A. K., Tiwari, A. K., & Dixit, A. R. (2016). Rheological behaviour of nanofluids: A review. *Renewable and Sustainable Energy Reviews*, 53, 779–791. <https://doi.org/10.1016/j.rser.2015.09.033>
- Sharma, D., Pandey, K. M., Debbarma, A., & Choubey, G. (2017). Numerical Investigation of heat transfer enhancement of SiO₂-water based nanofluids in Light water nuclear reactor. *Materials Today: Proceedings*, 4(9), 10118–10122. <https://doi.org/10.1016/j.matpr.2017.06.332>
- Sharma, S., Tiwari, A. K., Tiwari, S., & Prakash, R. (2018). Viscosity of hybrid nanofluids: Measurement and comparison. *Journal of Mechanical Engineering and Sciences*, 12(2), 3614–3623. <https://doi.org/10.15282/jmes.12.2.2018.8.0320>
- Sharma, V., Rajaura, R., Sharma, P. K., Srivastava, R. R., Sharma, S. S., & Agrawal, K. (2016). Studying the effect of graphene-ZnO nanocomposites on polymerase chain reaction. *AIP Conference Proceedings*, 1728.

<https://doi.org/10.1063/1.4946577>

- Shen, C., Yang, W., Ji, Q., Maki, H., Dong, A., & Zhang, Z. (2009). NanoPCR observation: Different levels of DNA replication fidelity in nanoparticle-enhanced polymerase chain reactions. *Nanotechnology*, 20(45), 455103. <https://doi.org/10.1088/0957-4484/20/45/455103>
- Shen, C., & Zhang, Z. (2013). An Overview of Nanoparticle-Assisted Polymerase Chain Reaction Technology. *Bio-Nanotechnology: A Revolution in Food, Biomedical and Health Sciences*, 97–106. <https://doi.org/10.1002/9781118451915.ch5>
- Sidik, N. A. C., Adamu, I. M., Jamil, M. M., Kefayati, G. H. R., Mamat, R., & Najafi, G. (2016). Recent progress on hybrid nanofluids in heat transfer applications: A comprehensive review. *International Communications in Heat and Mass Transfer*. <https://doi.org/10.1016/j.icheatmasstransfer.2016.08.019>
- Siqueira, J. F., & Rôças, I. N. (2003). PCR methodology as a valuable tool for identification of endodontic pathogens. *Journal of Dentistry*, 31(5), 333–339. [https://doi.org/10.1016/S0300-5712\(03\)00051-4](https://doi.org/10.1016/S0300-5712(03)00051-4)
- Sokolov, K., Tam, J., Tam, J., Travis, K., Larson, T., Aaron, J., Johnston, K. (2009). Cancer imaging and therapy with metal nanoparticles. In *2009 Annual International Conference of the IEEE Engineering in Medicine and Biology Society* (pp. 2005–2007). IEEE.
- Sridhara, V., & Satapathy, L. N. (2011). Al₂O₃-based nanofluids: A review. *Nanoscale Research Letters*, 6(1), 1–16. <https://doi.org/10.1186/1556-276X-6-456>
- Sun, C., Cheng, Y., Pan, Y., Yang, J., Wang, X., & Xia, F. (2020). Efficient polymerase chain reaction assisted by metal-organic frameworks. *Chemical Science*, 11(3), 797–802. <https://doi.org/10.1039/c9sc03202a>
- Suresh, S., Venkitaraj, K. P., Selvakumar, P., & Chandrasekar, M. (2011). Synthesis of Al₂O₃-Cu/water hybrid nanofluids using two step method and its thermo physical properties. *Colloids and Surfaces A: Physicochemical and Engineering Aspects*, 388(1–3), 41–48. <https://doi.org/10.1016/j.colsurfa.2011.08.005>
- Talib, S. F. A., Azmi, W. H., Zakaria, I., Mohamed, W., Mamat, A. M. I., Ismail, H., & Daud, W. R. W. (2015). Thermophysical Properties of Silicon Dioxide (SiO₂) in Ethylene Glycol/Water Mixture for Proton Exchange Membrane Fuel Cell Cooling Application. *Energy Procedia*. <https://doi.org/10.1016/j.egypro.2015.11.504>
- Talyzin, A. V., & Engström, I. (1998). C70 in benzene, hexane, and toluene solutions. *The Journal of Physical Chemistry B*, 102(34), 6477–6481.
- Tan, L. L., Ong, W. J., Chai, S. P., & Mohamed, A. R. (2013). Reduced graphene oxide-TiO₂ nanocomposite as a promising visible-light-active photocatalyst for the conversion of carbon dioxide. *Nanoscale Research Letters*, 8(1), 465. <https://doi.org/10.1186/1556-276X-8-465>

- Tang, S., Chen, M., & Zheng, N. (2014). Sub-10-nm Pd Nanosheets with renal clearance for efficient near-infrared photothermal cancer therapy. *Small*, *10*(15), 3139–3144.
- Thamilselvi, V., & Radha, K. V. (2017). A Review On The Diverse Application Of Silver Nanoparticle. *IOSR Journal of Pharmacy (IOSRPHR)*, *07*(01), 21–27. <https://doi.org/10.9790/3013-0701012127>
- Thomas, R. T., Abdul Rasheed, P., & Sandhyarani, N. (2014). Synthesis of nanotitania decorated few-layer graphene for enhanced visible light driven photocatalysis. *Journal of Colloid and Interface Science*, *428*, 214–221. <https://doi.org/10.1016/j.jcis.2014.04.054>
- Tomblin, G., Bellizzi, D., & Sgaramella, V. (1996). Heterogeneity of primer extension products in asymmetric PCR is due both to cleavage by a structure-specific exo/endonuclease activity of DNA polymerases and to premature stops. *Proc Natl Acad Sci U S A*, *93*(7), 2724–2728. <https://doi.org/DOI 10.1073/pnas.93.7.2724>
- Tong, L., Wei, Q., Wei, A., & Cheng, J. (2009). Gold nanorods as contrast agents for biological imaging: optical properties, surface conjugation and photothermal effects. *Photochemistry and Photobiology*, *85*(1), 21–32.
- Tong, W., Cao, X., Wen, S., Guo, R., Shen, M., Wang, J., & Shi, X. (2012). Enhancing the specificity and efficiency of polymerase chain reaction using polyethyleneimine-based derivatives and hybrid nanocomposites. *International Journal of Nanomedicine*. <https://doi.org/10.2147/IJN.S28947>
- Tsai, T. H., Kuo, L. S., Chen, P. H., & Yang, C. T. (2008). Effect of viscosity of base fluid on thermal conductivity of nanofluids. *Applied Physics Letters*, *93*(23), 23–25. <https://doi.org/10.1063/1.3046732>
- Uddin, M. E., Kuila, T., Nayak, G. C., Kim, N. H., Ku, B. C., & Lee, J. H. (2013). Effects of various surfactants on the dispersion stability and electrical conductivity of surface modified graphene. *Journal of Alloys and Compounds*, *562*, 134–142. <https://doi.org/DOI 10.1016/j.jallcom.2013.01.127>
- Upadhyay, A., Yang, H., Zaman, B., Zhang, L., Wu, Y., Wang, J., ... Han, Q. (2020). ZnO nanolower-based nanoPCR as an efficient diagnostic tool for quick diagnosis of canine vector-borne pathogens. *Pathogens*, *9*(2), 1–14. <https://doi.org/10.3390/pathogens9020122>
- Ussery, D. W. (2013). DNA Denaturation. *Brenner's Encyclopedia of Genetics: Second Edition*, 353–355. <https://doi.org/10.1016/B978-0-12-374984-0.00418-6>
- Varadaraj, K., & Skinner, D. M. (1994). Denaturants or cosolvents improve the specificity of PCR amplification of a G+C-rich DNA using genetically engineered DNA polymerases. *Gene*, *140*(1), 1–5.
- Velasco-Soto, M. A., Pérez-García, S. A., Alvarez-Quintana, J., Cao, Y., Nyborg, L., & Licea-Jiménez, L. (2015). Selective band gap manipulation of graphene oxide by its reduction with mild reagents. *Carbon*, *93*, 967–973.

<https://doi.org/10.1016/j.carbon.2015.06.013>

- Vo, B. T., Wolf, E., Kawauchi, D., Gebhardt, A., Rehg, J. E., Finkelstein, D., Han, Y.-G. (2016). The interaction of Myc with Miz1 defines medulloblastoma subgroup identity. *Cancer Cell*, 29(1), 5–16.
- Wan, W. W. W., Yeow, J. T. W., & Dyke, M. I. Van. (2009). Effect of silver and titanium dioxide nanoparticles on PCR efficiency. *2009 9th IEEE Conference on Nanotechnology (IEEE-NANO)*, 8, 458–461.
- Wang, J., Cheng, Y., Zhang, M., Zhao, H., Lin, P., Yi, L., & Cheng, S. (2015). Development of a nanoparticle-assisted PCR (nanoPCR) assay for detection of mink enteritis virus (MEV) and genetic characterization of the NS1 gene in four Chinese MEV strains. *BMC veterinary research*, 11(1), 1-8.
- Wang, B., Wang, X., Lou, W., & Hao, J. (2012). Thermal conductivity and rheological properties of graphite/oil nanofluids. *Colloids and Surfaces A: Physicochemical and Engineering Aspects*, 414, 125–131. <https://doi.org/10.1016/j.colsurfa.2012.08.008>
- Wang, J., Xu, D., & Polsky, R. (2002). Magnetically-induced solid-state electrochemical detection of DNA hybridization. *Journal of the American Chemical Society*, 124(16), 4208–4209. <https://doi.org/10.1021/ja0255709>
- Wang, M., Yan, Y., Wang, R., Wang, L., Zhou, H., Li, Y., Qiao, X. (2019). Simultaneous Detection of Bovine Rotavirus, Bovine Parvovirus, and Bovine Viral Diarrhea Virus Using a Gold Nanoparticle-Assisted PCR Assay with a Dual-Priming Oligonucleotide System. *Frontiers in Microbiology*, 10(December), 1–9. <https://doi.org/10.3389/fmicb.2019.02884>
- Wei, D., & Liu, Y. (2010). Controllable synthesis of graphene and its applications. *Advanced Materials*, 22(30), 3225–3241.
- Wen, D., & Ding, Y. (2004). Experimental investigation into convective heat transfer of nanofluids at the entrance region under laminar flow conditions. *International Journal of Heat and Mass Transfer*. <https://doi.org/10.1016/j.ijheatmasstransfer.2004.07.012>
- Wen, T., Gao, J., Shen, J., & Zhou, Z. (2001). Preparation and characterization of TiO₂ thin films by the sol-gel process. *Journal of Materials Science*, 36(24), 5923–5926. <https://doi.org/10.1023/A:1012989012840>
- Williams, Oliver A, Douhéret, O., Daenen, M., Haenen, K., Ōsawa, E., & Takahashi, M. (2007). Enhanced diamond nucleation on monodispersed nanocrystalline diamond. *Chemical Physics Letters*, 445(4–6), 255–258.
- Williams, Oliver Aneurin, Kriele, A., Hees, J., Wolfer, M., Müller-Sebert, W., & Nebel, C. E. (2010). High Young's modulus in ultra-thin nanocrystalline diamond. *Chemical Physics Letters*, 495(1–3), 84–89.
- Wong, K. V., & Castillo, M. J. (2010). Heat transfer mechanisms and clustering in

- nanofluids. *Advances in Mechanical Engineering*, 2010. <https://doi.org/10.1155/2010/795478>
- Xu, S., & Yao, M. (2013). NanoPCR detection of bacterial aerosols. *Journal of Aerosol Science*, 65, 1–9. <https://doi.org/10.1016/j.jaerosci.2013.06.005>
- Xu, X., Zhang, K., Zhao, L., Wang, D., Bu, W., Zheng, C., & Sun, H. (2014). Characteristics of three sizes of silica nanoparticles in the osteoblastic cell line, MC3T3-E1. *RSC Advances*, 4(87), 46481–46487.
- Xu, Z., Gao, H., & Guoxin, H. (2011). Solution-based synthesis and characterization of a silver nanoparticle-graphene hybrid film. *Carbon*, 49(14), 4731–4738. <https://doi.org/10.1016/j.carbon.2011.06.078>
- Xue, L., Keblinski, P., Phillpot, S. R., Choi, S. U. S., & Eastman, J. A. (2004). Effect of liquid layering at the liquid-solid interface on thermal transport. *International Journal of Heat and Mass Transfer*. <https://doi.org/10.1016/j.ijheatmasstransfer.2004.05.016>
- Yang, H., Yao, G., & Wen, D. (2020). Experimental investigation on convective heat transfer of Shear-thinning fluids by elastic turbulence in a serpentine channel. *Experimental Thermal and Fluid Science*, 112, 109997. <https://doi.org/10.1016/j.expthermflusci.2019.109997>
- Yang, L., Ji, W., Mao, M., & Huang, J. nan. (2020). An updated review on the properties, fabrication and application of hybrid-nanofluids along with their environmental effects. *Journal of Cleaner Production*, 257, 120408. <https://doi.org/10.1016/j.jclepro.2020.120408>
- Yang, W., Auciello, O., Butler, J. E., Cai, W., Carlisle, J. A., Gerbi, J. E., ... Russell, J. N. (2002). DNA-modified nanocrystalline diamond thin-films as stable, biologically active substrates. *Nature Materials*, 1(4), 253–257.
- Yang, Y., Oztekin, A., Neti, S., & Mohapatra, S. (2012). Particle agglomeration and properties of nanofluids. *Journal of Nanoparticle Research*, 14(5), 852. <https://doi.org/10.1007/s11051-012-0852-2>
- Yu, M.-F., Lourie, O., Dyer, M. J., Moloni, K., Kelly, T. F., & Ruoff, R. S. (2000). Strength and breaking mechanism of multiwalled carbon nanotubes under tensile load. *Science*, 287(5453), 637–640.
- Yuan, W., Li, Y., Wang, J., Wang, J., & Sun, J. (2016). A nanoparticle-assisted PCR assay for the detection of encephalomyocarditis virus. *Veterinarski Arhiv*, 86(1), 1–8.
- Yuce, M., Kurt, H., Mokkaṭpati, V. R. S. S., & Budak, H. (2014). Employment of nanomaterials in polymerase chain reaction: insight into the impacts and putative operating mechanisms of nano-additives in PCR. *RSC Adv.* <https://doi.org/10.1039/C4RA06144F>
- Zakaria, I., Azmi, W. H., Mohamed, W. A. N. W., Mamat, R., & Najafi, G. (2015).

Experimental Investigation of Thermal Conductivity and Electrical Conductivity of Al₂O₃ Nanofluid in Water - Ethylene Glycol Mixture for Proton Exchange Membrane Fuel Cell Application. *International Communications in Heat and Mass Transfer*, 61, 61–68. <https://doi.org/10.1016/j.icheatmasstransfer.2014.12.015>

- Zawawi, N. N. M., Azmi, W. H., Redhwan, A. A. M., Sharif, M. Z., & Sharma, K. V. (2017). Propriétés thermo-physiques du nanolubrifiant composite Al₂O₃-SiO₂/PAG pour les systèmes frigorifiques. *International Journal of Refrigeration*, 80, 1–10. <https://doi.org/10.1016/j.ijrefrig.2017.04.024>
- Zhang, H., Wang, X., Li, N., Xia, J., Meng, Q., Ding, J., & Lu, J. (2018). Synthesis and characterization of TiO₂/graphene oxide nanocomposites for photoreduction of heavy metal ions in reverse osmosis concentrate. *RSC Advances*, 8(60), 34241–34251. <https://doi.org/10.1039/c8ra06681g>
- Zhang, Y., Yang, M., Portney, N. G., Cui, D., Budak, G., Ozbay, E., ... Ozkan, C. S. (2008). Zeta potential: a surface electrical characteristic to probe the interaction of nanoparticles with normal and cancer human breast epithelial cells. *Biomedical Microdevices*, 10(2), 321–328.
- Zhang, Zhiyang, Chen, Z., Wang, S., Qu, C., & Chen, L. (2014). On-site visual detection of hydrogen sulfide in air based on enhancing the stability of gold nanoparticles. *ACS Applied Materials & Interfaces*, 6(9), 6300–6307.
- Zhang, Zhizhou, Shen, C., Wang, M., Han, H., & Cao, X. (2008). Aqueous suspension of carbon nanotubes enhances the specificity of long PCR. *BioTechniques*, 44(4), 537–545. <https://doi.org/10.2144/000112692>
- Zhang, Zhizhou, Wang, M., & An, H. (2007a). An aqueous suspension of carbon nanopowder enhances the efficiency of a polymerase chain reaction. *Nanotechnology*. <https://doi.org/10.1088/0957-4484/18/35/355706>
- Zhong, Y., Huang, L. H., Zhang, Z. Sen, Xiong, Y. J., Sun, L. P., & Weng, J. (2016). Enhancing the specificity of polymerase chain reaction by graphene oxide through surface modification: Zwitterionic polymer is superior to other polymers with different charges. *International Journal of Nanomedicine*, 11, 5989–6002. <https://doi.org/10.2147/IJN.S120659>
- Zhu, H., Wei, J., Wang, K., & Wu, D. (2009). Applications of carbon materials in photovoltaic solar cells. *Solar Energy Materials and Solar Cells*, 93(9), 1461–1470.

PUBLICATIONS

Published/Under Review Journals

FROM THESIS				
NAME OF JOURNAL	RANKI NGS	IMPACT FACTOR	NAME OF MANUSCRIPT	REMARKS
Journal of Thermal Science and Engineering Applications	Q3	1.787	Synthesis and character hybrid nanoparticles as	Communicated – Submitted revision
DNA Research	Q1	5.371	Enhancing the efficiency of PCR using ternary hybrid nanoparticles and its effect on sequence barcode reads	Communicated – Under revision
Journal of Experimental Nanoscience	Q2	2.169	Experimental investigation on rheological properties of water-based novel ternary hybrid nanofluids	Communicated – Under revision
Data In brief	Q4		Dataset on Characterization and Thermal Conductivity Measurements of the Novel Ternary Hybrid Nanoparticles	Communicated – Under review
IIUM Engineering Journal	Q4	0.69	Effect of ternary hybrid nanoparticles on DNA denaturation	Communicated – Under review
			Critical review on nanoPCR: limitations and future prospects	In Preparation

OTHER CONTRIBUTIONS				
NAME OF JOURNAL	RANKI NGS	IMPACT FACTOR	NAME OF MANUSCRIPT	REMARKS
Pathogens	Q1	3.018	hBN Nanoparticle-Assisted Rapid Thermal Cycling for the Detection of Acanthamoeba	Published

Advances in Materials Research	Q2	0.810	Experimental and numerical investigation on a gas turbine blade with the application of thermal barrier coatings	Published
Actuators	Q2	1.957	A review of piezoelectric material applications in engineering structures: challenges and opportunities	Published
Drones		Indexed	Survey on Design and Application of UAV (Drone) Including COVID-19 Duration	Communicated – Under review
Sensors	Q1	3.275	A systematic review of piezoelectric materials and energy harvesters for industrial applications	Published
Journal of modern mechanical Engineering		Indexed	Statistical analysis of adhesive bond parameters in a single lap joint system	Published

APPENDIX A: SEQUENCING FASTA FORMAT

3911756_1-2

TCCGGCCTNGTCCCCCATTGACGTCAATGGGGAGTTTGT TTTTGGCACCA
AAATCAACGGGACTTTCCAAAATGTCGTAACAAC TCCGCCCCATTGACGC
AAATGGGCGGTAGGCGTGTACGGTGGGAGGTCTATA TAAGCAGAGCTCTC
TGGCTAACTAGAGAACCCACTGCTTACTGGCTTATCG AAATTAATACGAC
TCACTATAGGGAGACCCAAGCTTGGTACCGAGCTCGG ATCCACTAGTAAC
GGCCGCCAGTGTGCTGGAATTCTGCAGATATCCATC ACACTGGCGGCCGC
TCCTGATGGAGAGGAGCGCGGAGCAGCGCTTGACTC GGGCGATGCTGAGT
CTGGTCGATCTGGATAAGCAAGTAAGCAGCGACTAGT CCAGCGTGTCCGG
CGAGGGCGAGGGCGATGCCACCTACGGGTAGCTGACC CTGAAGTTCATCT
GCACCACCGGCAAGCTGCCCCGTGCCCTGGCCCACCCT CGTGACCACCCTG
ACCTACGGCGTGCAGTGCTTCAGCCGCTACCCCGACC ACATGAAGCAGCA
CGACTTCTTCAAGTCCGCCATGCCCGAAGGCTACGTCC AGGAGCGCACCA
TCTTCTTCAAGGACGACGGCAACTACAAGACCCGCGCC GAGGTGAAGTTC
GAGGGCGACACCCTGGTGAACCGCATCGAGCTGAAGGG CATCGACTTCAA
GGAGGACGGGCAACATCCTGGGGGCACAAGCTGGAGTACA AACTACAACA
G

CCACAACGTCTATATCATGGCCGACAAGCANCAGAAAAA

>3911757_1-3

GGCTNGTCTNCCATTGACGTCAATGGGGAGTTTGT TTTTGGCACCAAAA
TCAACGGGACTTTCCAAAATGTCGTAACAAC TCCGCCCCATTGACGCAA
TGGGCGGTAGGCGTGTACGGTGGGAGGTCTATA TAAGCAGAGCTCTCTGG
CTAACTAGAGAACCCACTGCTTACTGGCTTATCG AAATTAATACGACTCA

CTATAGGGAGACCCAAGCTTGGTACCGAGCTCGGATCCACTAGTAACGGC
CGCCAGTGTGCTGGAATTCTGCAGATATCCATCACACTGGCGGCCGCTCG
AGATGGTGAGGAGCGCGGAGGAGCGGTTCACTGGGGTGGTGCCGATCCTG
GTCGAGCTGGACGGGGACGTAAGCGGCCACAAGTTCAGCGTGTCCGGCGA
GGGCGAGGGCGATGCCACCTACGGCAAGCTGACCCTGAAGTTCATCTGCA
CCACCGGCAAGCTGCCC GTGCCCTGGCCCACCCTCGTGACCACCCTGACC
TACGGCGTGCAGTGCTTCAGCCGCTACCCCGACCACATGAAGCAGCACGA
CTTCTTCAAGTCCGCCATGCCCGAAGGCTACGTCCAGGAGCGCACCATCT
TCTTCAAGGACGACGGCAACTACAAGACCCGCGCCGAGGTGAAGTTCGAG
GGCGACACCCTGGTGAACCGCATCGAGCTGAAGGGCATCGACTTCAAGGA
GGACGGCAACATCCTGGGGCACAAGCTGGAGTACA ACTACAACAGCCACA
ACGTCTATATCATGGCCGACAAGCAAAAG

>3911758_1-4

CGGGTAGTCCCACCCATTGACGTCAATGGGAGTTTGT TTTGGCACCAAAA
TCAACGGGACTTTCCAAAATGTCGTAACA ACTCCGCCCCATTGACGCAAA
TGGGCGGTAGGCGTGTACGGTGGGAGGTCTATATAAGCAGAGCTCTCTGG
CTAACTAGAGAACCCACTGCTTACTGGCTTATCGAAATTAATACGACTCA
CTATAGGGAGACCCAAGCTTGGTACCGAGCTCGGATCCACTAGTAACGGC
CGCCAGTGTGCTGGAATTCTGCAGATATCCATCACACTGGCGGCAGCTCG
AGATGGTGAGCAAGGGCGAGGAGCTGTTACCCGGGGTGGTGCCCATCCTG
GTCGAGCTGGACGGCGACGTA AACGGGCCACAAGTTCAGCGTGTCCGGCGA
GGGCGAGGGCGATGCCACCTACGGCAAGCTGACCCTGAAGTTCATCTGCA
CCACCGGCAAGCTGCCC GTGCCCTGGCCCACCCTCGTGACCACCCTGACC
TACGGCGTGCAGTGCTTCAGCCGCTACCCCGACCACATGAAGCAGCACGA
CTTCTTCAAGTCCGCCATGCCCGAAGGCTACGTCCAGGAGCGCACCATCT

TCTTCAAGGACGACGGCAACTACAAGACCCGCGCCGAGGTGAAGTTCGAG
GGCGACACCCTGGTGAACCGCATCGAGCTGAAGGGCATCGACTTCAAGGA
GGACGGCAACATCCTGGGGCACAAGCTGGAGTACAACACTACAACAGCCACA
ACGTCTATATCATGGCCGACAAGCAAAGAACGGN

>3911759_2-2

GCCTNGTCTNCCCATTGACGTCAATGGGGAGTTTGTGTTTTGGCACCAAAT
CAACGGGACTTTCCAAAATGTCGTAACAACCTCCGCCCCATTGACGCAAAT
GGGCGGTAGGCGTGTACGGTGGGAGGTCTATATAAGCAGAGCTCTCTGGC
TAACTAGAGAACCCACTGCTTACTGGCTTATCGAAATTAATACGACTCAC
TATAGGGAGACCCAAGCTTGGTACCGAGCTCGGATCCACTAGTAACGGCC
GCCAGTGTGCTGGAATTCTGCAGATATCCATCACACTGGCGGCCGCTCCT
GATGGAGAGGAGCGCGGAGCAGCGCTTGACTGGGGTGATGCTGAGCCTGG
TCGAGCTGGACGGGGACGTAAACGGCCACAAGTTCAGCGTGTCCGGCGAG
GGCGAGGGCGATGCCACCTACGGCAAGCTGACCCTGAAGTTCATCTGCAC
CACCGGCAAGCTGCCCGTGCCCTGGCCCACCCTCGTGACCACCCTGACCT
ACGGCGTGCAGTGCTTCAGCCGCTACCCCGACCACATGAAGCAGCACGAC
TTCTTCAAGTCCGCCATGCCCGAAGGCTACGTCCAGGAGCGCACCATCTT
CTTCAAGGACGACGGCAACTACAAGACCCGCGCCGAGGTGAAGTTCGAGG
GCGACACCCTGGTGAACCGCATCGAGCTGAAGGGCATCGACTTCAAGGAG
GACGGCAACATCCTGGGGCACAAGCTGGAGTACAACACTACAACAGCCACAA
CGTCTATATCATGGCCGACAAGCAAAC

>3911760_2-3

CGGCCTAGTCCCCCATTGACGTCAATGGGGAGTTTGTGTTTTGGCACCAA
ATCAACGGGACTTTCCAAAATGTCGTAACAACCTCCGCCCCATTGACGCAA
ATGGGCGGTAGGCGTGTACGGTGGGAGGTCTATATAAGCAGAGCTCTCTG

GCTAACTAGAGAACCCACTGCTTACTGGCTTATCGAAATTAATACGACTC
ACTATAGGGAGACCCAAGCTTGGTACCGAGCTCGGATCCACTAGTAACGG
CCGCCAGTGTGCTGGAATTCTGCAGATATCCATCACACTGGCGGCCGCTC
GAGATGGTGAGGAGCGGCGAGGAGCGGTTACCGGGGTGGTGCCCATCCT
GGTCGAGCTGGACGGGCACGTAAGCGGCCACTAGTTCAGCGTGTCCGGCG
AGGGCGAGGGCGATGCCACCTACGGCAAGCTGACCCTGAAGTTCATCTGC
ACCACCGGCAAGCTGCCCCGTGCCCTGGCCCACCCTCGTGACCACCCTGAC
CTACGGCGTGCAGTGCTTCAGCCGCTACCCCGACCACATGAAGCAGCACG
ACTTCTTCAAGTCCGCCATGCCCGAAGGCTACGTCCAGGAGCGCACCATC
TTCTTCAAGGACGACGGCAACTACAAGACCCGCGCCGAGGTGAAGTTCGA
GGGCGACACCCTGGTGAACCGCATCGAGCTGAAGGGCATCGACTTCAAGG
AGGACGGCAACATCCTGGGGCACAAGCTGGAGTACA ACTACAACAGCCAC
AACGTCTATATCATGGCCGACAAGCAACGNAAG

>3911761_2-4

GTNNCCCCATTGACGTCAATGGGAGTTTGT TTTGGCACCAAATCAACGG
GACTTTCCAAAATGTCGTAACA ACTCCGCCCCATTGACGCAAATGGGCGG
TAGGCGTGTACGGTGGGAGGTCTATATAAGCAGAGCTCTCTGGCTAACTA
GAGAACCCACTGCTTACTGGCTTATCGAAATTAATACGACTCACTATAGG
GAGACCCAAGCTTGGTACCGAGCTCGGATCCACTAGTAACGGCCGCCAGT
GTGCTGGAATTCTGCAGATATCCATCACACTGGCGGCAGCTCGAGATGGT
GAGCAGGGGCGAGGAGCTGTTACCGGGGTGGTGCCCATCCTGGTCGAGC
TGGACGGCGACGTA AACGGCCACAAGTTCAGCGTGTCCGGCGAGGGGCGAG
GGCGATGCCACCTACGGCAAGCTGACCCTGAAGTTCATCTGCACCACCGG
CAAGCTGCCCCGTGCCCTGGCCCACCCTCGTGACCACCCTGACCTACGGCG
TGCAGTGCTTCAGCCGCTACCCCGACCACATGAAGCAGCACGACTTCTTC

AAGTCCGCCATGCCCCGAAGGCTACGTCCAGGAGCGCACCATCTTCTTCAA
GGACGACGGCAACTACAAGACCCGCGCCGAGGTGAAGTTCGAGGGCGAC
A

CCCTGGTGAACCGCATCGAGCTGAAGGGCATCGACTTCAAGGAGGACGGC
AACATCCTGGGGCACAAGCTGGAGTACAACACTACAACAGCCACAACGTCTA
TATCATGGCCGACAAGCAGAAGAACGGCATCAAGGTGAACTTCAAGATCC
GCCACAACATCGAGGACGGCAGCGTGCAGCTCGCCGACCACTACCAGTAG
AACACCCTCATCGGGCAGGGCCCCGTGCTGCTGCCGAACATCACTATCTG
AGTATCTAGTCCGCCTTGATCAAAGAC

>3911762_3-2

CGGGTTAGTNCACCCATTGACGTCAATGGGGAGTTTGT TTTGGCACCAAA
ATCAACGGGACTTTCCAAAATGTCGTAACAACCTCCGCCCCATTGACGCAA
ATGGGCGGTAGGCGTGTACGGTGGGAGGTCTATATAAGCAGAGCTCTCTG
GCTAACTAGAGAACCCACTGCTTACTGGCTTATCGAAATTAATACGACTC
ACTATAGGGAGACCCAAGCTTGGTACCGAGCTCGGATCCACTAGTAACGG
CCGCCAGTGTGCTGGAATTCTGCAGATATCCATCACACTGGCGGGCCGCTC
CAAGTGGAGCCGAGCGCGGAACAGCGCTTGGGTCGCGCGATGGTGAGTCG
GGTCGAGCTGGATAGGCACGTAAGCAGCGACAAGTTCAGCGTGTCCGGCG
AGGGCGAGGGCGATGCCACCTACGGCAAGCTGACCCTGAAGTTCATCTGC
ACCACCGGCAAGCTGCCCCGTGCCCTGGCCCACCCTCGTGACCACCCTGAC
CTACGGCGTGCAGTGCTTCAGCCGCTACCCCGACCACATGAAGCAGCACG
ACTTCTTCAAGTCCGCCATGCCCCGAAGGCTACGTCCAGGAGCGCACCATC
TTCTTCAAGGACGACGGCAACTACAAGACCCGCGCCGAGGTGAAGTTCGA
GGGCGACACCCTGGTGAACCGCATCGAGCTGAAGGGCATCGACTTCAAGG
AGGACGGCAACATCCTGGGGCACAAGCTGGAGTACAACACTACAACAGCCAC

AACGTCTATATCATGGCCGACAAGCAACANNNG

>3911763_3-3

GCTNGTNCCCCATTGACGTCAATGGGGAGTTTGTGTTTGGCACCAAATC
AACGGGACTTTCCAAAATGTCGTAACAACCTCCGCCCCATTGACGCAAATG
GGCGGTAGGCGTGTACGGTGGGAGGTCTATATAAGCAGAGCTCTCTGGCT
AACTAGAGAACCCACTGCTTACTGGCTTATCGAAATTAATACGACTCACT
ATAGGGAGACCCAAGCTTGGTACCGAGCTCGGATCCACTAGTAACGGCCG
CCAGTGTGCTGGAATTCTGCAGATATCCATCACACTGGCGGCCGCTCCTG
ATGGAGACGAGCGCGGAACAGCGCTTGACTGGCGGATAGTGAGTCGGGT
CGAGCTGGATAAGCCAGTAAGCAGTGACTACTCCAGCGAGCCCGACAACG
GCGAGGGCGATGCCACCTACGGGTAGCTGACCCTGGAGTTCATCTGCACC
ACCGGCAAGCTGCCCCGNTGCCCTGGGCCACCCCTTCGTGACCACCCTGAA
ACCTACGGCGTGCAGTGGGCTTCAGCCGCTACCCCGACCACATGAAGCAG
CACGACTTCTTCAAGTCCGCCATGCCCGAAGGCTACGTCCAGGAGCGCAC
CATCTTCTTCAAGGACGACGGCAACTACAAGACCCGCGCCGAGGTGAAGT
TCGAGGGCGACACCCTGGTGAACCGCATCGAGCTGAAGGGCATCGACTTC
AAGGAGGACGGCAACATCCTGGGGCACAAGCTGGAGTACAACACTACAACA
G

CCACAACGTCTATATCATGGCCGGACAAGCAAAACA

>3911764_3-4

GGCTTCGTCTNCCCATTGACGTCAATGGGGAGTTTGTGTTTGGCACCAAAA
TCAACGGGACTTTCCAAAATGTCGTAACAACCTCCGCCCCATTGACGCAAA
TGGGCGGTAGGCGTGTACGGTGGGAGGTCTATATAAGCAGAGCTCTCTGG
CTAACTAGAGAACCCACTGCTTACTGGCTTATCGAAATTAATACGACTCA
CTATAGGGAGACCCAAGCTTGGTACCGAGCTCGGATCCACTAGTAACGGC

CGCCAGTGTGCTGGAATTCTGCAGATATCCATCACACTGGCGGCCGCTCG
AGATGGAGAGGAGCGGGGAGGAGCGGTTCACTGGGGTGATGCCGATCCT
G
GTCGAGCTGGACGGGCACGTAAGCAGCCACAAGTTCAGCGTGCCCGACAA
CGGCGAGGGCGATGCCACCTACGGGTAGATGACCCTGGAGTACATCTGTA
CCACCGGCGAGCTGCCCCTGCCCTGGCCCACCCTCGTGACCACCCTGACC
TACGGCGTGCAGTGCTTCAGCCGCTACCCCGACCACATGAAGCAGCACGA
CTTCTTCAAGTCCGCCATGCCCGAAGGCTACGTCCAGGAGCGCACCATCT
TCTTCAAGGACGACGGCAACTACAAGACCCGCGCCGAGGTGAAGTTCGAG
GGCGACACCCTGGTGAACCGCATCGAGCTGAAGGGCATCGACTTCAAGGA
GGACGGCAACATCCTGGGGCACAAGCTGGAGTACAACACTACAACAGCCACA
ACGTCTATATCATGGCCGGACAAGCAAAAAG

>3911765_4-2

GCTTNGTCTNCCCATTGACGTCAATGGGGAGTTTGTTTTGGCACCAAAT
CAACGGGACTTTCCAAAATGTCGTAACAACCTCCGCCCCATTGACGCAAAT
GGGCGGTAGGCGTGTACGGTGGGAGGTCTATATAAGCAGAGCTCTCTGGC
TAACTAGAGAACCCACTGCTTACTGGCTTATCGAAATTAATACGACTCAC
TATAGGGAGACCCAAGCTTGGTACCGAGCTCGGATCCACTAGTAACGGCC
GCCAGTGTGCTGGAATTCTGCAGATATCCATCACACTGGCGGCCGCTCGA
GATGGAGAGGAGCGCGGAGGAGCGGTTCACTGGGGTGATGCCGATCCTGG
TCGAGCTGGACGGGCACGTAAGCAGCGACTAGTTCAGCGTGTCCGGCAAC
GGCGAGGGTGATGCCACCTACGGGTAGATGCCTCTGGAGTTCATCTGTAC
CACCGGCGAGCTGCCCCTGCCCTGGCCCACCCTCGTGACCACCCTGACCT
ACGGCGTGCAGTGCTTCAGCCGCTACCCCGACCACATGAAGCAGCACGAC
TTCTTCAAGTCCGCCATGCCCGAAGGCTACGTCCAGGAGCGCACCATCTT

CTTCAAGGACGACGGCAACTACAAGACCCGCGCCGAGGTGAAGTTCGAGG
GCGACACCCTGGTGAACCGCATCGAGCTGAAGGGCATCGACTTCAAGGAG
GACGGCAACATCCTGGGGCACAAGCTGGAGTACAACAGCCACAA
CGTCTATATCATGGCCGACAAGCAAAAGA

>3911766_4-3

GCCTNGTCTNCCCATTGACGTCAATGGGGAGTTTGTGTTTGGCACCAAAT
CAACGGGACTTTCCAAAATGTCGTAACAACCTCCGCCCCATTGACGCAAAT
GGGCGGTAGGCGTGTACGGTGGGAGGTCTATATAAGCAGAGCTCTCTGGC
TAACTAGAGAACCCACTGCTTACTGGCTTATCGAAATTAATACGACTCAC
TATAGGGAGACCCAAGCTTGGTACCGAGCTCGGATCCACTAGTAACGGCC
GCCAGTGTGCTGGAATTCTGCAGATATCCATCACACTGGCGGCCGCTCGA
GATGGAGAGGAGCGCGGAGGAGCGGTTCACTGGGGTGATGCCGAGCCTG
G

TCGAGCTGGACGAGCGACGTAAGCAGCGACTAGTTCAGCGTGCCCGAGAA
CGGCGAGGGTGATGACACCTACGGGTAGATGCCCATGGAGTACATCTGTA
CCACCGGCGAGCTGCCCGTGCCCTGGCCCACCCTCGTGACCACCCTGACC
TACGGCGTGCAGTGCTTCAGCCGCTACCCCGACCACATGAAGCAGCACGA
CTTCTTCAAGTCCGCCATGCCCGAAGGCTACGTCCAGGAGCGCACCATCT
TCTTCAAGGACGACGGCAACTACAAGACCCGCGCCGAGGTGAAGTTCGAG
GGCGACACCCTGGTGAACCGCATCGAGCTGAAGGGCATCGACTTCAAGGA
GGACGGCAACATCCTGGGGCACAAGCTGGAGTACAACAGCCACA
ACGTCTATATCATGGCCGACAAGCAACT

>3911767_4-4

GCTNGTCTCCCCATTGACGTCAATGGGGAGTTTGTGTTTGGCACCAAATC
AACGGGACTTTCCAAAATGTCGTAACAACCTCCGCCCCATTGACGCAAATG

GGCGGTAGGCGTGTACGGTGGGAGGTCTATATAAGCAGAGCTCTCTGGCT
AACTAGAGAACCCACTGCTTACTGGCTTATCGAAATTAATACGACTCACT
ATAGGGAGACCCAAGCTTGGTACCGAGCTCGGATCCACTAGTAACGGCCG
CCAGTGTGCTGGAATTCTGCAGATATCCATCACACTGGCGGCCGCTCCTG
ATGGAGACGAGCGCGGAGCAGCGCTTGACTGGGGCGATGCTGAGTCGGGT
CGAGCTGGATAAGCAAGTAAGCAGCGACTAGTTCAGCGTGTCCGGCGACG
GCGAGGGCGATGCCACCTACGGCAAGCTGACCCTGAAGTTCATCTGCACC
ACCGGCAAGCTGCCCCTGCCCTGGCCCACCCTCGTGACCACCCTGACCTA
CGGCGTGCAGTGCTTCAGCCGCTACCCCGACCACATGAAGCAGCACGACT
TCTTCAAGTCCGCCATGCCCGAAGGCTACGTCCAGGAGCGCACCATCTTC
TTCAAGGACGACGGCAACTACAAGACCCGCGCCGAGGTGAAGTTCGAGGG
CGACACCCTGGTGAACCGCATCGAGCTGAAGGGCATCGACTTCAAGGAGG
ACGGCAACATCCTGGGGCACAAGCTGGAGTACAACACTACAACAGCCACAAC
GTCTATATCATGGCCGGACAAGCAAACACGNNNGN

>3911768_Control

GCCTNGTCTNCCCATTGACGTCAATGGGGAGTTTGTTTTGGCACCAAAT
CAACGGGACTTTCCAAAATGTCGTAACAACCTCCGCCCCATTGACGCAAAT
GGGCGGTAGGCGTGTACGGTGGGAGGTCTATATAAGCAGAGCTCTCTGGC
TAACTAGAGAACCCACTGCTTACTGGCTTATCGAAATTAATACGACTCAC
TATAGGGAGACCCAAGCTTGGTACCGAGCTCGGATCCACTAGTAACGGCC
GGCCAGTGTGCTGGGAATTCTGCAGATATCCATCACACTGGCGGCCGCTC
CTAATGGAGACGAGCGCGGAGCAGCGCTTGGCTGGCGCGATAGTGAGTCG
GATCGAGCTGGATAAGCCAGTAAGCAGTGACTACTCCAGCGAGCCCGAGA
ACGGCGAGGGCGATGCCACCTACGGGTAGCTGACCCTGACGTTTCATCTGC
ACCACCGGCAAGCTGCCCCTGCCCTGGCCCACCCTCGTGACCACCCTGAC

CTACGGCGTGCAGTGCTTCAGCCGCTACCCCGACCACATGAAGCAGCACG
ACTTCTTCAAGTCCGCCATGCCCGAAGGCTACGTCCAGGAGCGCACCATC
TTCTTCAAGGACGACGGCAACTACAAGACCCGCGCCGAGGTGAAGTTCGA
GGGCGACACCCTGGTGAACCGCATCGAGCTGAAGGGCATCGACTTCAAGG
AGGACGGCAACATCCTGGGGCACAAGCTGGAGTACAACACTACAACAGCCAC
AACGTCTATATCATGGCCGACAAGCAACAAC